Methane Hydrate Production Using Mixture Of CO2 and N2

Master of Science Thesis in Process Technology

By Aruna Sapate

Department of Physics and Technology

University of Bergen, Norway

June 2015

Abstract

Gas Hydrates (GHs) are naturally occurring solid, crystalline compounds in which natural gas is trapped inside the cage like structures formed by water molecules. Lately a novel technology has been developed for the production of methane from in-situ GHs by injection of CO2. Addition of N2 to CO2 for hydrate production has an advantage of both higher methane recovery and CO2 sequestration. Injected CO2/N2 mixture into in-situ methane hydrate replaces the CH4 molecules in the hydrate cage and form new CO2 dominated CO2 hydrate or mixed CO2-CH4 hydrate. This conversion is based on two primary mechanisms; first is through formation of new hydrate and second is direct solid state exchange.

The main goal of this master thesis is to study the feasibility of CO2-N2 gas mixture injection method in methane recovery. In pursuit of this goal hydrate stability limits for different mixtures of CO2/N2 in terms of chemical potentials as function of gradual decrease in CO2 content in gas mixture have been evaluated. The CO2:N2 ratio is a sensitive balance. Nitrogen concentration applied in relevant simulations carried out in this thesis vary from 30% to 80%. Residual thermodynamics has been applied for all the components in all phases as a basis of free energy analysis of hydrate stability in order to have same reference level of chemical potentials for all components in all phases. The kinetics of hydrate phase transition in porous media is implicit function of mass-transport dynamics, heat transport dynamics and the kinetics of the phase transition itself.

The work presented in this thesis is a contribution to the description of the thermodynamic forces related to the phase transition kinetics. A natural extension of this work would be the inclusion into a hydrate reservoir simulator in order to complete the couplings to mass and heat-transport. For this reason, as a service to external researchers that might want to incorporate these models into their simulator, a fairly detailed description of the thermodynamic models is presented.

As examples for examining possible limitations of nitrogen addition to the carbon dioxide, a selection of real hydrate reservoirs have been examined in terms of local range of thermodynamic conditions for hydrate zones considered to be large enough in thickness and extension of hydrate filled sediments to be of interest for possible production. For this purpose using different concentrations of CO2 & N2, hydrate stability limitations have been evaluated at hydrate bearing layers in Eileen area at Prudhoe Bay field on the North Slope of Alaska, USA; Mallik field at Mackenzie Delta River, Canada; MITI Nankai Trough at Japan and Bjørnøya Basin in SW-Barents Sea. For each study area, regional stratigraphic data for hydrate bearing sediments has been analyzed.

The fastest mechanism for conversion of CH4 hydrate through CO2 injection goes through the formation of new CO2 dominated hydrate and subsequent dissociation of in-situ hydrate assisted by the released heat from this new hydrate formation. An important focus of the analysis is the necessary CO2 content in the gas mixture needed for generation of new hydrate. CO2 will dominate new hydrate and will therefore be extracted from the injected gas mixture. A second focus is the implication of a nitrogen dominated gas (after gradual CO2

extraction) on stability of the hydrates in reservoir, both in-situ CH4 hydrate and new CO2 dominated hydrate.

This method of injection of CO2/N2 mixture into in-situ hydrate for CH4 production has been proven beneficial in many aspects over injection of pure CO2 method. The development of such production methods may help us to overcome the environmental issues as well as challenges related to economy recovery. On the basis of simulation results obtained, it seems feasible to produce in-situ methane hydrate by injection of CO2/N2 mixture. In summary the evaluation performed in this thesis indicate that the thermodynamic stability of hydrate depends on temperature, pressure and concentration (corresponding chemical potential) of all components in all phases entering the hydrate in all co-existing phases.

The second part of this thesis deals with the evaluation of maximum permissible water content in gas stream while gas is transported through pipelines without facing the risk of hydrate formation. The transport of CO2 to its underground storage destination through pipelines occurs at low temperature and high pressure which favors the hydrate formation. There are several different routes to hydrate formation depending on number of phases containing hydrate formers, but in this master thesis three possible routes of hydrate formation have been evaluated.

Simulation results indicate that the most dominant route for hydrate formation is through the adsorbed water on rusty pipeline surfaces and hydrate formers in gas phase. The obtained results also indicate that with addition of N2 to CO2 and with increase in pressure, maximum water content permitted in gas stream during transport through pipeline decreases. Estimated results indicate that the system containing 1/3 CO2 + 2/3 N2, at pressure 170 bar and temperature 222 K, the mole-fraction of water before liquid drop out is 0.85 times higher than the mole-fraction of water before adsorption on hematite.

Acknowledgements

_____

Aruna Sapate,

June 2015.

Table of Contents

List of Figures

List of Tables

<u>Abbreviations</u>

GHs – Gas Hydrates

NGHs – Natural Gas Hydrates

CO_2 – Carbon dioxide

N_2 – Nitrogen

USGS – U.S. Geological Survey

LNG – Liquefied Natural Gas

STP – Standard Temperature Pressure

tcf – Trillion Cubic Feet

R&D – Research and Development

JOGMEC – Japan Oil, Gas & Metals National Corporation.

ppt – Parts per thousand

GHSZ – Gas hydrate stability zone

DOE – Department of energy

GSC – Geological Survey of Canada

JNOC – Japan National Oil Corporation

Mbsl – Meters below sea level

Mbsf – Meters below sea floor

BSRs – Bottom simulating reflectors

Nomenclature

T – Temperature

P – Pressure

μ – Chemical potential

U – Internal energy

S – Entropy

V – Volume

R – Universal gas constant

K – Kelvin

°C – Degree Celsius

$\boldsymbol{\theta_{ik}}$ – Filling fraction of component in cavity type k.

f_i – Fugacity coefficient

y – Mole-fraction of gas

x – Mole-fractions of liquid

γ_i – Activity coefficient

β – Inverse of Boltzmann constant times temperature

Z – Distance from surface

T_c – Temperature at critical point

P_c – Pressure at critical point

ω – Acentric factor

G – Gibbs free energy

Δg_{ik}^{inc} - Gibbs free energy of inclusion of component i in cavity type k.

Subscripts & Superscripts

μ_i^{H2O} – Chemical potential of component i in water

$\mu_{i,}^{pure\ water}$ – Chemical potential of component i in pure liquid water

μ_w^{H} – Chemical potential of water in hydrate

$\mu_w^{0,H}$ – Chemical potential of water in empty hydrate

In above terms, subscript represents denotes component and superscript denotes phase, μ is chemical potential.

1. Introduction

1.1 Gas Hydrates

Gas Hydrates (GHs) are solid crystalline compounds formed by combination of natural gas and water under specific pressure and temperature conditions. Commonly the gas molecules are designated as 'guest' molecules and water as 'host' molecules in the discussion of these hydrate structures. In chemical point of view hydrates are water clathrate of methane gas, where term 'clathrate' refers to rigid cage of hydrogen bonded water molecules, more commonly known as 'Methane/Gas hydrate'. The guest gas molecules could be polar or non-polar in nature and more than one type of guest molecules can participate in the formation of Gas Hydrates (GHs) (Chejara, 2012). In the oil and gas industry the most typical guest molecules are Methane (CH_4), Ethane (C_2H_6), Carbon dioxide (CO_2), Nitrogen (N_2) and Hydrogen sulfide (H_2S). In this project work, the gas molecules considered are CH_4, CO_2 & N_2. In the term 'Natural Gas Hydrate (NGHs)' the word 'Natural' indicates two meanings. First is that the GHs occur naturally on the Earth or not synthesized in laboratory and second is the methane gas, main component of natural gas encaged inside the cavities of hydrogen bonded water molecules.

 GHs are formed under following four essential conditions,

1. When adequate supply of hydrate formers for the initiation of formation and stability of hydrate structure
2. When sufficient amount of water is available
3. High pressure
4. Low temperature

The hydrate formation condition restricts the occurrence of NGHs to two types of geologic locations, first under permafrost in the polar continental shelves and second in sediments beneath the seafloor. Typical conditions for the formation of hydrate are when temperature is (0 °C < Temperature < 20 °C) and pressure greater than 30 bar (Sinquine et.al, 2004).

The NGH deposits are found all over the world in deep water and in the Arctic. The investigation of NGHs and their exploitation researches has become very active in recent few years. For the exploration of NGHs more than hundred wells has been drilled. In last 50 years hydrates have been found in more than 79 countries. In many countries national programs have been laid for the research and production of NGHs. For the countries such as Japan and India who have not blessed with traditional gas reserves, GHs may play important role as energy suppliers. Japan is the first country who successfully produced gas from methane hydrate deposits under the Pacific Ocean in a pilot test for 6 days. India also has long been known to have massive deposits of methane hydrate. Even though the NGHs are distributed worldwide, limited number of GH accumulations has been studied in detail. The experimental exploitation research was carried out in the following few areas (Collett, 2002).

- On the Black Ridge along the southern continental margin of the United States.

- At the Cascadia continental margin off the Pacific coast of Canada.
- Near the Nankai Trough off the coasts of Japan.
- On the North Slope of Alaska.
- In the Mackenzie River Delta of northern Canada.

A map of the discovered NGH deposits is shown in figure 1.
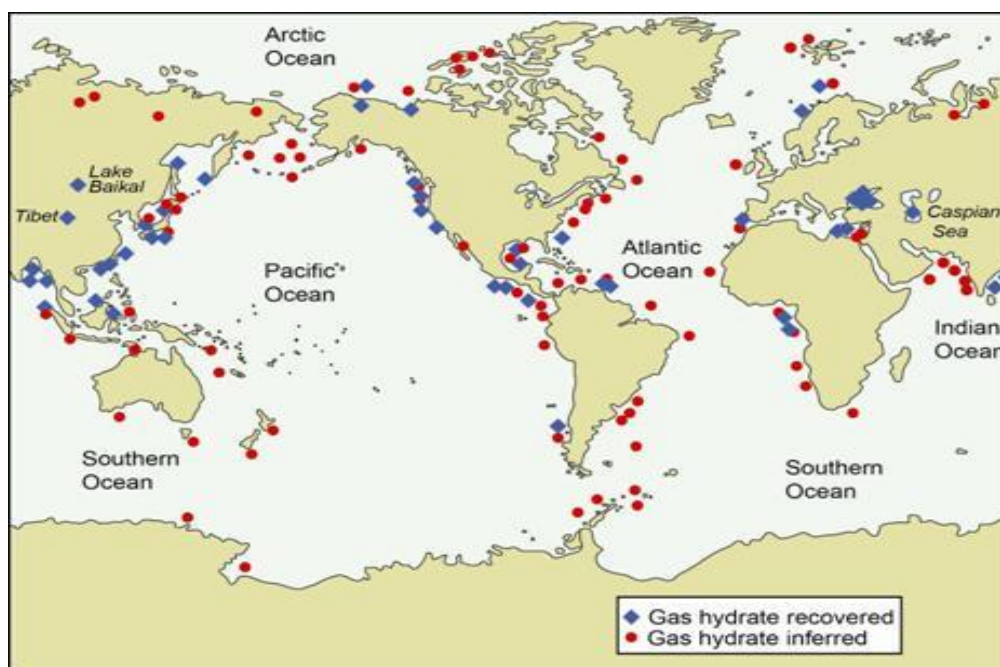
Figure 1: Location of sampled and inferred gas hydrates occurrences worldwide (map courtesy by USGS).

Many scientists and researchers have been proposed that the enormous amount of natural gas is trapped in the form of hydrates and also they have proposed very optimistic methods for the production of methane from GHs to prove them as potential energy source. This is one of the reasons that researchers and engineers are interested in methane hydrate production. Moreover, there is growing evidence for the production of natural gas from hydrates with existing oil and gas technologies (Dallimore et.al, 2008a., Dallimore et.al, 2008b., Yamamoto and Dallimore, 2008). For an accurate estimation of how much gas is trapped within gas hydrate, one should understand the fundamental aspects about GHs like how do they occur? Where do they occur in nature? And why do gas hydrates occur at particular settings?

Due to their global occurrences and containing enormous amount of natural gas, GHs may represent future energy source for the world if efficient methods are developed for extraction of methane gas from hydrate. Natural gas has important uses such as fuel for residential heating, fuel for many industries and also can be used as feedstock to produce chemicals, fabrics, fertilizers etc. For decades GHs have been discussed as a potential resource, particularly for countries with limited access to conventional hydrocarbons (Japan, India etc.). The wide distribution of GHs throughout the world makes them interesting as a substantial future energy source.

1.2 Hydrate History

In the early 1800, scientists were used to synthesize GHs just for a laboratory curiosity. In the early 19th century, Humphrey Davy and Michael Faradays during their studies realized that sometimes chlorine atom become encaged inside the ice structure, they named it as chlorine clathrate hydrate (Sloan & Koh, 2007). According to some scientists Davy was the one who discovered the GHs first time, but however scientist Priestley synthesized the GHs first time in 1778 in laboratory. Then GHs has drawn much attention in 1930s in oil & gas industries. Hammerschimidt observed that some ice-like compound blocking the flow in gas pipelines and later on he investigated that these solid plugs consist not of ice, but ice wrapped methane hydrate (Makogon, Y.F). During this period scientists were trying to develop new methods to inhibit the pipeline blockages due to hydrate formation.

But in 1960s, first time scientist discovered the existence of NGHs in natural world in subsurface sediments of Messoyokha gas field in western Siberia. In 1970s, another research team found the presence of gas hydrates on the North Slope of Alaska as well. From 1960s to till date, research on GHs has gained much fame and more than 12,000 research papers have been published on these GHs since then.

1.3 Hydrate Structures and Basic Properties

In hydrate structure cavities are filled by slightly polar or non-polar guest molecules. Generally a single cage can hold single molecule. In order to stabilize these cavities, guest molecules should fit volumetrically within the cavity and guest molecules must not compete with already existing hydrogen bond (Jeffrey, 1984). The vital condition for a guest molecule to be able to fit within the cavities and stabilize them is the diameter ratio between guest and cavity should be within the range of 0.70 - 1.0. The empty space in the cavity may cause collapsing of structure. Nitrogen is the smallest hydrate former. Presently three distinct crystalline structures has been determined by Sloan and Koh in 2007 (Sloan & Koh, 2007), among them Structure I (sI) and Structure II (sII) are common (sI and sII are cubic structures) in oil industry and the third Structure H (sH, hexagonal structure) is rarely found. The classification of hydrate is based on the geometries of their constituent water cages.

1.3.1 Structure I (sI)

These hydrate structures are commonly occurring in nature which encases small molecules of a diameter 4.2 Å – 6Å such as CH4, CO2, H2S, C2H6 gas etc. One unit cell of sI consists of 46 water molecules and this is made up of six large cages and two small cages. The large cage called as 'tetrakaidecahedron' ($5^{12}6^2$) since it has shape of 14 sided cavity with 12 pentagonal faces and 2 hexagonal faces. The small cage called as 'pentagonal dodecahedron' (5^{12}) as it has the shape of 12 sided cavity with 12 pentagonal faces each side. The small and large cavities are shown in figure 2.

1.3.2 Structure II (sII)

One unit cell of sII consist 136 water molecules. These hydrate structures (sII) are formed either by small size of molecules (with diameter < 4.2 Å) such as Nitrogen, Hydrogen etc. or by large guest molecules (with diameter 6 Å to 7 Å) like Propane, Iso-butane. One unit cell has 16 small cages and 8 large cages. Large cage called as 'hexakaidecahedron' ($5^{12}6^4$) since it has 16 sided cavity with 12 pentagonal faces and 4 hexagonal faces. Small cage has the same shape as in sI of 'pentagonal dodecahedron' (5^{12}).

1.3.3 Structure H (sH)

This type of structure is very rarely found in nature. The structure H has an intermediate size cavity in addition to small and large cavities. sH is formed by large guest molecules like Iso-pentane or neo-hexane when accompanied by small guest molecules $CH4$, $N2$ or $H2S$ etc. (Sloan and Koh, 2007). One unit cell of sH consists 3 small, 2 medium and 1 large cages. Large cage is called 'icosahedron' ($5^{12}6^8$) since it has 20 sided cavity with 12 pentagonal faces and 8 hexagonal faces. Medium cage called as 'irregular dodecahedron' ($4^35^66^3$) since it has 12 sided cavity with 3 square faces, 6 pentagonal faces & 3 hexagonal faces. Small cages form the shape of 'pentagonal dodecahedron' (5^{12}) as in sI and sII.

The main properties of three hydrate structures sI, sII & sH can be systemized in the table format as follows (Table 1).

Hydrate Crystal Structures	sI		sII		sH		
Cavity	Small	Large	Small	Large	Small	Medium	Large
Description	5^{12}	$5^{12}6^2$	5^{12}	$5^{12}6^4$	5^{12}	$4^35^66^3$	$5^{12}6^8$
Number of cavities per unit cell	2	6	16	8	3	2	1
Average cavity radius (Å)	3.95	4.33	3.91	4.73	3.91[d]	4.06[d]	5.71[d]
Number of water per unit cell	46		136		34		
Crystal system	Cubic		Cubic		Hexagonal		

Table 1: Main properties of the different hydrate structure (Sloan & Koh, 2007) (d = From the atomic coordinates measured using single crystal x-ray diffraction on 2,2-dimethylpentane 5(Xe,H2S)-34H2O at 173 K).

The cage configuration for three crystalline hydrate structures (sI, sII, & sH) can be represented as in figure 2.

Small cages | Large cages | Unit Cell Formula

5^{12} | $5^{12}6^2$ | $S_2L_6 \cdot 46H_2O$

5^{12} | $5^{12}6^4$ | $S_{16}L_8 \cdot 136H_2O$

5^{12} | $4^35^66^3$ | $5^{12}6^8$ | $S_3S_2L \cdot 34H_2O$
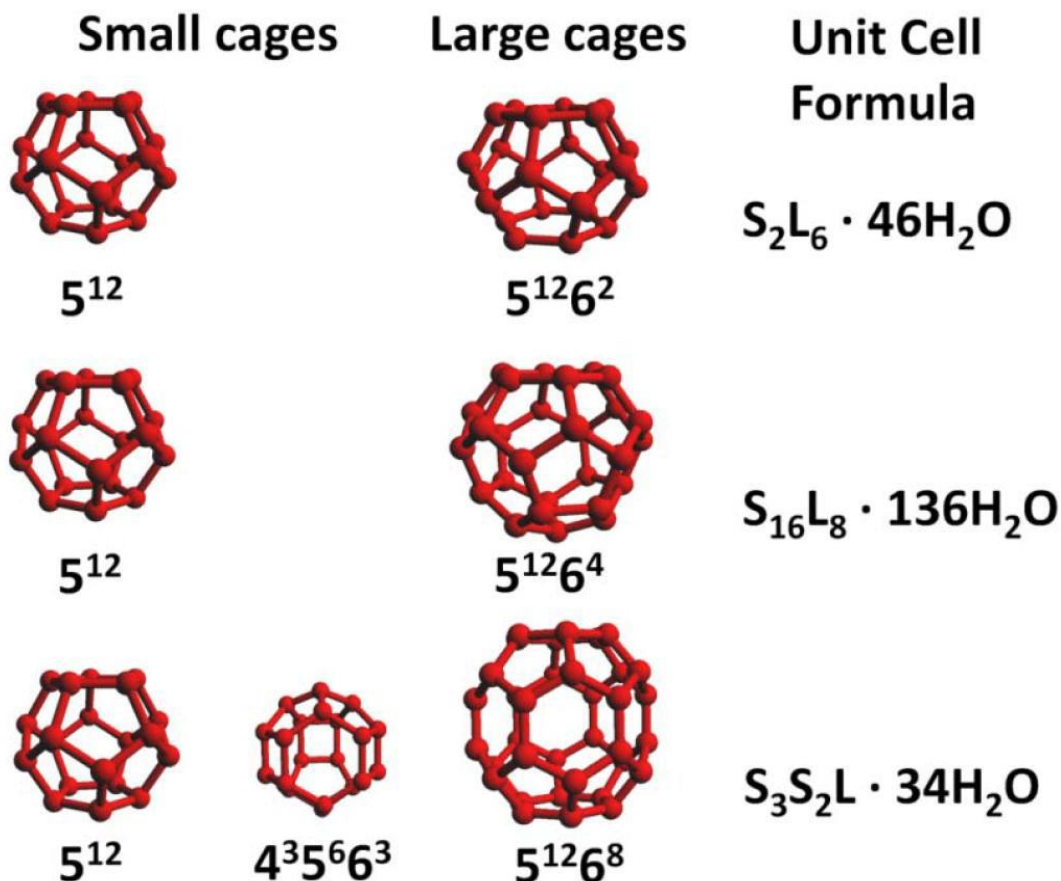
Figure 2: Hydrate polyhedron. The figure shows cage structures of small cavity, large cavity, and unit cell formula for sI, sII, sH respectively from top to bottom (Husebø, 2008).

So generally hydrates are classified on the basis of arrangement of host i.e. water molecules in the crystal structure. The requirement for a guest molecule is that it needs to fit into the cavity it enters without destroying the hydrogen bonds due to expansion. Small molecules compared to cavity sizes might induce collapse due to excessive empty space in cavity, unless double occupancy can counteract that. A crystalline property of NGHs has been studied in detail by (Sloan & Koh, 2007).

Some of the guest molecules that forms hydrate with water are,

- Methane, Ethane, Propane, Iso-butane, or light hydrocarbons
- Carbon dioxide
- Nitrogen
- Hydrogen Sulfide
- Oxygen etc.

In this master thesis the hydrate formers or guest molecules considered are methane, carbon dioxide, & nitrogen. The hydrate formers CH4, CO2, H2S form structure I hydrate whereas components like N2, propane, Iso-butane forms structure II type hydrate. Nitrogen being smallest natural gas hydrate former, it can provide insignificant stability to the large cavity in either structure (sI or sII), so nitrogen forms sII with a fractionally higher number of small cavities in unit cell (Sloan and Koh, 2007). For the stabilization of hydrate structure, the volume and shape of guest molecule must be sufficient to prevent collapse (Kvamme, 2014b).

1.4 Similarities between Ice and Hydrate

The natural gas hydrates are also called as "Burning Ice" because on primary view they look like ice but they are highly flammable. Since all of the three hydrate structure contains about 85% water, many of the hydrate mechanical properties resemble to those of ice but some of the properties are different like thermal conductivity, thermal expansion, electrical property and elasticity etc. Electrical and thermal conductivity of hydrate is lower than Ice. The electrical property is used in technology for detecting hydrate (Kvamme, 2014b). Hydrates have a density and texture similar to ice.

Properties	Ice	Structure I	Structure II
Number of water molecules	4	46	136
Dielectric constant at 273 K	94	~58	~58
Thermal conductivity at 263 K [$Wm^{-1}K^{-1}$]	2.23	0.49 ± 0.02	0.51 ± 0.02
Density (g/cm^3)	0.917	0.94^b	1.291^c
Lattice parameters (at 273K)	a=4.52,c=7.36	12	17.30
H2O diffusion jump time (µs)	2.70	>200	>200
H2O reorientation time[µs]	21	10	10

Table 2: Comparison of some properties between ice and hydrate structures (Sloan & Koh, 2008) (In table b = based on methane hydrate density in large polyhedral, c = calculated for 2,2-dimethylpentane 5(Xe,H2S)·34H2O,)

1.5 Hydrate as a problem in industry

As mentioned previously Hammerschimidt first time discovered that the hydrate plugs are the culprits for pipeline blockages and it is one of the major problems that oil and gas industries suffering from. In an oil and gas industries the conditions at which oil and gas are produced, transported, and processed provides suitable conditions for hydrate formation. During 1930s scientists were interested in developing new technology for prevention of hydrate formation since gas hydrates always provided challenges for production of natural oil and gas. But with the time it becomes clear that hydrate risk management is more economical than complete hydrate prevention. However for the gas industries, for safe dissociation of formed NGHs in pipeline may cost approximately $1 million each day and once a hydrate plug has formed in the pipeline it takes few weeks or even a month to dissociate it. Moreover requires very complex operation for removal (Guo et.al, 2005).

The complete blockage of pipelines causes severe issues and it can completely stop production for several days or even months. Currently few interesting methods are developed for the prevention of hydrate formation in pipelines as follows,

1. Injection of thermodynamic inhibitors to decrease the hydrate formation temperature and inhibit the formation of NGH crystals.

2. Injection of anti-agglomerants to prevent the aggregation of hydrate crystals.

3. Maintaining the pipeline operating conditions outside the zone of hydrate stability.

The most common flow assurance method is based on injection of organic inhibitors like methanol, mono-ethylene glycol which suppresses the temperature at which hydrates are stable. The companies like Gassled who successfully transport gas from Norwegian continental shelf to Europe, are looking for new methods for developing assurance of smooth flow of gases through transport pipeline. Flow assurance is the operation that provides a reliable flow of fluids from the reservoir to sales point.

The second major problem while producing energy from NGHs from the ocean bed deposits is the release of uncontrolled methane into the ocean may increases the salinity of ocean. NGHs can cause some climate issues because when these hydrate deposits decomposes and dissociates into water and methane gas due to rise in temperature or depressurization. Methane is a greenhouse gas; the large amount of discharge in atmosphere would cause the global warming.

1.6 Hydrate as Energy Source and Methods for Production

It is believed that the amount of natural gas trapped within the gas hydrate accumulations is greater than the known volume of conventional gas reserves. At STP (standard conditions of 1 atm pressure and 298 K temperature) one volume of solid methane hydrate can contain as many as 164 volumes of methane gas (Ginley & Cahen, 2012).
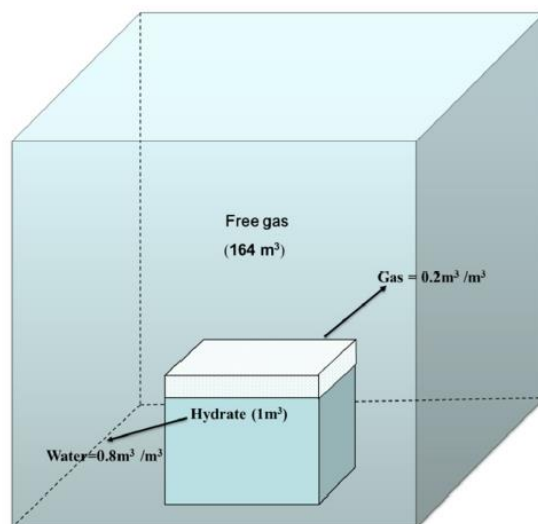
Figure 3: Methane Hydrate composition (Makogon, 1966).

In 1970 Chersky & Makogon proposed the amount of methane in naturally occurring gas hydrates is potentially enormous but the estimated amounts were highly speculative because of lack of sufficient knowledge about occurrences of GHs (Chersky & Makogon, 1970). The current estimate shows that around 20,000 trillion cubic meter of gas is deposited in the form of hydrate in the world's marine and permafrost region (Collett, 2002).

In last decades the increased rate of energy production has been considerably higher than the rate of increase of new proven hydrocarbon resources, resulting in a serious energy crisis in some countries. In order to reduce the cost and risk while transporting the natural gas via pipelines or LNG-boats (Liquefied Natural Gas) an alternative technology for NGHs production has been developed. The methane hydrate production means dissociation of methane hydrate into methane and water and collecting the resultant methane gas through wells. Two different approaches has been proposed for production, either by changing thermodynamic conditions resulting in hydrate decomposition or by exposing the hydrate to a thermodynamically more stable hydrate former inducing a replacement process of the encaged CH4 molecule in the lattice structure with the introduced new hydrate former. Carbon dioxide is an attractive candidate for such process due to both offering a better hydrate stability and possibilities for sequestrating a greenhouse gas as hydrates in the earth.

1.6.1 Methane Production by Hydrate Dissociation

The production of natural gas accumulated in oceanic and permafrost sediments is currently being developed by using depressurization, thermal stimulation & inhibitor injection. These methods are explained in detail in section 1.6.1.1, 1.6.1.2 & 1.6.1.3.

1.6.1.1 Depressurization

This method refers to the lowering of pressure inside the well and stimulates the methane hydrate to dissociate. It has been proven that depressurization method for production is one of the most promising and economical method because it doesn't require large expenditure and it can manage dissociation of significant amount of gas hydrate relatively rapidly. Depressurization which occurs when pressure is lowered below the pressure of hydrate stability at given temperature is schematically represented as shown in figure 4.
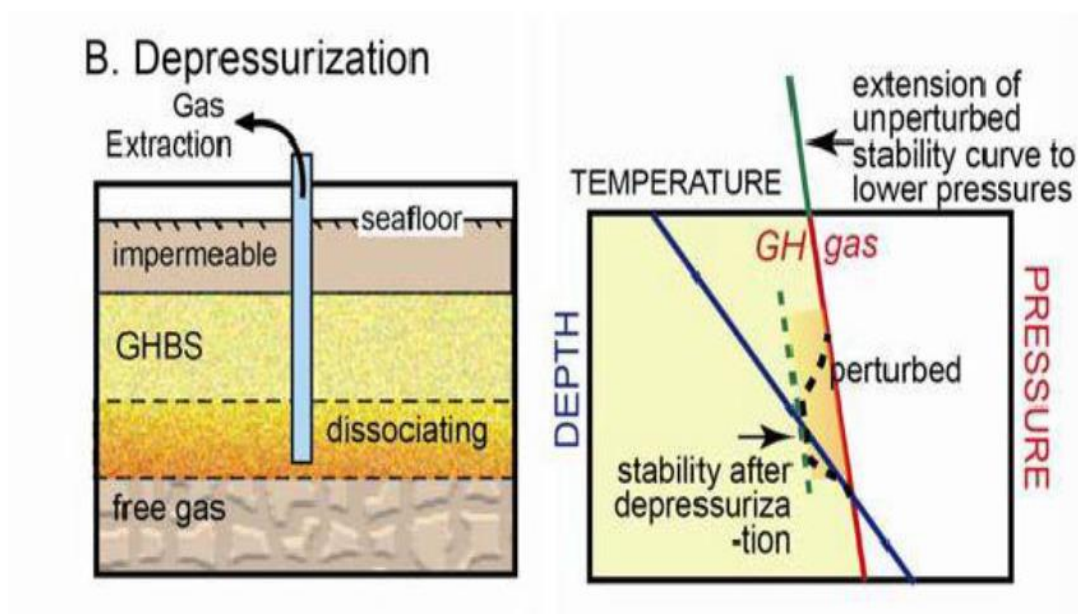
Figure 4: Schematic representation of depressurization production method (Ruppel, 2011).

In the depressurization method, hydrate stability conditions are shifted by lowering the pressure below the equilibrium pressure, so hydrates can become unstable and dissociates into methane and water. Heretofore the only method that has been successfully used to produce gas economically from GHs is the "depressurization". This method is applicable to only those hydrates that exist in Polar Regions below permafrost and underlying sediments containing free gas. Depressurization method has been successfully applied in the second onshore production test at Mackenzie delta, Canada during 2007-2008 for hydrate dissociation, producing 13,000 m^3 of gas in six days first time in world. It is generally agreed that the depressurization method is much more efficient method of gas production than the current thermal methods.

1.6.1.2 Thermal Stimulation

Thermal stimulation refers to rise in temperature of the hydrates above their stability zone at systems pressure, resulting in hydrate dissociation. Since hydrate dissociation is an endothermic process, thermal energy required is provided directly either by injecting steam or hot water or another heated liquid. In this method steam or hot water is pumped into the hydrate bearing layer through drill hole, so that methane hydrate can dissociate and release methane gas. The methane gas mixes with water and returns to the surface where gas and water are separated. The production of methane hydrate using thermal stimulation can be schematically represented as shown in figure 5.
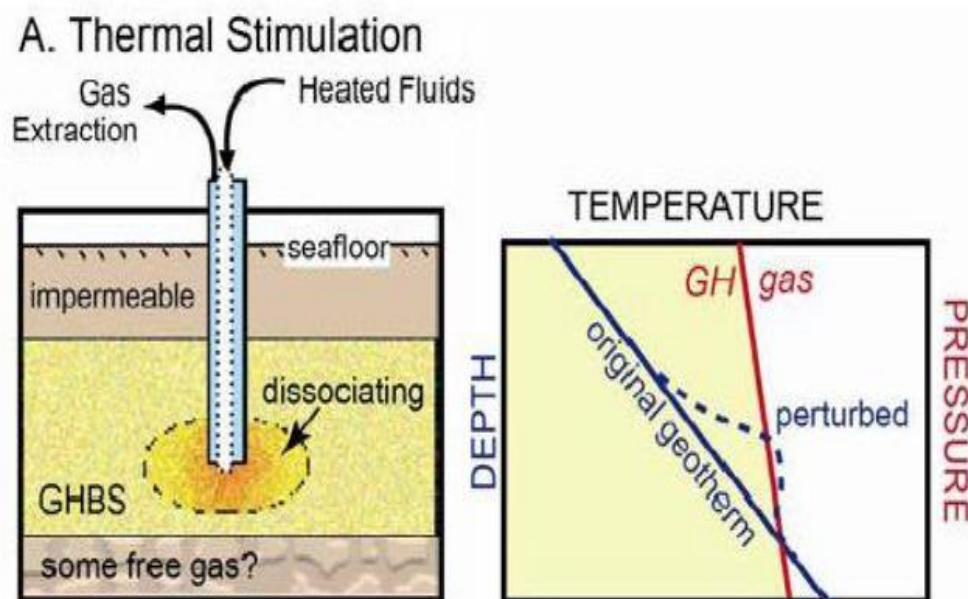
Figure 5: Gas production by thermal stimulation process (Ruppel, 2011).

In this method, heat is introduced into the reservoir resulting increase in surrounding temperature. Methane hydrate production by using thermal stimulation method has an advantage that this method is simple and comparably easy to handle. However this method has a major disadvantage that the loss of considerable amount of provided energy (up to 75%) to non-hydrate bearing strata. This drawback makes the thermal stimulation method very expensive (Demirbas, 2010). The endothermic nature of gas hydrate dissociation also presents a challenge to thermal stimulation, the cooling associates with dissociation will partially offset artificial warming of the formation, meaning that more heat must be introduced to drive continued dissociation and prevent formation of new GH (Ruppel, 2011).

"Hot water circulation" method was applied for methane production from hydrate bearing layers in the Mackenzie River Delta, Canada which involve the injection of hot water ($\approx 80\ ^\circ$C) in 17 m thick hydrate layer with high saturation. This method successfully produces 470 m^3 of gas within a period of five days. This was the first time in the world that anyone has ever produced methane gas from hydrate bearing layers.

1.6.1.3 Inhibitor Injection

Inhibitor injection method refers to the injection of chemicals such as alcohols, methanol, brine, ethylene glycol etc. which inhibits the formation hydrate crystals (Demirbas, 2010). In this inhibitor injection method chemical such as methanol is injected into the hydrate bearing layer. So that they can shift the pressure-temperature equilibrium and hydrates are no more stable at disturbed in situ pressure-temperature conditions resulting in hydrate dissociation (Demirbas, 2010). Injection of inhibitors into the hydrate zone dissociates the methane hydrate by altering the chemical composition of liquid pore water to no longer suitable conditions of hydrate stability. In this inhibitor injection method injected chemicals lowers the freezing point of neighboring water, free gas and the gases would be collected by same well head. This method of injection of chemical inhibitor schematically represented as shown in figure 6.
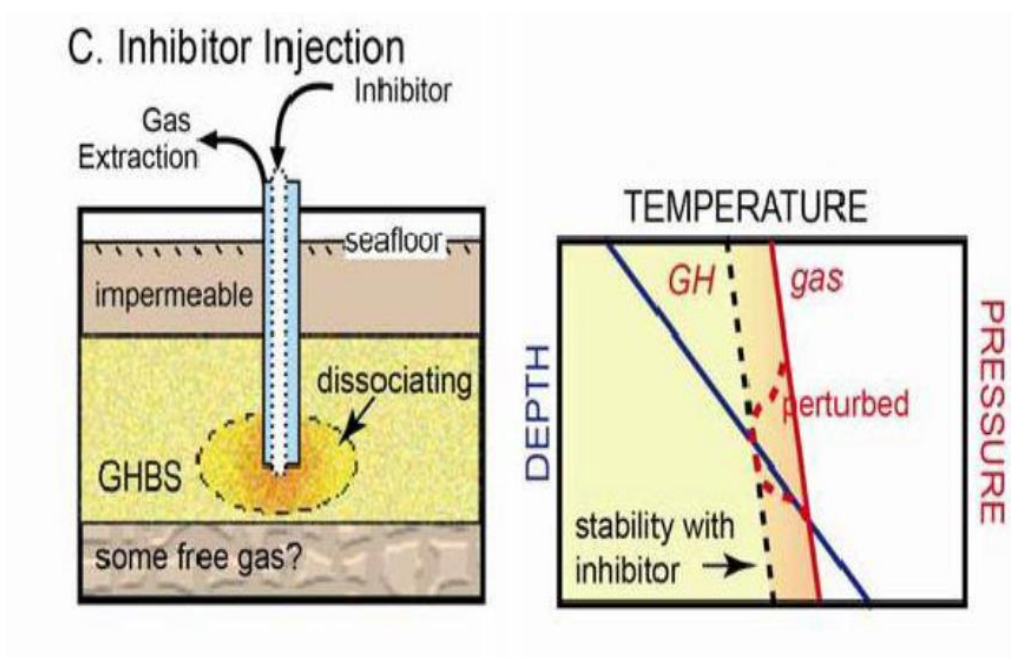
Figure 6: Gas production by inhibitor injection process (Ruppel, 2011).

It has been suggested that the GH production using chemical inhibitor injection is divided into four stages (Demirbas, 2010),

i. The initial injection of inhibitors,
ii. The dilution of injected inhibitor,
iii. The hydrate dissociation,
iv. Gas output.

The advantage of this method is that the dissociation of hydrate can be controlled by adjusting the amount of inhibitors injection. Moreover, inhibitor injection prevents the hydrates from blocking the pipeline and well heads during collection. But the major dis-advantage of this method is this method is quite expensive.

1.6.2 Production of CH4 from hydrate by CO2 injection (CH4-CO2 exchange)

The global warming and energy crisis are two big problems that the whole world is dealing with. The new technologies are developing in order to reduce the global warming and to increase the energy production from unconventional energy sources. Methane hydrate as unconventional source of energy has gained much fame in recent years because conventional gas reserves are dwindling day by day due to their massive use. For the purpose of methane hydrate production an alternative technology has been developed by injecting CO2 called 'CO2 sequestration'. CO2 sequestration means to capture the atmospheric carbon dioxide before it releases in atmosphere which is responsible for global warming from its source point, to transport at its storage site, safe and long term storage of carbon dioxide into deep underground rock formations and monitoring of stored CO2. This process is also known as carbon capture, storage & transport (CCS).

The above proposed conventional production methods in section 1.6.1, dissociates in-situ methane hydrate & releases significant amount of water which may cause geomechanical stresses on reservoir that could lead to decrement. A novel technology has been introduced for methane production by replacing in-situ CH4 with injected CO2. The idea of accessing methane present in the form of hydrate by introducing a thermodynamically more stable hydrate was first time introduced by Japanese researchers. This strategy towards production of methane from in-situ methane hydrate by injecting CO2 (greenhouse gas) is beneficial, resulting in increased methane recovery while CO2 being trapped underground. This innovative method has several advantages over other conventional methods,

a) Injection of CO2 into in-situ gas hydrate reservoir forms CO2 hydrate which is thermodynamically more stable than CH4 hydrate under low temperature conditions, below 283 K, because the equilibrium pressure for CO2 is lower than that of CH4 hydrate (Seo et.al, 2001).

b) Heat released from formation of CO2 hydrate is higher than the heat of dissociation of CH4 hydrate.

c) During the CH4-CO2 exchange production method the mechanical stability of the hydrate bearing formation was maintained.

d) Reducing anthropogenic CO2 in atmosphere and simultaneously releasing natural gas (Khaled et.al, 2014).

Injection of carbon dioxide into in-situ methane hydrate will lead to conversion of the methane hydrate into CO2 dominated CO2 hydrate or mixed CO2-CH4 hydrate in which CO2 fills the large cavities. This conversion process is governed by two principal mechanisms; first mechanism involves the formation of new hydrate and second direct solid state exchange. These two mechanisms are discussed in detail in section 2.
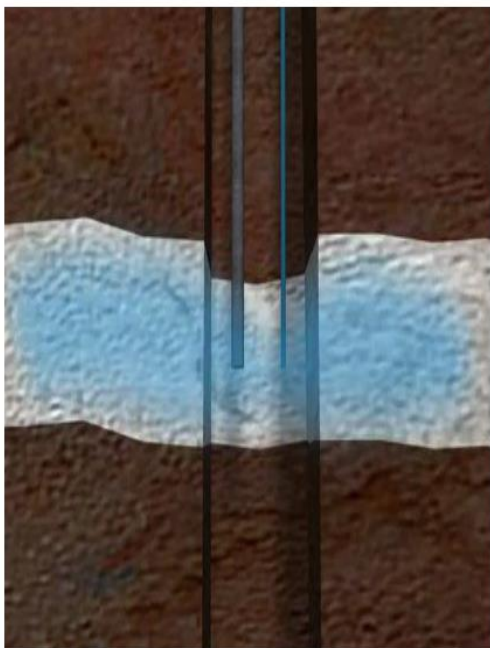
Figure 7: Injection of CO2 into well (Blue stream) (Khamneh et.al, 2012).
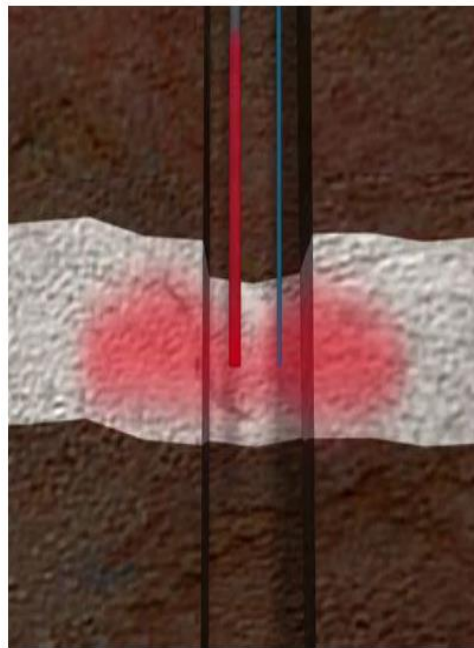
Figure 8: Released methane from hydrate (Red stream) (Khamneh et.al, 2012).

Methane production by injecting CO2 & N2 mixture into hydrate bearing zone has been successfully applied at the U.S department of energy on Ignik Sikumi #1 well located on the North Slope of Alaska. Since 2003 ConocoPhillips has been conducting laboratory experimentation with the University of Bergen, Norway in hopes of developing commercially viable technology to produce natural gas from hydrates. Ignik Sikumi #1 a project with U.S Department of Energy and Japan Oil, Gas & Metals National Corporation (JOGMEC) is the first experiment of this production technology outside the laboratory. In 2010-2011 Ignik Sikumi #1 gas hydrate test well drilled and logged in order to study the efficiency of CO2/CH4 exchange at the Prudhoe Bay area on the North Slope of Alaska and in winter 2011-2012 the gas hydrate production testing was carried out. The representative East-West structural cross section is illustrated in figure 9 below.
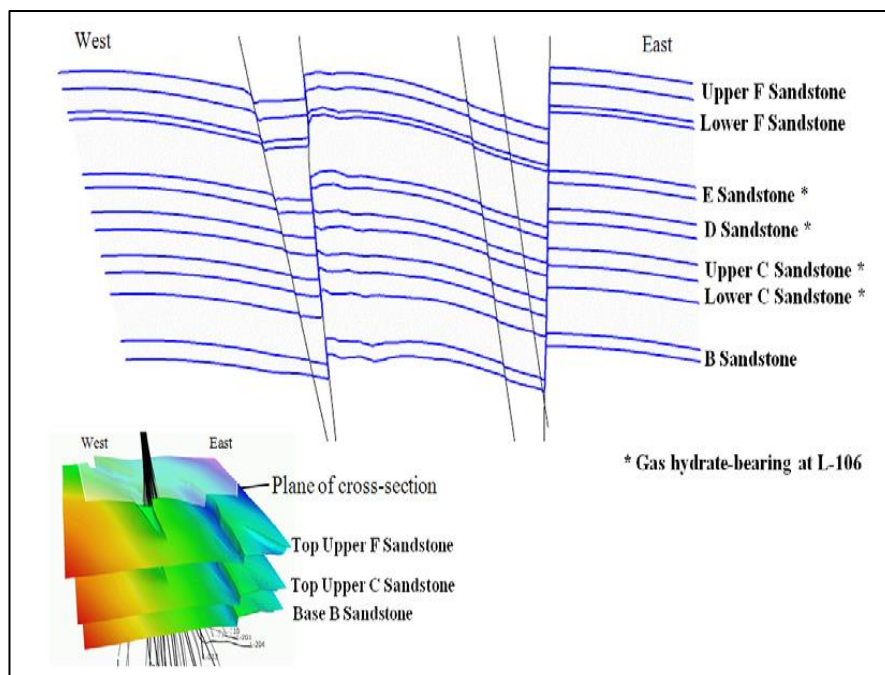
Figure 9: East-west-oriented structural cross-section across the framework model (Schoderbek et.al, 2013).

In above figure 9, the plane cross section in left corner is 16,000 feet x 16,000 feet in plane projection. Minimum depth in the model is 1136 feet and maximum depth is 3025 feet. Thickness of the formation is 1,045 feet from the top of the Upper F sandstone to the base of the B sandstone. In above figure 9; zone D, zone E, upper and lower C zone are the gas hydrate bearing sandstones. According to (Schoderbek et.al, 2013) the permeability in the hydrate bearing sandstone corresponds to 1 mDarcy or less, depending on TIMUR & SDR methods. In above figure 9, zone B & zone F are liquid water bearing sandstone having permeability greater than 1 Darcy.

In this test program 167.3 Mscf of Nitrogen and 48.6 Mscf CO_2 i.e. 77.5% N_2 and 22.5% CO_2 was injected. In the following figure 10, the average injection rates over the injection period have been plotted for the Ignik Sikumi #1 pilot test. This production test was carried out using a "huff and puff" injection/production cycle from a single well to demonstrate the CO_2/CH_4 exchange concept at larger scale.
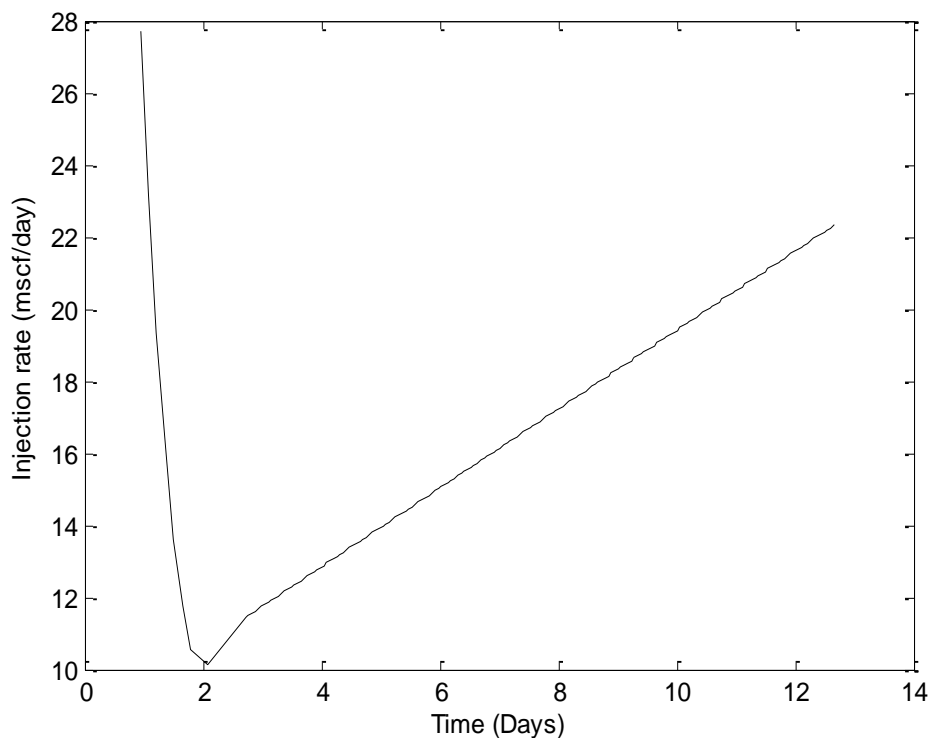
Figure 10: Average injection rates for the Iġnik Sikumi pilot test for CO2/N2 based production of CH4 from in situ hydrate (Kvamme, 2015b).

During this production test ≈ 210,000 standard cubic feet mixture of CO2 & N2 was injected in hydrate bearing portion of the well. It was observed that approximately 70% injected nitrogen and 40% CO2 was recovered among the total injected quantity. In short period of 12 days, over 855 Mscf of methane in total was produced throughout the total production period during this test program.

Figure 11, summarizes the important well logging data for upper C hydrate bearing zone which is thick, homogeneous, and clean with uniform hydrate saturation. Hydrate bearing zones are identified by high resistivity values, high velocities, and low NMR porosities in column number 4, 5 & 6 respectively.
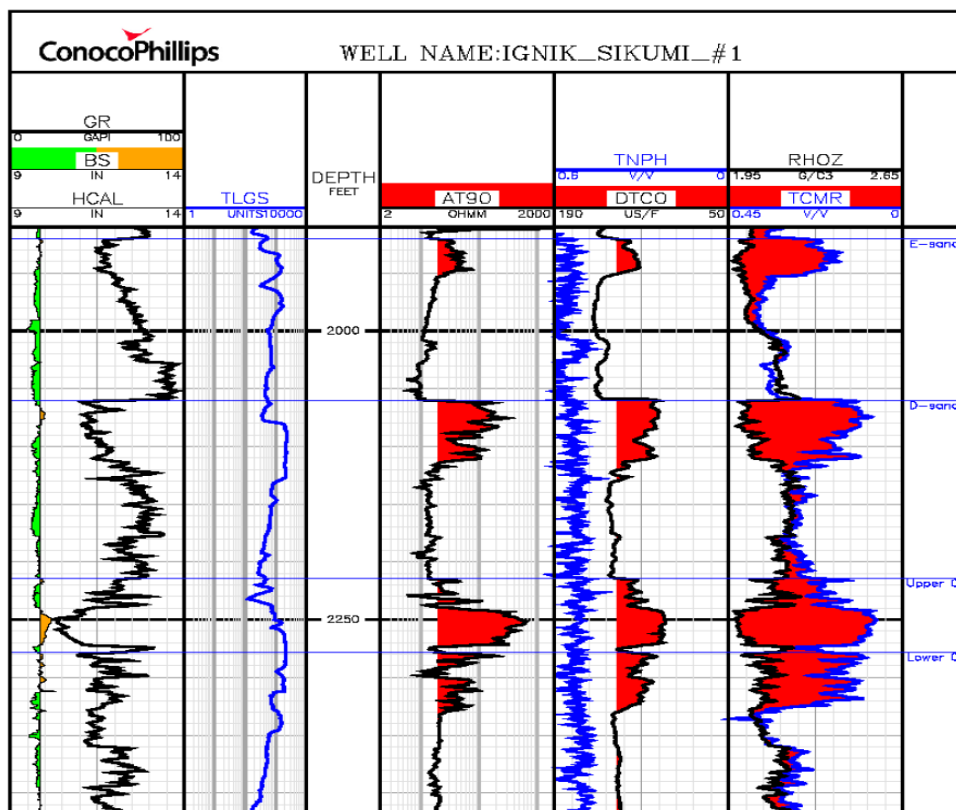
Figure 11: Ignik Sikumi Log responses with hydrate-bearing intervals (Schoderbek et.al, 2013).

Well log results obtained for this method are used for the calculation of hydrate saturation in the upper C zone. According to NMR and Archie's method the average hydrate saturation in the upper C zone is approximately 75% of available pore volume, ten percent pore bounded water and remaining is free water. More details on production can be seen in the report by (Schoderbek et.al, 2013).

2. Definition of Project and Choice of Scientific Methods

This section proves a detailed overview of this master thesis.

Injection of CO_2 into hydrate bearing reservoirs is an interesting, advanced method for methane hydrate production. In this method the conversion of in-situ methane hydrate into CO_2 dominated CO_2 hydrate (Kvamme et.al, 2007) or CO-CH_4 mixed hydrate takes place (Khuram et.al, 2014a). Injected CO_2 into in-situ methane hydrate replaces the CH_4 molecules from the hydrate lattice and serves a dual purpose of both producing natural gas from hydrates and safe, long term storage of CO_2. Theoretical and experimental studies indicate that this method of conversion of in-situ methane hydrate into new solid CO_2-hydrate or mixed CO_2-CH_4 hydrate is based on two primary mechanisms (Khuram et.al, 2014a., Kvamme et.al, 2014f). First mechanism, injected CO_2 reacts with residual water in the porous media and forms new CO_2 dominated hydrate. The reaction is exothermic and heat released in this process dissociates the surrounding methane hydrate. Then the water generated in this methane hydrate will form additional CO_2 hydrate. This is because of heat generated from hydrate formation is greater than the heat required to dissociate CH_4 hydrate. This mechanism of formation of new CO_2 hydrate from injected CO_2 is dominating and faster as compare to direct solid state exchange mechanism. The second mechanism is solid state exchange. In this mechanism the direct conversion of CH_4 hydrate over CO_2 hydrate (Kvamme et.al, 2007) or CO_2-CH_4 mixed hydrate take place and dominates when there is no sufficient free water available. This mechanism will be slow since it is kinetically controlled by solid state mass transport through the hydrate.

This method of methane hydrate production using CO_2 is practically challenging because density of CO_2 at the time of injection is high and relatively lower permeability of injected CO_2 at relevant conditions, especially when the in-situ methane hydrate saturation is high. As soon as the CO_2 injects into the in-situ methane hydrate reservoir, there will be rapid formation of new CO_2-hydrate which reduces the available pore volume for flow and also reduces the injectivity and permeability of CO_2 (Kvamme, 2015a). In order to mitigate these problems nitrogen will be injected along with CO_2 into the hydrate which has an advantage of higher gas permeability. Addition of nitrogen to CO_2 reduces the thermodynamic driving force for the formation of new hydrate and consequently flow permeability increases as the nitrogen content increases in the mixture (Kvamme, 2015a). Adding N_2 to CO_2 also reduces the risk for blocking the flow path through reservoir due to reduced formation of new hydrate from CO_2/N_2 mixture. This is one of the reasons for the increased research effort on using carbon dioxide with nitrogen.

This exchange process includes replacing of CH_4 molecules from in-situ methane hydrate by injected CO_2 molecules shown in figure 12. The following figure 12, indicate that the injected CO_2 replaces CH_4 molecules present in the large cavities only.
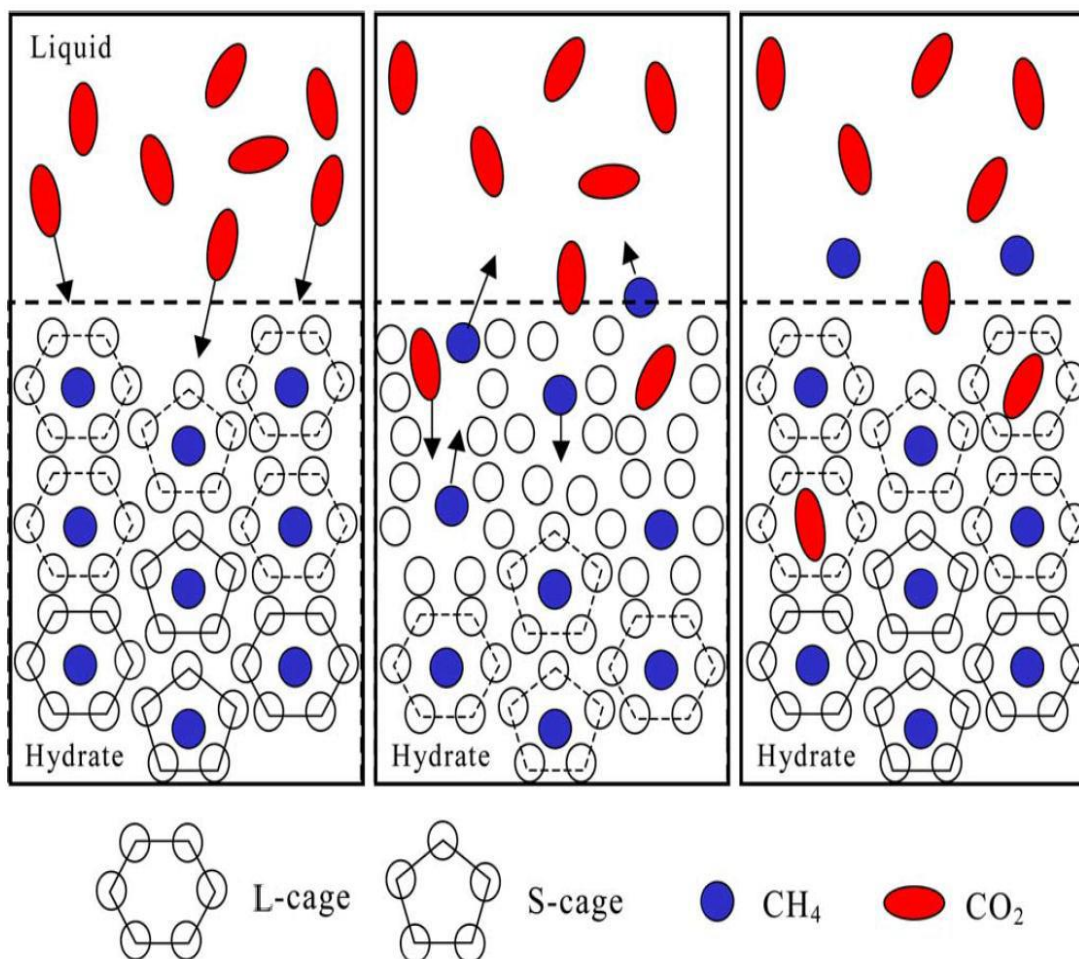
Figure 12: Illustration of CO2 replacing methane as guest molecule in structure I bulk hydrate. CO2 is only replacing methane in large cages (Christian, 2013).

Newly formed CO2-hydrate or mixed CO2-CH4 hydrate from injected CO2/N2 mixtures and liquid water, under suitable hydrate forming temperature-pressure conditions in the reservoir is generally assumed to be stable and blocks the flow paths of fluids in the region where it is formed. In some limits this could be practically true, but according to Gibbs phase rule hydrates formed in sediments are thermodynamically unable to reach equilibrium. Even though the new hydrate formed under suitable T-P stability zone, the hydrate may be unstable with respect to different concentration of all components entering the hydrate in all co-existing phases (Khaled et.al, 2014). In the non-equilibrium situation, hydrate formed from different phases will have different free energies since the chemical potential of all the guest molecules will be different. Thus the study is based on free energy analysis. The estimation of chemical potential for different phases is based on molecular simulations by (Kvamme & Tanaka, 1995) & SRK equation of state has been used.

In equilibrium situation the classical way to solve for equilibrium is to solve simultaneously the conditions for equilibrium, mass-conservation, and energy-conservation. In a non-equilibrium situation the equilibrium conditions will be replaced by the combined 1st and 2nd

law of thermodynamics through some schemes for minimizing free energy locally under constraints of mass- and energy-conservation. Phase field theory (PFT) (Kvamme et.al, 2014f) is one example which require free energies for each phase, interphase free energies a barrier for each phase transition corresponding to the work need to push away initial phase. In this work we use an easier and more feasible approach in which we discretely evaluate some of the possible changes from injection of pure CO2 over to mixtures of CO2 and N2. In order to be able to compare phase transitions and levels of chemical potentials of the different components in different phases, all thermodynamic data are based on absolute thermodynamics often called residual thermodynamics (ideal gas as reference). The analysis is based on a classical thermodynamic approach.

The primary focus of this thesis is,

1. Theoretical study of GH bearing fields.
2. Estimation of hydrate stability limits in terms of chemical potential for different mixtures of CO2 & N2 at varying pressure and temperature relevant for each specific field.
3. Calculation of maximum permissible water content in gas streams supplying gas and produced gas.

3. Thermodynamics

This chapter gives a detailed overview of the thermodynamic functions required for the calculation of chemical potentials in different phases. In this project Residual thermodynamics (ideal gas phase as reference) is applied for all components in all phases as a basis for free energy analysis of hydrate stability. Residual thermodynamics is denoted by R and is a thermodynamic deviation from the ideal gas behavior.

3.1 Fluid Thermodynamics

Formally, a thermodynamic equilibrium is achieved when the temperature, pressure and chemical potentials of all co-existing phases are uniform across all phase boundaries i.e. in simple words we can say that the system can reach equilibrium when,

$$T^{(I)} = T^{(II)} = T \qquad \text{Thermal Equilibrium} \qquad (1)$$

$$P^{(I)} = P^{(II)} = P \qquad \text{Newton's law, Mechanical Equilibrium} \qquad (2)$$

$$\mu^{(I)} = \mu^{(II)} = \mu \qquad \text{Chemical Equilibrium} \qquad (3)$$

In equation (1), (2) & (3) superscript I, II indicates phase number. To insure the same reference values for free energy of all phases, the calculation of chemical potential of all components in the different phases should use ideal gas as reference state. The combined first and second law of thermodynamics (minimum free energy) (Kvamme, 2014b) can be expressed as,

$$dU \leq T.dS - P.dV + \sum_{i=1}^{n} \mu_i.\, dN_i \qquad (4)$$

Here summation is done over all present phases, i=1, 2, 3……n. S is entropy. N is the number of particles of particular compound & μ is chemical potential.

$$d\mu_i = RTdlnf_i \qquad (5)$$

With ideal gas as a reference state, limits of equation (5) as,

$$\lim (f_i) = y_i.P \qquad \text{.......when } P \to 0$$

$$\&$$

$$\mu_i(T,P,\vec{y}) - \mu_i^{\text{ideal gas}}(T,P,\vec{y}) = RT\ln f_i(T,P,\vec{y}) \tag{6}$$

Where f_i is fugacity coefficient for component in the given phase and

$$\lim (f_i) \rightarrow 1.0 \quad \dots \text{for ideal gas}$$

Here as an intermediate state, one more reference state for the chemical potential of component i in a liquid phase is also considered,

$$\mu_i(T,P,\vec{x}) - \mu_i^{\text{ideal liquid}}(T,P,\vec{x}) = RT\ln \gamma_i(T,P,\vec{x}) \tag{7}$$

In equation (6) & (7); y and x are mole fractions of gas & liquid respectively. γ_i is activity coefficient for component i in the liquid mixture and limits of γ_i can be expressed as,

$$\lim \gamma_i = 1.0 \text{ when } x_i \rightarrow 1.0$$

From above equation (7), it is seen that the chemical potential of a species in ideal solution is lower than the chemical potential of pure component.

Equation (6), (7) and much of the data in this section 3.1 are found in (kvamme, 2015a).

$$Q^{1D} \approx \int \left[\exp(-\beta\Gamma_{smooth}(z)) - 1 \right] dz \tag{8}$$

Where β = inverse of Boltzmann constant times temperature

Q = configurational part of the canonical partition function

z = distance from the surface.

The above equation applied to water, is based on absolute thermodynamics when chemical potential of pure water is calculated from models using molecular simulations. More specifically the data has been used from (Kvamme & Tanaka, 1995).

SRK (Soave-Redlich-Kwong) EOS

The most applied Equation of State in Oil and Gas Industry is SRK (Mingjian et.al, 2007),

$$P = \frac{RT}{v-b} - \frac{a(T)}{v(v+b)}$$ (9)

$$a(T) = a_c \alpha(T)$$

$$a_c = 0.42747 \frac{R_c^2\, T_c^2}{P_c}$$

$$a(T) = 1 + (0.480 + 1.574\omega + 0.176\omega^2)(1 - T_r^{0.5})$$

$$b = 0.08664 \frac{R\, T_c}{P_c}$$

Where,   v = molar volume

R = Ideal gas constant (8.314 J/mole.K)

b = excluded molecule volume

T_c = absolute temperature at critical point

P_c = pressure at the critical point

ω = acentric factor

a = specific constant

α(T) is added so that SRK reproduces pure component vapor pressure.

3.2 Water Thermodynamics

When equation (6) applied for water, the chemical potential of pure water has been calculated from models using molecular simulations. The data used here is from Kvamme and Tanaka (Kvamme & Tanaka, 1995).

a) Symmetric Excess

Chemical potential of component i in water phase,

$$\mu_i^{H2O} = \mu_i^{ideal\ liquid} + RT\ln\left[X_i.\Upsilon_i^{H2O}(T,P,\vec{x})\right] \qquad (10)$$

Where $\Upsilon_i \rightarrow 1.0$

$x_i \rightarrow 1.0$

b) Asymmetric Excess

When chemical potential of component i in aqueous phase uses asymmetric excess/non-symmetric convention as a reference state which is useful for gases with low solubility in water,

$$\mu_i^{H2O}(T,P,\vec{x}) = \mu_i^{\infty}(T,P,\vec{x}) + RT\ln\left[x_i.\,\Upsilon_i^{\infty}(T,P,\vec{x})\right] \qquad (11)$$

$$\lim \Upsilon_i^{\infty} \rightarrow 1.0\ ;\ x_i \rightarrow 0$$

In above equation (11) superscript ∞ denotes the chemical potential of i in water at infinite dilution. Υ_i^{∞} is the activity coefficient of component i in aq. phase. The limit of activity coefficient approaches to unit as mole fraction becomes zero. Here to estimate the absolute values of chemical potentials at infinite dilution the molecular dynamics simulation & Gibbs-Duhem relation (Kvamme et.al, 2014c., Kvamme et.al, 2014d) is used which describes the relationship between changes in a thermodynamic system.

The bulk of the actual pressure and temperature range corresponds to a liquid state for all the phases except the hydrate. The brief discussion on hydrate phase can be read in (Kvamme et.al, 2013a).

In this work the solubility of H2O in CO2/N2 considered is very low. So in this case the following approximation of infinite dilution should prove sufficiently accurate for CO2 with small amount of N2.

$$\mu_{i,j}(T,P,\vec{x}) \approx \mu_{i,j}^{\infty}(T,P) + RT\ln\left[X_{i,j}\,\Upsilon_{i,j}^{\infty}(T,P,\vec{x})\right] \qquad (12)$$

Where subscript j denotes the component & i denotes the phase. Much of the data in section 3.2 is taken from (Kvamme, 2013b).

3.3 Hydrate Thermodynamics

The chemical potential of water in hydrate is expressed as follows. This equation is obtained by applying statistical mechanical model for water in hydrate (Kvamme & Tanaka, 1995). This equation is based on adsorption theory,

$$\mu_w^H = \mu_w^{0,H} - \sum_{k=1,2} RTV_k \ln(1+\sum_i h_{ik}) \tag{13}$$

Where, H refers to hydrate phase.

μ_w^H = Chemical potential of water in hydrate

$\mu_w^{0,H}$ = Chemical potential of water in empty hydrate (no filling in any cavity)

V_k = Fraction of cavity type k per water.

The unit cell of structure 1 consists of 46 water molecules (12.01 Å cubic box). It has two small and six large cavities (Sloan & Koh, 2007).

For large Cavity $V_1 = 6/46 = 3/23$
For small cavity $V_2 = 2/46 = 1/23$

In above equation (13) the cavity partition functions are integrated under the assumption that the water molecules are fixed and normally also neglecting interaction with surrounding molecule. For a molecule like methane won't have a significant effect on water movements. On other hand CO_2 will change chemical potential by roughly ≈ 1 KJ/mole at 0 °C when compared to the assumption of undisturbed fixed water molecules (Kvamme et.al, 2014e).

The canonical partition function for a k cavity type containing a guest molecule of type i is given by,

$$h_{ik} = e^{\beta} (\mu_i^H - \Delta g_{ik}^{inc}) \tag{14}$$

$\beta = 1/RT$ ….in molar units

Where ß is the inverse of gas constant times temperature and Δg_{ik}^{inc} = impact on hydrate water from the inclusion of the guest molecule i in the cavity i.e. free energy change of putting the molecule inside the cavity k (Kvamme & Tanaka, 1995).

3.4 Equilibrium Thermodynamics of Hydrate

At equilibrium chemical potential of i in hydrate has to be identical to chemical potential of molecule i in the phase it has been extracted from (Chemical potential of dissolved CO2 or CH4 for the case of hydrate formation from aqueous solution) (Kvamme et.al, 2014e).

Now the hydrate content of all gas components can be estimated by applying equation (6) to calculate their chemical potential when dissolved in the gas (here methane) phase. Water will totally dominate the dew point. The hydrate formation in case of liquid water drop out can be obtained by applying equation below (Kvamme et.al, 2015b).

$$\mu_w^{0,H} - \sum_{k=1,2} RT\ V_k\ \ln(1+\textstyle\sum_i h_{ik}) = \mu_{i,H2O}^{pure\ water}(T,P) + RT\ln\left[x_{i,H2O}\ \Upsilon_{i,H2O}(T,P,\vec{x})\right] \qquad (15)$$

The chemical potential of empty hydrate structure estimated based on (model based on Kvamme & Tanaka, 1995). The free energy change related to a hydrate phase transition ΔG^H, can be written as equation (16).

$$\Delta G^H = d \sum_{i=1}^{n^H} x_i^H(\mu_i^H - \mu_i^p) \qquad (16)$$

In above equation (16), H represents hydrate phase & p represents parent phase of molecule i.

The non-equilibrium description of hydrate by (Kvamme et.al, 2013a) can be applied for this purpose to follow free energy gradients until the CO2/N2 phase has been mostly depleted in the most aggressive hydrate former CO2.

The relation between the filling fraction, the mole fractions & cavity partition function is given by equation (17),

$$\theta ik = \frac{x_{i,k}^H}{vk(1-XT)} = \frac{hik}{1+\sum_i hik} \qquad (17)$$

Where x_T = total mole fraction of all guests in the hydrate
θ_{ik} = Filling fraction of component in cavity type k
$x_{ik}{}^H$ = Mole fraction of component i in cavity type k.

4. Theoretical Case Studies

In this section, a selection of the hydrate bearing reservoir fields has been studied with respect to physical properties mainly temperature, pressure conditions in order to estimate the hydrate stability limits for mixtures of CO2 & N2 in terms of chemical potentials. This section also provides some of the details on different experiments performed by different groups on gas hydrate field production.

Seismic data provides us most accurate graphic representation of particular portion of the Earth's surface geologic structure i.e. seismic data provides information about physical properties such as depth, temperature, pressure, geothermal gradient in hydrate bearing layers but we need concentration dependency for stability which is more important. For the stability analyses and in order to produce gas safely from hydrate bearing sediments, the accurate data about physical properties of hydrate bearing sediments are required. For this purpose the physical properties of hydrate bearing units in different fields; in this thesis Eileen area on the North Slope of Alaska, USA., Mallik field, Canada & MITI Nankai Trough, Japan and Bjørnøya Basin in Barents Sea has been studied.

4.1 Eileen Area on the North Slope of Alaska

The main body of this section describes the known and inferred gas hydrate accumulations in the Prudhoe Bay region. GH reservoirs occur within and below the ice-bearing permafrost on the Alaska North Slope because the gas hydrate stability zone includes temperatures that are below and above the freezing point of water.

4.1.1 Occurrences of Methane Hydrate on the North Slope of Alaska

Almost 40 years of GH research in northern Alaska has confirmed the occurrences of at least two large gas hydrate accumulations. Interest in hydrates as a potential energy source has been enhanced further by reports of feasible gas production from hydrates (Makogon & Sayakhov, 1988). The occurrence of NGHs on the North Slope of Alaska was confirmed in 1972 when ARCO\Exxon well were successful in recovering the first sample of a NGH in a solid state (Kvenvolden & McMenamin, 1980). This sample was obtained from the depth of 666 m. The well was drilled with cool drilling muds in an attempt to reduce thawing of the permafrost and decomposition of the GHs.
A methane hydrate sample was recovered in pressurized core barrel. This study of pressurized core barrel confirms the presence of gas in hydrate state. The well logging data from Prudhoe Bay field in northern Alaska confirms the existence of gas hydrates at depth of 210 m to 1100 m (Kvenvolden & McMenamin, 1980). A previous study shows that the hydrates would be stable on northern Alaska for depths up to 1200 m (Katz, 1971). GHs exist under a limited range of temperature and pressure conditions. Well logging data from Eileen State-2 well (shown in the following figure) gives another evidence for existence of gas hydrate.
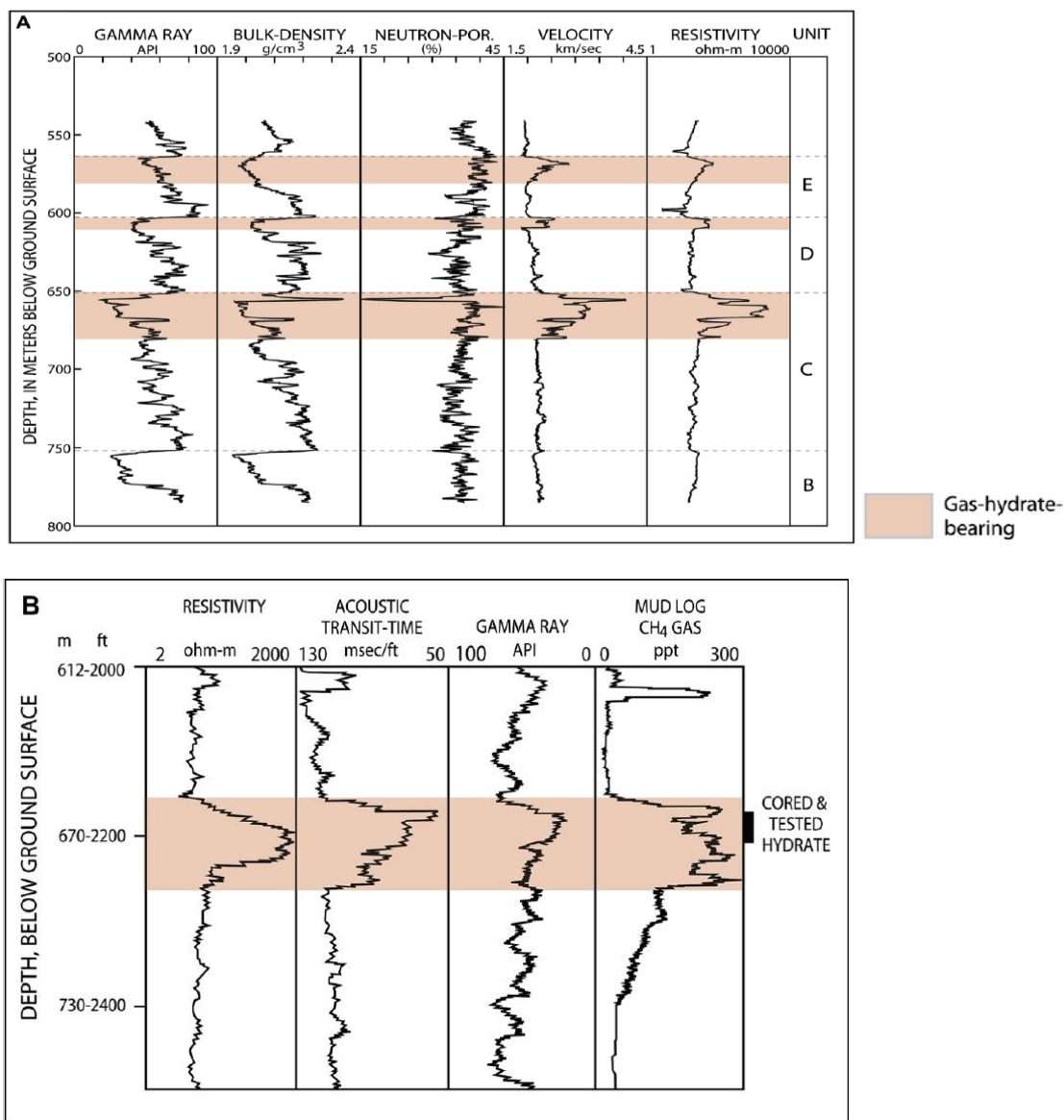
Figure 13: (A) Downhole logs from the Northwest Eileen State-2 well depicting the depth of units B, C, D, and E. (B) Insert of well logs from the cored (664–667 m) gas hydrate interval (unit C) in the Northwest Eileen State-2 well (Collett et.al, 2009).

Well logging data indicates the presence of hydrate zone due to the hydrate bearing sediments has a relatively high resistivity as shown in above figure 13. Spontaneous potential (SP) curves show very little deflection in hydrate zones in comparison with deflections in free-gas and free-water zones. Sonic log shows high acoustic velocity. In combination with the resistivity log & sonic log, mud logs as well pointed out the presence of hydrates in this area (Kvenvolden & McMenamin, 1980).

Studies of pressurized core samples, downhole well logging data, and the results of formation production testing have confirmed the presence of three gas hydrate bearing stratigraphic units in the Northwest Eileen State-2 well. In Kuparuk oil field, GHs are present in about four to six laterally continuous units that can be delineated in cross section. These six gas hydrate-bearing sedimentary units in the Eileen accumulation have each been assigned by a reference letters A to F, as shown in the following figure 14.
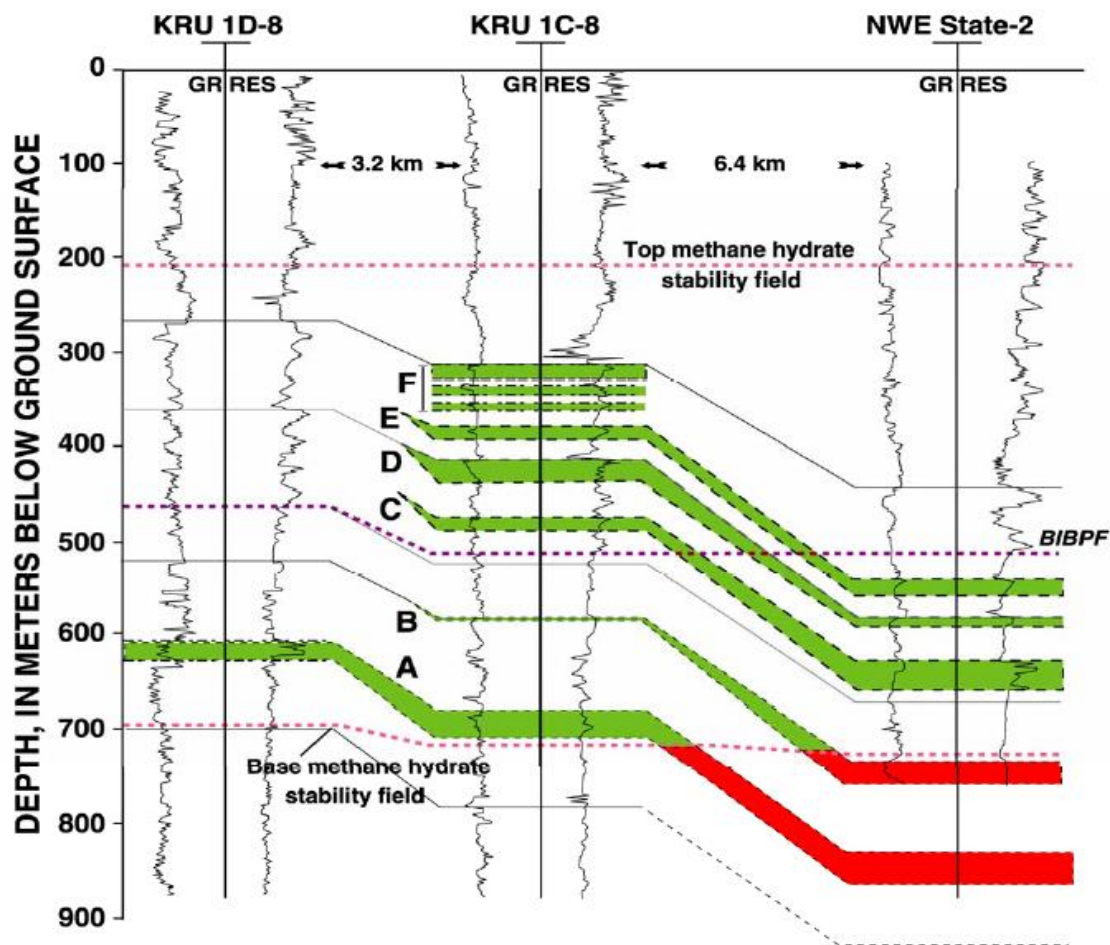
Figure 14: Cross section showing lateral and vertical extent of gas hydrates and underlying free-gas occurrences in Prudhoe Bay-Kuparuk River area. Gas-hydrate-bearing units are identified with reference letters A through F. Gamma-ray (GR) and resistivity (RES) logs are shown for three wells (Collett, 1993b).

The recognized GHs appear to be laterally continuous and extensive; these widespread distributions of in-situ GHs on the North Slope suggest that they may be an unconventional source of natural gas. The main focus of this section is to evaluate the geological and geophysical data that aid in the delineation of hydrate prospects.

The volume of gas that may be contained in a gas hydrate accumulation depends on five primary reservoir parameters (parameters modified from Collett, 1993b),

(1) Areal extent of the GH occurrence
(2) Reservoir thickness
(3) Sediment porosity
(4) Degree of GH saturation
(5) Volume of Gas within hydrate.

1. Areal Extent of the GH Occurrence – Well logging data confirms the existence of GHs on the North Slope of Alaska at the depth of 210 m to 1100 m.

2. Reservoir Thickness or Area – The total mapped area of all six gas hydrate units in the Eileen accumulation is about 1643 km^2, the areal extent of the individual units range from 3 km^2 to 404 km^2**.**

3. Porosity – The density log derived sedimentary porosities for the three gas hydrate bearing units in the Eileen area average about 36% to 39%.

4. Gas Hydrate Saturation – The average value of gas hydrate saturation in the three hydrate bearing units (Unit C, D, E) ranges from about 33% to 61%. These values are estimated from the available downhole log data. Thicknesses of individual zones are listed in Table 3 below.

5. Volume of Gas within Hydrate – The volume of the gas within the Eileen gas hydrate accumulation is estimated about the twice the volume of known conventional gas in the Prudhoe Bay Field (Collett, 1993b), range between 1.1 to 1.2 trillion cubic meter (at STP) (Collett, 2009). Total volume of gas within hydrate for Northwest Eileen State-2 well corresponds to 2 to 1,511,216,069 Km^2 (m^3).

Some of the other properties are as follows,

6. Biogenic or Thermogenic Sources – The hydrocarbon gas available for hydrate formation is basically from either bacterial decay of organic rich sediments or thermogenic sources. Generally biogenic gas is generated at shallow depths compared to thermogenic gas (below 1000 m). The molecular and isotopic analysis indicates the occurrence of methane in gas hydrates at northern Alaska is of thermal origin.

7. Salinity – The presence of salts such as NaCl in gas hydrate system lowers the hydrate formation temperature. The results from 55 analyses of pore waters from the North Slope region collected between depths of 400 m to 2000 m indicate salinity vary from 0.5 to 19.0 parts per thousand (ppt) with no marked correlation between depth and salinity. For the calculation of GHSZ in northern Alaska (Collett et.al, 2009) the pore-water salinity of 5.00 ppt has been assumed.

8. Geothermal Gradient & Permafrost Thickness – The geothermal gradient needed for the prediction of depth of hydrate stability is not easily obtained, especially when hydrate bearing permafrost is present. After evaluating logs from 125 wells on the North Slope, it was determined that in order to have an intersection between the methane hydrate stability curve and a geothermal gradient, the projected gradient within the ice-bearing permafrost must be equal to or less than 4.32 °C/100 m (Collett, 1983). Values in the ice-bearing permafrost vary from ≈1.5 °C/100 m in the Prudhoe Bay area to ≈ 4.5 °C/100 m in the east-central portion of the National Petroleum Reserve in Alaska. Geothermal gradients below the ice-bearing permafrost sequence range from ~ 1.6 °C/100 m to ~ 5.2 °C/100 m. Much of the analysis depends on interpretation of this gradient change. In the phase diagram (figure 15) obtained from the Northwest Eileen State-2 well, mean annual temperature of ground surface -10 °C is assumed (Collett, 2002). Geothermal gradient above the base of ice bearing permafrost is 1.9 °C/100 m and below the base of permafrost 3.2 °C/100 m is considered for the calculations of temperature conditions (Collett & Kvenvolden, 1987).

9. Phase Diagram – The conditions necessary for formation and stability of GHs are controlled largely by temperature and pressure as shown in the constructed phase diagram. In figure 15, the previously calculated geothermal gradients below & above the base of permafrost has been plotted on a methane hydrate stability curve. The gas-hydrate phase diagram graphically demonstrates that the geothermal gradient has to be known before the limits of the GH stability field can be calculated. Earlier studies by (Lachenbruch et.al, 1982, Lachenbruch et.al, 1985) explained the methods for obtaining geothermal gradients and surface temperatures.
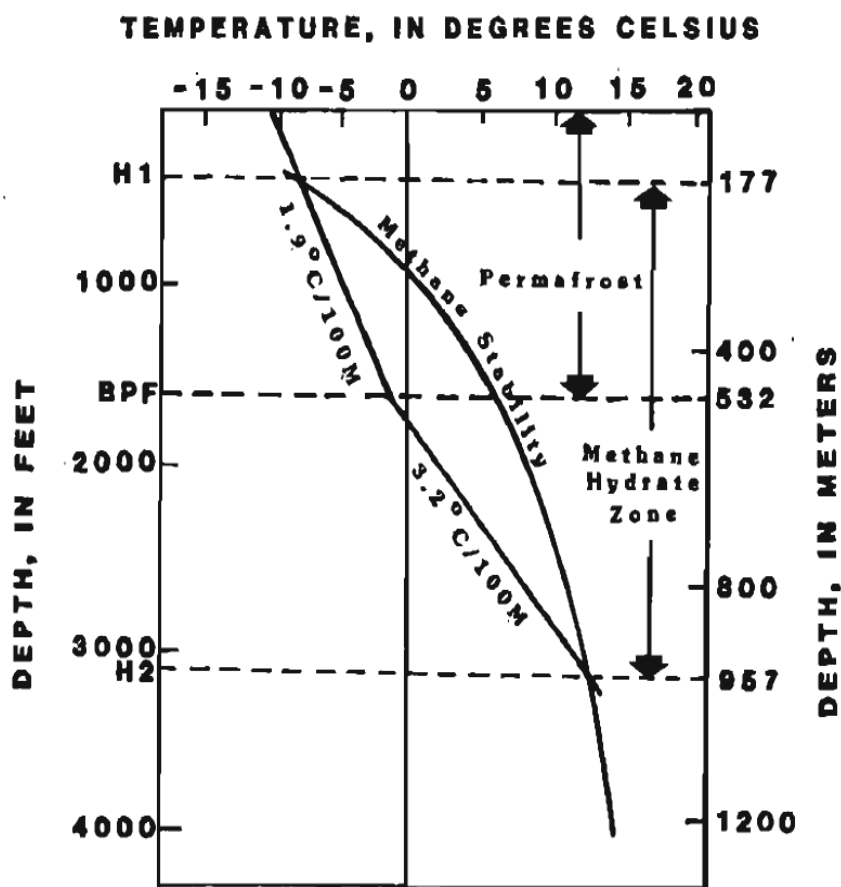
Figure 15: Gas hydrate phase diagram from the Northwest Eileen State-2 well (Collett & Kvenvolden, 1987).

The above phase diagram is constructed by considering hydrostatic pore-pressure gradient of 9.795 KPa/m (0.1 bar). The methane stability curve and the base of ice-bearing permafrost can be used to determine the depth and zone of potential methane hydrate stability. The phase diagram (figure 15) illustrates that the zone of potential gas hydrate stability in the Northwest Eileen State-2 well lies within the depths between two intersections of the geothermal gradient curve and hydrate stability curve.

10. Calculations of Temperature and Pressure Conditions –

The section 4.1 provides the depths and potential thicknesses of formations as a function of the permafrost thickness, geothermal gradient, pressure gradient, and ocean temperature in the Prudhoe Bay field on North Slope of Alaska. Here temperature range in the permafrost and below the base of permafrost is determined by multiplying depth by geothermal gradient and adding surface temperature. In a similar way the pressure range for hydrate bearing zones are calculated by multiplying pressure gradient by depth and adding surface pressure.

Field analysis provides,

Surface Temperature ≈ -10°C

Permafrost Thickness ≈ 532 m (±20 m)

Temperature at the base of permafrost i.e. at depth 550 m = (-0.1 °C)

Geothermal Gradient above the base of permafrost ≈ 1.9 °C/100 m

Geothermal Gradient below the base of permafrost ≈ 3.2 °C/100 m

Calculated temperature range for Unit C ≈ 3.15 °C to 4.17 °C

Calculated temperature range for Unit D ≈ 1.5 °C to 1.80 °C

Calculated temperature range for Unit E ≈ 0.35 °C to 0.89 °C

A hydrostatic pore-pressure gradient 9.795 KPa/m (0.1 bar) is generally assumed when calculating gas hydrate stability conditions in northern Alaska.

Calculated pressure range for Unit C ≈ 63.81 bar to 66.65 bar

Calculated pressure range for Unit D ≈ 59.03 bar to 59.69 bar

Calculated pressure range for Unit E ≈ 55.2 bar to 56.89 bar

Here temperature - pressure conditions required for stability evaluation has been calculated using geothermal gradient, pore-pressure gradient and depth profile. The hydrate stability limits in terms of chemical potential as a function of temperature with gradual decrease in CO_2 content in the mixture of CO_2 and N_2 for the log inferred hydrate region in the Northwest Eileen State-2 well and also for individual Units (Unit C, Unit D & Unit E) has been evaluated in Section 5.2. Temperature range assumed here for the hydrate stability evaluation ranges from 268 K to 288 K. The temperature - pressure profile with depth for separate hydrate bearing units is shown in figure 16 (schematic representation).

11. Schematic Representation –

The schematic of depth, temperature and pressure conditions calculated in three hydrate bearing units (Unit C, D & E) in Northwest Eileen State-2 well can be represented as in figure 16,
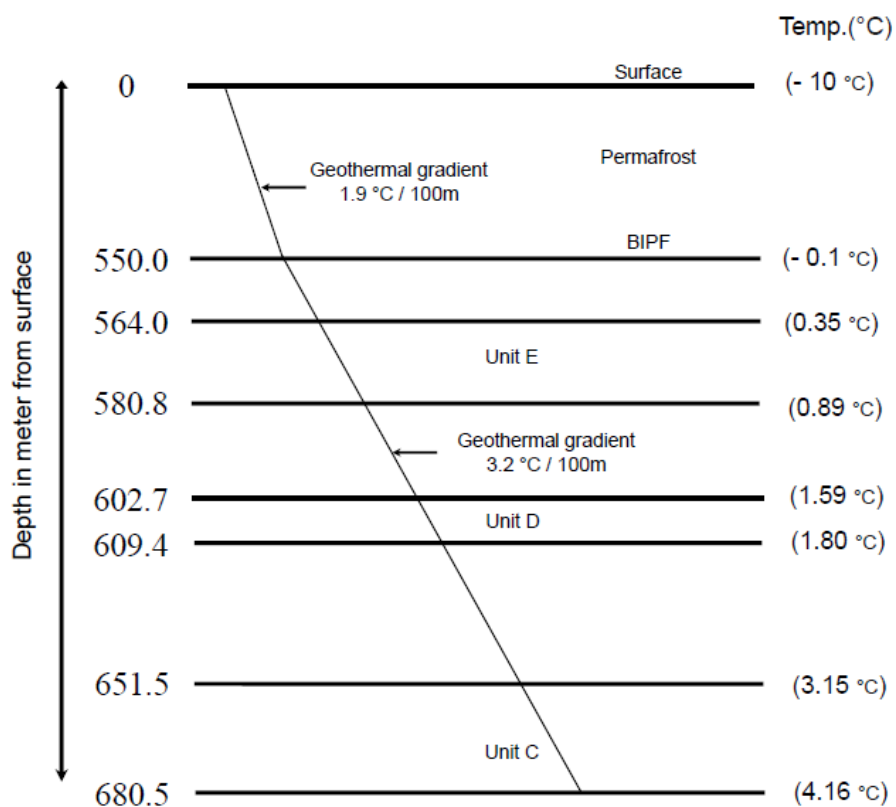
Figure 16: Schematic of depth, temperature, and pressure conditions in three hydrate bearing units (Unit C, D & E) in Northwest Eileen State-2 well (In figure BIPF refers to base of Ice-bearing permafrost) (Aruna Sapate).

In above figure the depth, calculated temperature-pressure conditions for the individual hydrate bearing units has been depicted. It is observed that the Unit C is thickest zone with average gas hydrate saturation 60.9%.

The physical properties of GH bearing sediments in the Eileen area can be summarized in table format as follows,

	Properties	Unit C	Unit D	Unit E
1	Depth of log-inferred GHs (m)	651.5 – 680.5	602.7 – 609.4	564.0 – 580.8
2	Thickness of hydrate bearing units (m)	29.0	6.7	16.8
3	Calculated temperature range (°C)	3.15 (276.3K) – 4.16 (277.2K)	1.5 (274.7K) – 1.80 (274.9K)	0.5 (273.5K) – 0.89 (274.04K)
4	Calculated pressure range (bar)	63.81 – 66.65	59.03 – 59.69	55.24 – 56.89
5	Average GH Saturation (%)	60.9	33.9	32.6
6	Salinity (ppt)	5	5	5
7	Average sediment porosity (%)	35.6	35.8	38.6
8	Saturation of pore bounded water (%)	-	-	-
9	Free water saturation	-	-	-
10	Biogenic\Thermogenic origin	Thermogenic	Thermogenic	Thermogenic
11	Volume of gas within hydrate per Km^2 (m^3)	1,030,904,796	133,382,462	346,928,811

Table 3: Geophysical properties of gas hydrate bearing units in Northwest Eileen State-2 well (data taken from Collett, 2002, Modified by Aruna Sapate).

Total volume of gas within hydrate for Northwest Eileen State-2 well corresponds to 1,511,216,069 Km^2 (m^3).

4.2 Mallik Field, Mackenzie River Delta, Canada

This section contains some important details on GHs inferred at Mallik L-38 well drill site. The Mallik methane hydrate field is located in the northern edge of Canada's Mackenzie Delta, Beaufort Sea, Canada. The location was chosen due to its high hydrate concentration. The Japan Petroleum Exploration Company (JAPEX)/Japan National Oil Corporation (JNOC), Geological survey of Canada (GOC) drilled a GH research well Mallik 2L in 1998 near the already existing Mallik L well which was drilled by Imperial Oil in 1972 (Bily & Dick, 1974). The Mallik 2L gas hydrate research well was designed to investigate the existence of naturally occurring GHs in the Mallik area of Mackenzie Delta River of Canada (Dallimore et.al, 1999). All of the inferred GHs occur within the clastic sandy sediments in Tertiary Kugmallit & Mackenzie Bay sequences.

4.2.1 Occurrences of GHs in Mallik Field

The well logging studies indicate that the Mallik L-38 drill site offers favorable logistics and has the thickest known GH accumulation in the region. Quantitative well log data and core studies confirmed the existence of ten gas hydrate bearing stratigraphic units within the depth interval of 810.1 m to 1102.3 m (Dallimore & Collett, 1998). In the Mallik L-38 well each of the hydrate bearing stratigraphic units contains substantial amount of energy. Till date Mallik site is one of the most concentrated GH reservoirs with pore space hydrate concentration exceeding 80%. In December 2001 to March 2002 under "The Mallik gas hydrate research well program" drilled three wells namely Mallik 3L-38, 4L-38 & production well 5L-38.The location of three wells drilled in this area is as shown in figure 17.
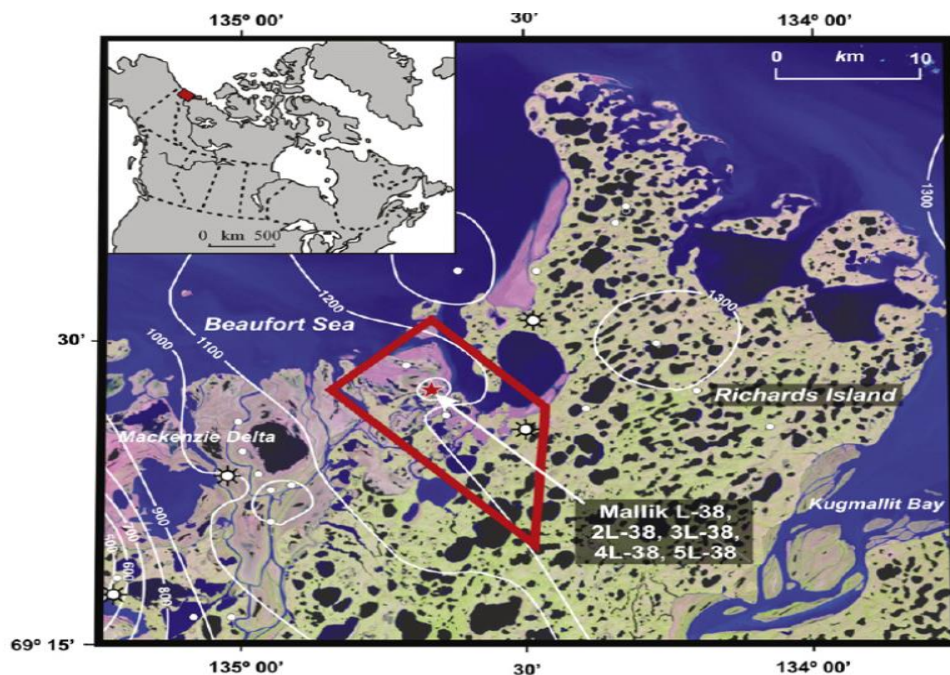
Figure 17: Map of the Mallik gas hydrate field, in the Mackenzie Delta, Northwest Territories, Canada (Collett, 2008).

The Mallik field is located onshore and first onshore production test was carried out at this Mallik site in the Mackenzie Delta in the Northwest Territories of Canada in 2002. The Mallik site has humid ground in summer and in winter the ground is found to be completely frozen. It is investigated that the permanently frozen ground (permafrost thickness) is found to a depth of approximately 640 m (Collett & Dallimore, 1998). Under these circumstances increase in pressure decreases the underground temperature and which provides a favorable conditions of high pressure and low temperature for the stability of methane hydrate at Mallik site.

As mentioned previously the drilling at Mallik site provides information about the existence of ten methane hydrate bearing stratigraphic units at the depth between 810.1 m to 1102.3 m, these hydrate bearing units and their respective thicknesses can be listed in table number 4.

Hydrate Unit	Depth from Ground Surface (m)	Thickness (m)
1	810.1 - 817.0	6.9
2	880 - 905.4	25.4
3	910.3 - 925.5	15.2
4	936.5 - 948.1	11.6
5	951.1 - 954.5	3.4
6	963.3 - 973.4	10.1
7	978.6 - 987.7	9.1
8	1003.2 - 1006.3	3.1
9	1066.9 - 1073.7	6.8
10	1082.2 - 1102.3	20.1
	Total thickness	= 111.4

Table 4: Depth and thickness of log inferred gas hydrate bearing stratigraphic units in the Mallik L-38 well (Data taken from Collett & Dallimore, 1998).

This analysis provides the detailed overview of GHs in the Mallik L-38 drill site. While drilling Mallik 3L-38 well, they placed great emphasis on core analysis. Approximately 37 m of core were recovered from the depth of 878 m to 944 m in the Mallik 2L-38 well. In this case GHs were observed in the pore spaces and several forms of visible gas hydrates in the unconsolidated sands & gravels (Dallimore et.al, 1999). Well logging data has been used to evaluate local geology, permafrost and gas hydrate conditions. In the upper 1500 m, three sequences has been identified namely Iperk sequence (0-350 m), the Mackenzie Bay sequence (350 m - 935 m) & Kugmallit sequence (935 m - bottom of hole) (Dixon et.al, 1992). The well log data from Mallik L-38 well exhibits both high electrical resistivities and high acoustic velocities as shown in column 4 & 5 respectively in figure 18. In total 25 well (17%) recognizes the existence of GHs in this area (Collett & Dallimore, 1998). All of these existed GHs occur in the clastic sedimentary rock sequences as mentioned previously i.e. Iperk sequence, Kugmallit sequence, & Mackenzie sequence.
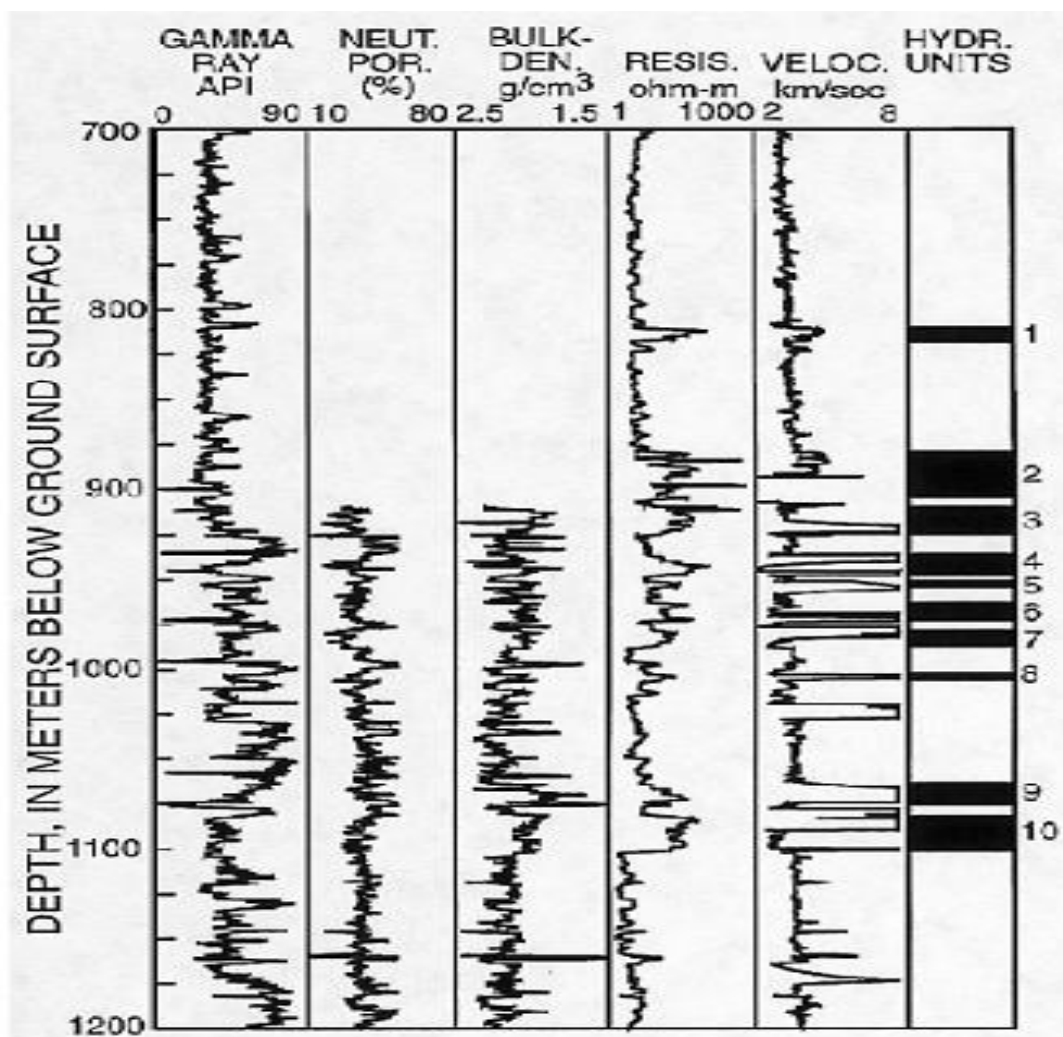
Figure 18: Downhole log data from the Mallik L-38 well. Data shown include the natural gamma ray log from the GR tool, neutron porosity data from SNP, bulk density data from FDC, deep reading electrical resistivity data from DIL & acoustic velocity data from BHC. On right hand side number indicates the depth of ten stratigraphic units (Collett & Dallimore, 1998).

The well log data indicates that the greatest concentration of GH is located within sand and gravel deposits between 897 m to 922 m. Hence open hole well logs reveal that the Mallik L-38 well drilled about 111 m of gas hydrate bearing strata within the depth interval from 810.1 m to 1102.3 m which is within the zone of predicted methane hydrate stability and below the base of ice bearing permafrost. Geochemical and isotopic determinations suggest that the methane hydrate observed in the core hole is biogenic (microbial) in origin (Dallimore & Collett, 1995).

1) Phase Diagram –

The conditions necessary for formation and stability of GHs are mainly controlled by some Physio-chemical properties such as temperature, pressure, gas chemistry etc. The major factors controlling the formation and stability of the inferred gas hydrates in the Mallik L-38 well site are represented in reconstructed phase diagram (Figure 19).
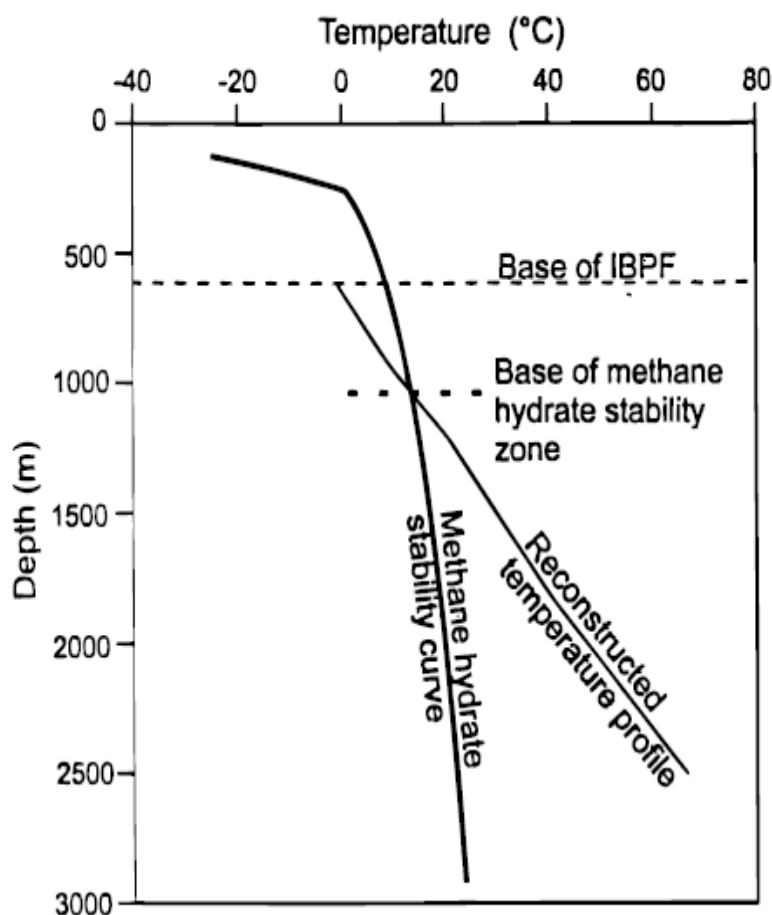
Figure 19: Reconstructed temperature – depth profile for Mallik L-38 site superimposed on methane hydrate stability curve. Methane hydrate stability field occurs to left of methane hydrate stability curve. (In figure BIPF refers to base of ice-bearing permafrost) (Majorowickz & Hannigan, 2000).

2) Permafrost Thickness –

Now days the Mackenzie Delta field has become an attractive centre for northern scientific research and hydrocarbon exploration. Both onshore and offshore drilling activities in 1970s provide knowledge about the presence of deep permafrost. Conventional logging studies acquired during the tentative drilling for oil & gas has been successfully accomplished to set up the depth of ice bearing permafrost (IBPF) i.e. permafrost thickness. Further information on the permafrost depth has been directly obtained by geophysical well log responses especially acoustic log and electrical log. The "Mallik 2002 Gas Hydrate Production Research Well" investigated that the permafrost layer is approximately 640 m thick (Collett & Dallimore, 1998) and overlies gas hydrate accumulation between about 800 m to 1100 m below ground level within sedimentary succession.

3) Surface Temperature and Geothermal Gradient –

In the Mackenzie Delta area subsurface temperature data comes from industry acquired production drill stem tests and bottom hole well log surveys (Collett & Dallimore, 1998). An average surface temperature conditions in the incipient areas of Mackenzie Delta has found to be -9 °C (Allen et.al, 1988). Geothermal gradient below the IBPF in Mackenzie Delta – Beufort sea region were more uniform, ranging from 3.0 °C/100 m to 4.0 °C/100 m (Majorowickz et.al, 1990). In this case study of field Mackenzie Delta, temperature range for the expected GH bearing units are calculated by considering sub-permafrost geothermal gradient of 2.7 °C/100 m & temperature predicted at the base of IBPF i.e. at depth of 640 m is -0.1 °C (Collett & Dallimore, 1998).

4) Pore Pressure –

The available information allows the assumption of the regional pore pressures for the upper 1500 m of strata in the Mackenzie Delta field is similar to that of hydrostatic pressure i.e. pore pressure gradient of 9.8 KPa/m (0.433 psi/ft) knowing that the main overpressure zone are at least thousand meter deeper within succession (Collett & Dallimore, 1998).

5) Calculations –

Permafrost thickness – 640 m

Geothermal gradient – 2.7 °C

Pore-pressure gradient – 9.8 KPa/m (0.1 bar)

Temperature provided at the base of ice-bearing permafrost – (-1°C)

Temperature at depth 810.1 m = start temp. + (geothermal gradient * depth)
$$= (-1°C) + (0.027 * 170)$$
$$= 3.6°C = 276.75 \text{ K}$$

Temperature at depth 1102.3 m = (-1) + (0.027 * 462)

$$= 11.48 °C = 284.63 \text{ K}$$

The physical properties of gas hydrates inferred sediments in the Mallik area can be summarized in the Table number 5.

	Mallik L- 38well	
	Properties	**Values**
1	Depth of log inferred gas hydrates (m)	810.1 – 1102.3
2	Thickness of hydrate bearing zone (m)	111.4
3	Geothermal gradient (°C/100 m)	2.7
4	Permafrost thickness (m)	640
5	Temperature at the BIPF (°C)	-1
6	Calculated temperature range °C (K)	3.6 (276.75) – 11.48 (284.63)
7	Calculated pressure range (bar)	79.38 – 108.03
8	Average gas hydrate saturation (%)	67
9	Water saturation (%)	33
10	Salinity (ppt)	25
11	Average sediment porosity (%)	35
12	Biogenic/ Thermogenic origin	Biogenic
13	Gas chemistry	Pure methane
14	Volume of gas within hydrate per Km^2 (m^3)	4,284,000,000

Table 5: Geophysical properties of GH bearing units in Mallik L-38 well (Data taken from Collett & Dallimore, 1998).

In 1998 the collaborative research program between Japan & India confirms the existence of methane GHs at the Mallik site by obtaining geological and geochemical data through wireline logging and coring. In 2002 first onshore GH production test was carried out by collaborative research project by five countries (Japan, Canada, USA, India & Germany) & seven research institutes (the former Japan National Oil Corporation – the predecessor of JOGMEC, Geological Survey of Canada (GSC), US Department of Energy (DOE), US

Geological Survey (USGS), German Research Center for Geosciences (GFZ), Indian Ministry of Petroleum and Natural Gas – Oil and Natural Gas Corporation (ONGC) in India, and Project of BP-Chevron Texaco Mackenzie Delta Joint Venture) (Yamamoto & Dallimore, 2008). In 2002 the collaborative research program successfully produced gas from methane GHs by using thermal stimulation production method. In this hot water circulation test, hot water heated up to 80 °C is pumped into the methane hydrate deposits existing within a depth approximately 1100 m below from the ground surface through a test well. The temperature of pumped hot water was estimated to be around 50 °C when it comes near the hydrate bearing layers & as a result rise in the temperature to a point that the hydrate breaks down and methane hydrate dissociates. The collaborative test program succeeded in producing approximately 470 m^3 of gas from methane hydrate over a five days production period. This was the first test at the Mackenzie Delta (permafrost area) in the northwest of Canada to produce methane gas by dissociating methane hydrate was conducted as a pioneer in the world.

4.3 MITI Nankai Trough, Japan

The main objective of this section is to investigate the geophysical properties of inferred GH bearing sediments in the Nankai Trough area, Japan which are necessary requirements for the interpretation of the stability limits of hydrate using mixture of CO_2 & N_2. The Nankai Trough is located beneath the Pacific Ocean off the southeast coast of Japan. Since Japan is high energy consumption country, they need to develop a technology for energy production from in-situ GH deposits and therefore heightened the interest in methane hydrate. So first time Ministry of Economy, Trade & Industry drilled a research well in 1999-2000 in offshore Tokai, Japan & after that Japan completed second methane hydrate exploration field program in 2004. The MITI Nankai Trough well was drilled to investigate the potential of deep marine in-situ methane hydrate resources. The Nankai Trough runs along the Japanese Islands from offshore Tokai to offshore Kyushu areas, where fore-arc basins and accretionary prisms have developed extensively. Geographically the eastern part of the Nanakai Trough is separated into three zones; fore-arc basins, outer ridges & through axis.

4.3.1 Occurrences of GHs in Nankai Trough

Over a last decade Nankai Trough has become the focus of GH studies because Japan as a high hydrocarbon consumption country, it is highly dependent on imported energy resources and lack of domestic fossil energy sources. From November 1999 to February 2000, the Nankai Trough wells were drilled by Japan National Oil Corporation (JNOC) & MITI (Ministry of International Trade & Industry, currently Ministry of Economy, Trade and Industry). The drilling location was selected in the Nankai Trough area where existence of Bottom Simulating Reflectors (BSRs) has been pointed out by scientific seismic program (Satoh et.al, 1996). The MITI Nankai Trough wells were drilled to provide the physical evidence for existence of gas in the Pacific Ocean 50 km offshore of the Tenryu River Mouth, Shizuoka Prefecture, Central Japan at a water depth of 945 m. The temperature range at sea bottom corresponds to 3 °C (Takahashi et.al, 2001).

The MITI Nankai Trough wells consist of total six wells and are drilled within 100 m distances through BSR horizon. These six wells consists two pilot holes, main hole, & three post - survey wells (PSW) were drilled 655 m and 544 m below the sea floor (1600 mbsl & 1489 mbsl), and main holes 2355 m below sea floor (3300 mbsl) respectively followed by three post survey wells (PSW) drilled to 355 m below sea floor (1300 mbsl) (Uchida et.al, 2004). The MITI Nankai Trough wells penetrated the sea floor at water depth about 945 m (Collett, 2002). In order to recover the in situ hydrate bearing core sample without dissociating it while bringing it to the surface a unique coring method of 'Pressure Temperature Core Sampler' (PTCS) has been developed. The PTCS technique succeed in recovering GH bearing sand core samples were successfully recovered from main hole and the post survey wells – 2. In the MITI Nankai Trough wells high gas hydrate saturation within the cored intervals is observed in the main hole at the depth 165 to 327 mbsf and at the depth 204 to 278 mbsf in PSW-2 well (Uchida & Tsuji, 2004).

Nankai Trough area is characterized by the wide distribution of BSRs, but they are discontinuous. The BSRs runs parallel to the topography of seafloor. Usually the base of hydrate stability zone on continental margin is identified by occurrence of BSRs. The BSRs are reflections generated at the boundary between the gas hydrate saturated sediments above & the underlying sediment containing free gas (Pecher et.al, 1996). The BSR reflections are primarily due to presence of free gas therefore GHs may exist without BSRs. Hence wide distribution of GHs around Japan is interpreted based on existence of BSRs (Singh et.al, 1993). In summary high amplitude of BSRs reveals the presence of gas hydrate bearing strata, in contrast the amplitudes are not so striking in hydrate free region.

Well logging data including resistivity data, acoustic transit time data & NMR data is used for the evaluation of GH saturation within the sediments. Hydrate bearing layers are identified by increased resistivity & acoustic velocity as shown in figure 20 below. Well logging data & core analysis indicates the existence of hydrate in pore spaces of several sand layers between 1135 mbsl and 1213 mbsl (i.e. 190 m to 268 m below sea floor) (details can be seen in Takahashi et.al, 2001). Well log analyses & pore water chloride anomalies confirms the occurrences of gas hydrates within the depth of 204 m & 268 m below sea floor in the main hole and as well as PSW-2 well indicates the GH saturation within the hydrate bearing sand layers are approximately about 60% to 90%. Well logging and core analysis shows that within the depth interval 204 mbsf to 268 mbsf, three distinct hydrate bearing sand layers are observed from 204-212 mbsf, 236-246 mbsf & 255-268 mbsf. It is observed that these hydrate bearing strata are 1cm to 1 m thick and are highly saturated (up to 90%).
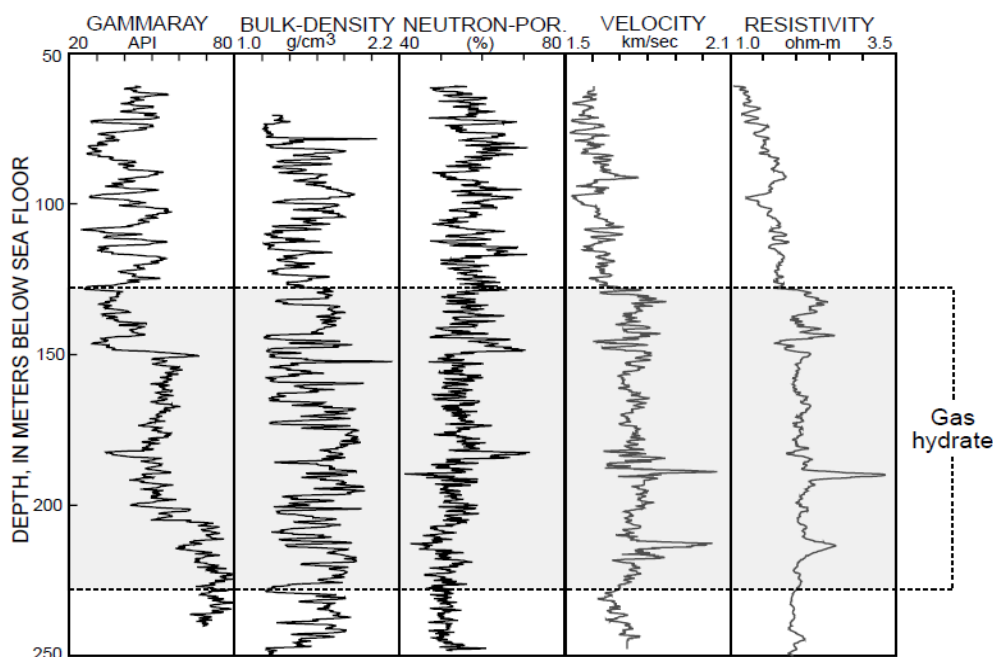
Figure 20: Downhole log data from ODP Site 889. Data shown include the natural gamma-ray log, bulk-density data, neutron porosities, compressional-wave acoustic velocities, and deep-reading electrical resistivities (Collett, 2002).

From above figure it is clear that the MITI Nankai Trough well analysis allows us to expect the subsurface distribution of GHs at a depth about 300 m below sea floor. According to (Waseda & Uchida, 2004), GHs in the Nankai Trough is composed of nearly by pure methane gas. The geochemical analysis of the samples collected by MITI Nankai Trough drilling reveals that the methane in hydrate bearing layer is of biogenic origin. Interstitial water extracted from the core sediments obtained from the exploratory MITI Nankai Trough well and analyzed for the chloride and sulfate concentrations in order to investigate the depth profile & occurrences of gas hydrates. Many similarities have been observed between Mallik site in Canada and the Nankai Trough wells regarding observations of well interconnected and highly saturated pore-space hydrate systems within sandy sediments.

A 2D and high resolution seismic study shows two BSRs in this study area of eastern Nankai Trough as shown in figure 21. Strong BSRs (BSR 1) at the depth of 263 m below sea floor were correlated to boundary between GH bearing sands and the shallower low velocity zone. The BSR 2 at depth of 289 m below sea floor corresponds to the top of deeper low velocity zone of sonic log. In the study area, the Nankai Trough has three 'BGHSs'. BGHS-0 exists at ~230 mbsf and is defined by temperature measurements. BGHS-1 exists at 265 mbsf and corresponds to the base of gas hydrate-bearing sands and BSR-1. BGHS-2 exists at 289~295 mbsf and corresponds to BSR-2 (as illustrated in figure 21). Based on research results, the world's first offshore natural hydrate exploration wells were successfully drilled from November 1999 to February 2000 at a single location in the Nankai Trough off Japan.
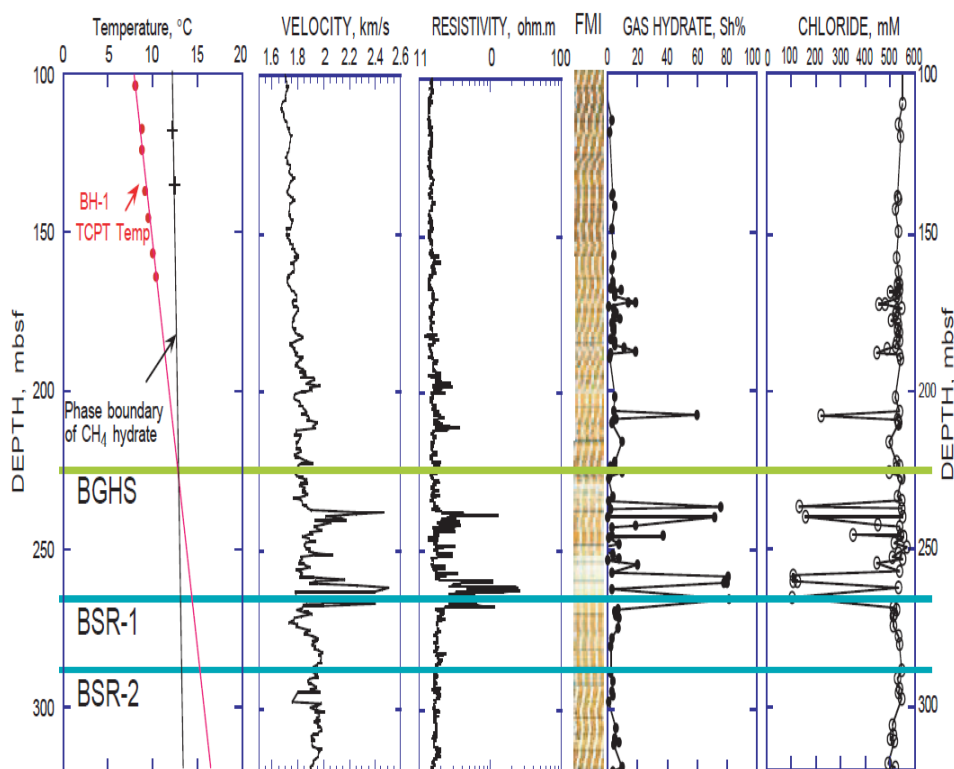
Figure 21: Correlation of temperature, velocity, resistivity, FMI (Formation Micro-Scanner), gas hydrate (Sh%) and chloride logs in the exploratory wells in the eastern Nankai Trough. [Solid horizontal lines indicate the predicted base of gas hydrate stability (BGHS-0), shallow BSRs (BSR-1) and deeper BSRs (BSR-2)](Ryo Matsuoto et.al, 2004).

1) Phase Diagram –

Geothermal gradient is needed in order to calculate the temperature at the hydrate bearing sediments in this area. The direct measurement of the formation temperature reveals the geothermal gradient of 4.3 °C/100 m. In below phase diagram the base of gas hydrate stability is observed at the depth of 230 mbsf which is shallower than the base of gas hydrates bearing layers (268 mbsf). But this discrepancy between the base of gas hydrate stability and base of the hydrate bearing layer has not been explained fully yet. Typically geothermal gradient strongly affects the thickness of GHSZ.
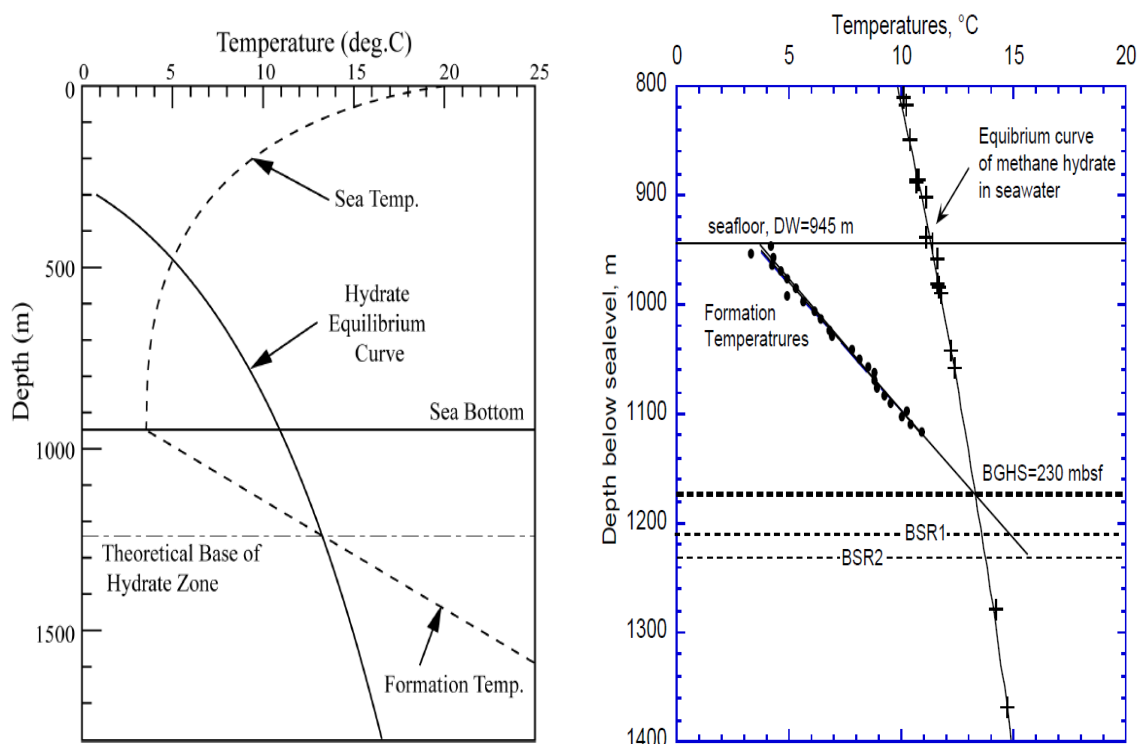
Figure 22: (a) Estimated downhole temperature and Methane-Hydrate equilibrium curve. (b) Theoretical base of gas hydrate stability (Takahashi et.al, 2001).

2) Calculations –

The temperature range for hydrate bearing sediments is calculated by multiplying the depth below seafloor by geothermal gradient and adding the sea-bottom temperature. Similar calculations did for pressure calculations.

Depth of log-inferred gas hydrates ranges considered from 190 m to 300 m below sea floor.

Geothermal gradient = 4.3 °C/100m

Sea-bottom temperature = 3 °C

Temperature at depth 190 mbsf = Sea-bottom temperature + (geothermal gradient * Depth)
$$= 3 \text{ °C} + (0.043*190)$$
$$= 11.2 \text{ °C} = 284.35 \text{ K}$$

Temperature at depth 268 mbsf = Sea-bottom temperature + (geothermal gradient * Depth)

$$= 3 \text{ °C} + (0.043*268)$$

$$= 14.5 \text{ °C} = 287.6 \text{ K.}$$

The pressure range at the hydrate bearing layer is calculated by considering the hydrostatic pore-pressure gradient of 9.8 KPa/m (0.1 bar).

Pressure at depth 1135 mbsl = 113 bar

Pressure at depth 1213 mbsl = 121 bar.

The geophysical properties required for the calculation of hydrate stability limits has been summarized in table format as below,

	MITI Nankai Trough Well	
	Properties	**Values**
1	Depth of log-inferred gas hydrates (m)	190 – 268
2	Thickness of hydrate-bearing zone(m)	16
3	Biogenic/Thermogenic origin	Biogenic
4	Average sediment porosity (%)	36
5	Average gas hydrate saturation (%)	80
6	Sea-bottom temperature (°C)	3
7	Geothermal gradient (°C/100 m)	4.3
8	Hydrostatic pressure gradient (bar)	0.1
9	Calculated temperature range °C (K)	11.2 (284) – 14.9 (288)
10	Calculated pressure range (bar)	113 – 121
11	Volume of Gas Within Hydrate per Km^2 (m^3)	755,712,000

Table 6: Geophysical properties of gas hydrate bearing sediments in MITI Nankai Trough Well (Collett, 2002).

4.4 Bjørnøya Basin, SW-Barents Sea

The inferred gas hydrate zone is located in Bjørnøya Basin, a large shelf through in the Southwestern (SW) Barents Sea. Barents Sea is bounded by, in the west by the Norwegian - Greenland Sea & in the north by the Eurasian Basin. Barents Sea is the largest epicontinental of 1.2 million km^2, located between Scandinavian penisula at south & Svalbard archipelago at the west. Barents Sea is comparatively deep (200 m – 400 m) epicontinental sea.

Generally BSRs are reflections generated at the boundary between above hydrate bearing layer and underneath free gas. Seismic data showing high amplitude reflections at a depth less than 1000 m from sea-floor from the Cenozoic sediments of the Bjørnøya Basin in SW-Barents Sea suspects the existence of GHs & free gas (Laberg & Andreassen, 1996). The data available until now for the late Cenozoic paleoenvironment in Svalbard & Barents Sea is limited, and gas hydrate accumulation in Barents Sea is not fully understood geographically yet.

4.4.1 Occurrences of GHs in Bjørnøya Basin

Indications for GHs and free gas at the SW Svalbard continental margin were first observed by (Vogt et.al, 1999). The evidences reveals that large amount of hydrocarbons are migrating upwards or leakages from deeper accumulations in Barents Sea and these leaked hydrocarbons have thought to be trapped in the shallow subsurface in the form of GHs (Laberg et.al, 1998., Chand et.al, 2012). Moreover 3D seismic data and occurrences of BSRs indicate the presence of gas hydrates in the shallow sediments in SW-Barents Sea.

The study area considered for the elucidation of the distribution of high amplitude reflections is located on the southeastern part of the Bjørnøya Basin in Barents Sea. In this area water depth varies from 350 m to 450 m (Laberg & Andreassen, 1996). Both Atlantic water and Arctic water influences the Barents Sea. In the Bjørnøya Basin the temperature of the bottom water is more or less constant around 2 °C and the temperature goes down up to -1.5 °C (Norwegian Oceanographic datacenter). Increase in bottom water temperature might have caused the decrease in GHSZ thickness because depth of gas hydrate stability is controlled by temperature. The calculations of GHSZ are carried out considering geothermal gradient 3.5 °C/100 m in Barents Sea, estimated by nearby exploration wells (Laberg & Andreassen, 1996).

The presence of natural submarine gas hydrate is commonly inferred from seismic reflection data. High amplitude BSRs on the Cenozoic succession are separated into three units; Unit TbA, Unit TbB, & Unit TbE. Units TbA & TbB correlate with units TtA1 & TtA2 in the Tromsø Basin while unit TbE correlates with unit TtE in Tromsø Basin as shown in figure 23.

			Vorren et al. (1991) (e = Egga Basin)	Knutsen et al (1992) (t = Tromsø Basin)	This work (T = Tertiary) (b = Bjørnøya Basin)
QUAT.		Pleisto.	TeE	TtE	TbE
TERTIARY	NEOGENE		TeD		
		Plio.	TeC		
		Miocene	TeB		
	PALEOGENE	Oligocene			
		Eocene		TtB₁ / Tt B₁	TbB
				TtA₂	
		Paleocene	TeA	TtA₁	TbA
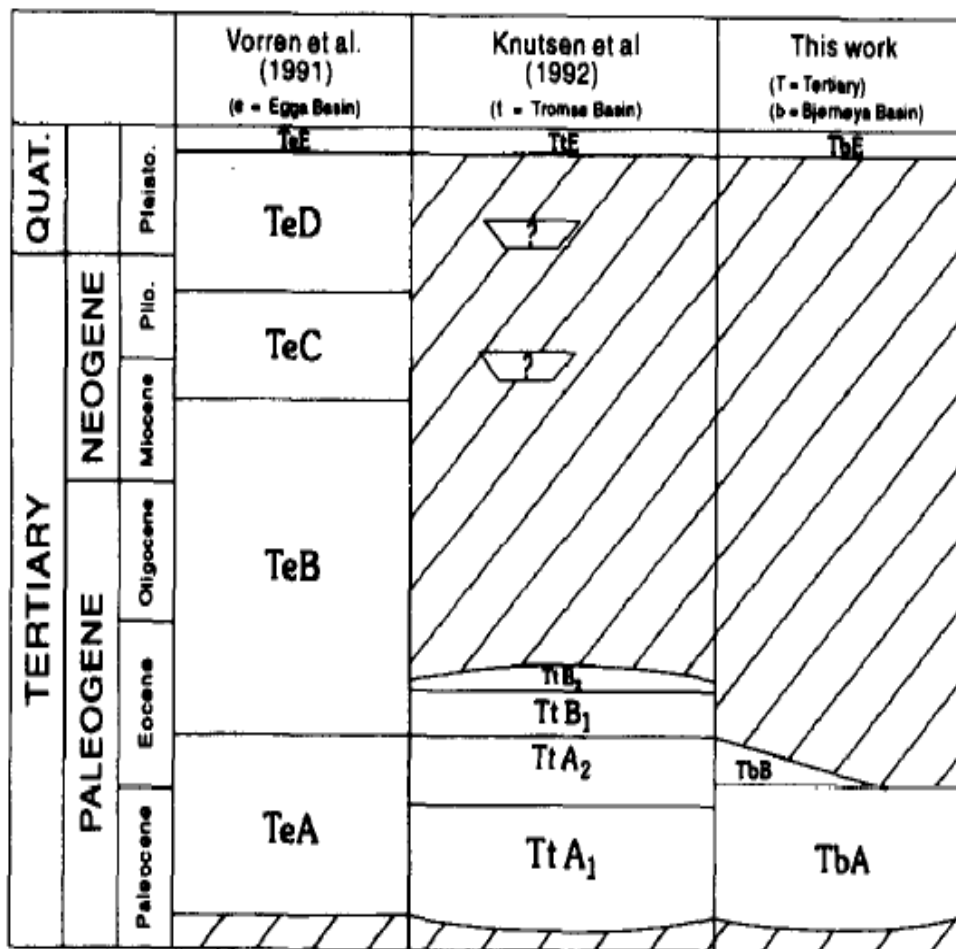
Figure 23: Simplified Cenozoic stratigraphy of the Bjørnøya Basin, the correlative sediments within the Tromsø Basin and their age relationships (Laberg & Andreassen, 1996).

The BSRs exists at comparatively shallower depth i.e. 220 m below from sea floor which makes the studied interval suitable for estimation of interval velocity and estimates of in-situ gas hydrates are made on the basis for interval velocity structure. The interval velocity studies indicate high amplitude reflections are observed at depth 620 m. A velocity structure (interval velocity 2210 m/s) indicate that the thickness of the GHs inferred zone might be up to 100 m & the inferred GH accumulations described in this study area occur at water depth 400 m. Areal extent of GHs within the study area considered corresponds to 55 km^2. Multichannel seismic data and well logging data tentatively indicate that $1.9 * 10^8$ m^3 of gas trapped in the form of GH in SW-Barents Sea (Laberg et.al, 1998). The maximum estimated volume of gas within this gas hydrate bearing area corresponds to $3.8 * 10^8$ m^3.

In this study two areas are considered,

Area 1 –

In area 1, three high-amplitude reflections are observed at the water depth 405 m (200 mbsf), but these amplitudes are in dis-agreement with the units TbA & TbB i.e. cross cut the dipping reflections of units TbA & TbB. According to (Laberg & Andreassen, 1996) above the high

amplitude seismic anomaly, interval velocity increases from 1960 m/s to 2375 m/s and below the anomaly velocity decreases up to 1700 m/s.

Area 2 –

Area 2 is situated 10 km south of area 1. In this area 2 high-amplitude reflections are observed at 1.15 s or 1.35 s below from sea floor. In contrast to area 1, these high amplitude reflections are parallel with overlying and underlying internal reflections of unit TbA. According to (Laberg & Andreassen, 1996) above to within the zone of high-amplitude reflections in area 2, interval velocity decreases from 2620 m/s to 1890 m/s. The decrease in velocity at the depth of high amplitude anomalies is probably due to presence of free gas. Even a very small amount of presence of gas causes the remarkable decrease in velocity.
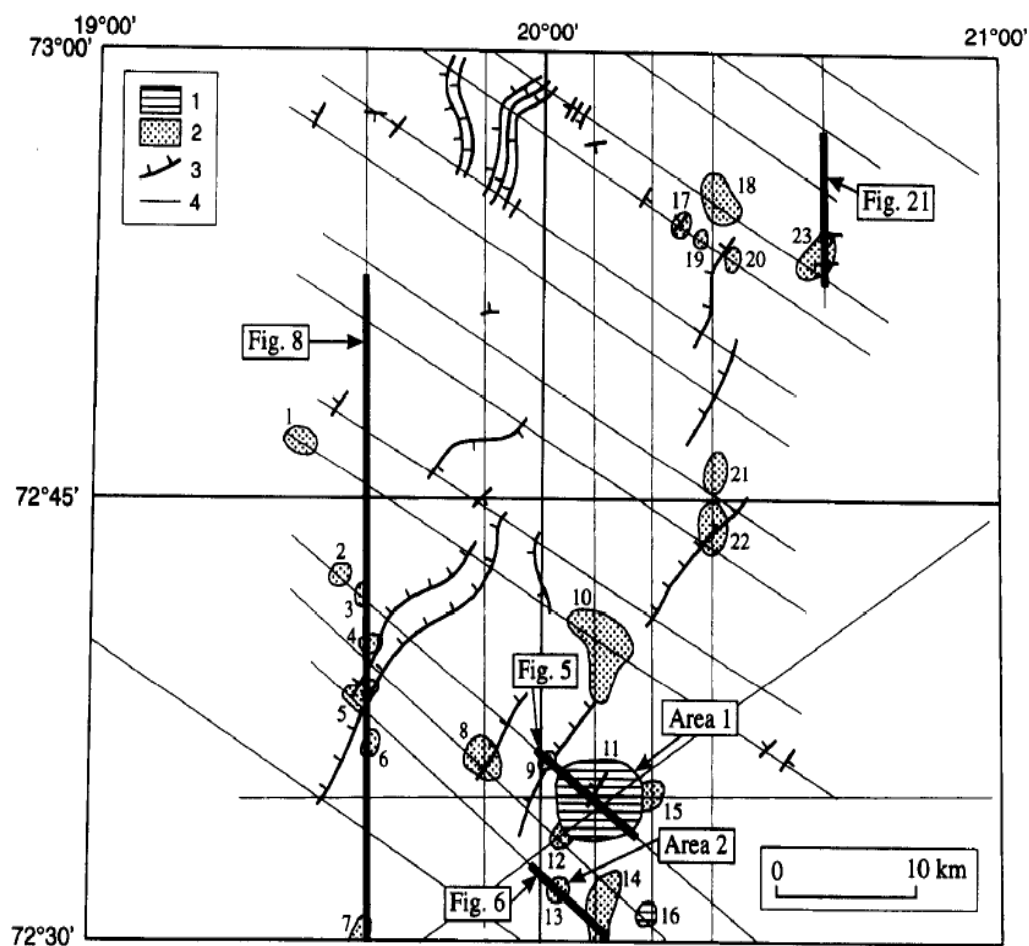
Figure 24: Distribution of high amplitude reflections. In figure group 1 indicates the bottom simulating reflections which are discordant with the overlying and underlying reflections, group 2 indicates high-amplitude reflections parallel with overlying and underlying reflections. Group 3 shows location of faults at the tertiary base, group 4 indicates seismic data. Two areas considered for the study (Laberg & Andreassen, 1996).

According to (Mathews & Von Huene, 1985), if there is high hydrate concentration in hydrate bearing sediments then interval velocity increases and decrease in interval velocity as in area 1 is expected to occur at the base of the gas hydrate zone because of the transition between the sediments with no hydrocarbons (having normal velocity) and to the gas bearing sediments (having lower velocity).

First well drilled in 1980 in Barents Sea aiming hydrocarbon exploration and after that more than 90 exploration wells has been drilled so far in the Norwegian parts of the Barents Sea. In SW- Barents Sea five exploration wells has been drilled in middle Eocene sediments which correlates with unit TbB in the Bjørnøya Basin as shown in figure 23. However the presence of GHs in this area has not been confirmed from drilling.

The inferred GHs accumulation described in this study area occurs at water depth 400 m. Based on interval velocity structure, the depth of the high amplitude reflections as well has been calculated which corresponds to 620 m below seafloor. Hydrostatic pressure gradient of 0.1 bar has been considered. Some of other the geophysical properties are calculated using well logging data and these properties are arranged in table number 7. Detailed studies shows that GHs are inferred to occur in six additional areas within the southeastern part of Bjørnøya Basin, and they all are located near the western flank of the Loppa high.

Multichannel seismic data reveals the existence of GHs that overlie free gas within the Cenozoic sediments of southwestern Barents Sea shelf. The Cenozoic sediments within the Bjørnøya Basin are dominated by claystone & siltstone.

1) Phase Diagram

The inferred GHs in Bjørnøya Basin exists at depth between 400 m to 620 m. Temperature is the vital factor which controls the gas hydrate stability. In this area water depth is 400 m and bottom water temperature predicted by Norwegian Oceanographic datacenter corresponds to 2 °C. An average geothermal gradient used for the construction of temperature-depth profile corresponds to 3.5 °C/100 m. In this study area, hydrostatic or lithostatic pressure gradients are 0.1 atmospheres/m i.e. 9.8 KPa/m.
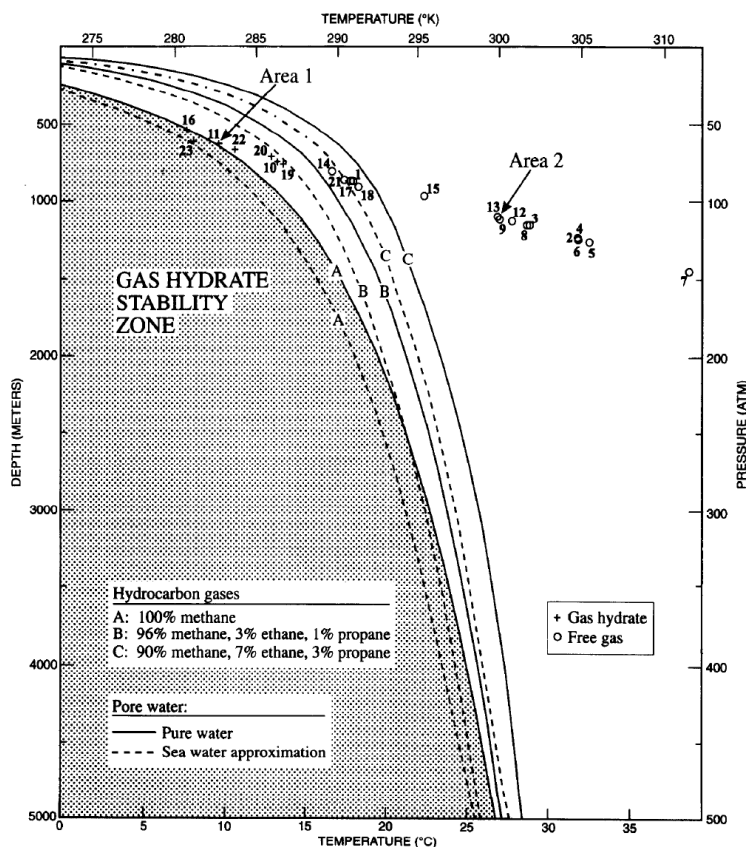
Figure 25: Estimated depth & temperature profile of all the high amplitude reflections within phase boundary diagram for fresh water - methane hydrate (shaded area)(Laberg & Andreassen, 1996).

2) Calculations

The temperature at the base of the suspected GH anomaly i.e. at depth 620 m has been calculated by using bottom water temperature and geothermal gradient.

Depth of water – 400 m

Bottom water temperature – 2 °C

Geothermal gradient – 3.5 °C/100 m

Pressure gradient – 0.1 bar

Temperature at the depth of 620 m = Bottom water temperature + (geothermal gradient * Depth from seafloor)

$$= 2 + (0.035 * 220)$$
$$= 9.7 \text{ °C} = 283 \text{ K.}$$

Pressure calculations are based on force exerted by overlying water column.

Calculated pressure range at the depth 620 m from the sea level = 62 bar.

The physical properties of suspected gas hydrate bearing sediments in Bjørnøya Basin are arranged in following table 7.

	Børnøya Basin in Barents Sea	
	Properties	**Values**
1	Depth of log inferred GHs (m)	400 – 620
2	Areal extent of GHs (km^2)	55
3	Thickness of hydrate bearing zone (m)	100
4	Geothermal gradient (°C/100 m)	3.5
5	Calculated temperature range °C (K)	2 (275) – 9.7 (282)
6	Pressure gradient (bar)	0.1
7	Calculated pressure range (bar)	40 – 62
8	Average interval velocity (m/s)	2200
8	Average hydrate saturation (%)	26
9	Average sediment porosity (%)	30
10	Density (g/cm3)	2.15
11	Biogenic/Thermogenic origin	Thermogenic
12	Maximum estimates for volume of gas within hydrate	$3.8 * 10^8$ m^3
11	Minimum estimates for volume of gas within hydrate	$1.9 * 10^8$ m^3

Table 7: Geophysical properties observed in hydrate bearing sediment in Bjørnøya Basin (data taken from Laberg et.al, 1998).

5. Results and Discussion

The theoretical data estimated by (Herri et.al, 2010) is used for the verification of our model system. Since the experimental data for 'Gas hydrate equilibria for CO2-N2 mixtures' has been used for comparison with our estimates, the experimental set up and procedure from (Herri et.al, 2010) is described briefly as follows.

Experimental Set-up

In their (Herri et.al, 2012) experiments, experimental set up has been built to investigate the thermodynamics equilibrium conditions of GHs (pressure and temperature) and to determine the composition of all existing phases like gas, liquid and hydrate. The apparatus consists of double jacket stainless steel high pressure batch reactor which is connected to an external cooler with a CC3 controller. Hydrate formation in the reactor is confirmed by visual appearances using two sapphire windows placed on both sides of the reactor. A Pyrex cylinder filled with 800 cm^3 1L of water containing LiNO3 as an anionic tracer is fixed in the reactor in which pressure can be increased up to 10 MPa. Liquid is injected in pressurized injector by using HPLC pump. During crystallization suspension was stirred by a four vertical blade turbine impeller. Two pt100 probes in liquid and gas phase monitor temperature while pressure measured by pressure transducer. The data acquisition unit (T, P) is connected to personal computer. Gas sampling is performed by the instrument ROLSI. This ROLSI tool collects little micro cubic gas and passes it into the gas chromatograph. Then gas phase composition is determined by means of gas chromatograph. The precision in gas composition is 2%. 1 ml of liquid sample is taken by classical valve & directed towards DIONEX ionic exchange chromatograph which measures the concentration of LiNO3. The gas mixtures are prepared by injecting each gas directly into the reactor. To obtain the exact composition of each gas, mixtures are analyzed with gas chromatography.

Experimental Procedure

• Crystallization of gas mixtures CO2 with N2 or CH4 in presence of a liquid phase (water +LINO3) forms hydrate.
• Initially reactor is closed and removes all the air, water and other contents by means of vacuum pump.
• To remove the other traces of gases, cell is flushed with nitrogen and again reactor is evacuated.
• In the beginning reactor is pressurized with CO2 gas, having maximum pressure in the bottle about 5 MPa.
• When pressure increases up to 10 MPa, N2 or CH4 gas is injected.
• With the help of stirrer the gas mixture is stirred and cooled down and maintained at a temperature around 273 to 283 K.
• Then 1L of liquid solution is injected in the reactor by using HPLC pump which increases both temperature and pressure because of the gas compression resulting from the reduction of gas volume by the liquid injection.
• The stirrer is started. The decrease in pressure was observed due to partial dissolution of the gaseous components in the liquid phase.
• After some time (from minutes to several hours), the crystallization starts accompanied by a sudden rise of temperature that dependence on the intensity of crystallization.
• During solid formation pressure decreases due to the consumption of gas and forms hydrate. Gas phase is sampled with the ROLSI instrument while crystallization and analyzed in-line gas chromatography.
• Liquid phase is sampled to be analyzed by off-line ion exchange chromatography.
• At the end of crystallization system reaches equilibrium and temperature-pressure values corresponds to a constant values.
• The gas hydrate dissociation is operated at constant volume and started by heating the reactor in increment of 1 K. After each increment of temperature, the pressure increases due to gas hydrate dissociation and reaches a constant value which represents the thermodynamic equilibrium.
• In the same way as in the case of the crystallization steps, the gas and the liquid phases are sampled to determine the compositions of the phases at equilibrium.

5.1 Verification of the Model

In this section the estimated data for mixtures of various compositions has been tried to match with the experimental data from (Herri et.al, 2010) as illustrated in graphs below. This was done in order to validate the calculated results with the experimental results from [Herri et.al, 2010]. The data calculated for the hydrate equilibrium curve is for mixtures of different compositions of gases as illustrated in figure below.

In figure 5.1 to 5.3, compared the estimated equilibrium temperature-pressure values estimated from software generated by Professor Bjørn Kvamme with experimental values from (Herri et.al, 2010). The thermodynamic parameters considered here are from (Kvamme, 2015a., Kvamme, 2015b).

The results estimated for considered thermodynamic model are equivalent with experimental results (as illustrated in figure 5.1 to 5.3) ensures that the model system considered in this study is suitable.

Figure 5.1: Estimated and experimental hydrate equilibrium curve, for a system of 0.19999999 (19.99%) CO_2, 0.79999999 (79.99%) N_2, 0.00000001 (0.01%) H_2S. Solid line (–) our estimates, asterisk (*) – experimental data from (Herri et.al, 2010).

Comparing figures 5.1 to 5.3 it is observed that, increase in nitrogen content in the CO_2+N_2 gas mixture from 70% to 80%, the hydrate formation pressure increases from 5.1 bar to 6.4 bar.
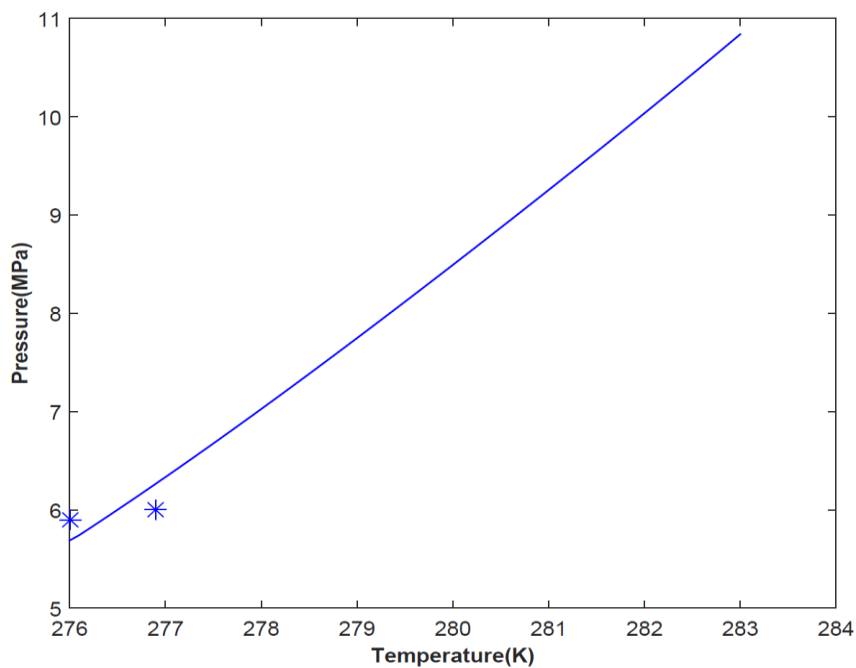
Figure 5.2: Estimated and experimental hydrate equilibrium curve, for a system of 0.24999999 (24.99%) CO_2, 0.74999999 (74.99%) N_2, 0.00000001 (0.01%) H_2S. Solid lines (–) our estimates, asterisk (*) – experimental data from (Herri et.al, 2010).
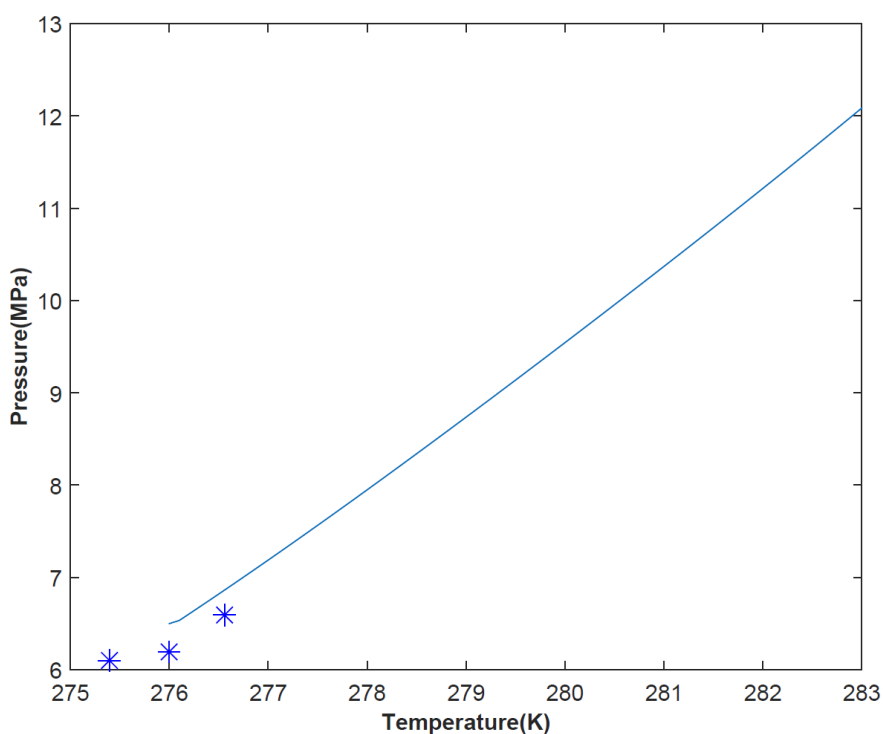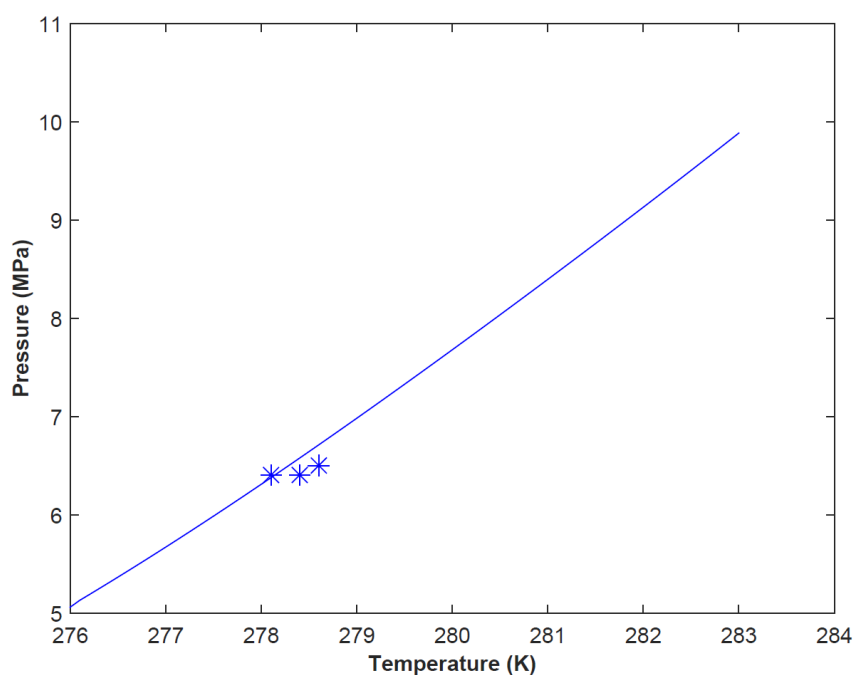

Figure 5.3: Estimated and experimental hydrate equilibrium curve, for a system of 0.29999999 (29.99%) CO_2, 0.69999999 (69.99%) N_2, 0.00000001 (0.01%) H_2S. Solid line (–) our estimates, asterisk (*) – experimental data from (Herri et.al, 2010).

6. Limits of Hydrate Stability for Mixtures of CO2 and N2

In this section hydrate stability limits for different mixtures of CO2 and N2, at specific T-P conditions calculated for the theoretically studied fields in section 4 has been evaluated. In the graphs constructed below, estimated water chemical potential in hydrate & liquid or ice water chemical potential for pressures of 90 bar, 100 bar, 150 bar, 200 bar & 250 bar are plotted under the assumption that the guest chemical potentials are same in the hydrate and in the gas but no water equilibrium constraints. This makes it possible to compare the difference in chemical potential for water in hydrate and the liquid water chemical potential. If the chemical potential of water in hydrate is lower than the liquid water chemical potential, then hydrate would be stable at those thermodynamic conditions. The values for chemical potentials are estimated by using the "Thermocode" generated by Prof. Bjørn Kvamme. The codes are in "FORTRAN" language & Microsoft Developer Studio (MSDEV) has been used as compiler.

Thermodynamic properties of hydrate, chemical potential for empty hydrate and liquid water chemical potential estimations are based on thermodynamic model by (Kvamme & Tanaka, 1995). Ideal gas phase chemical potentials are calculated from statistical mechanics. The chemical potential of water for the adsorbed phase was estimated from (Kivalæ et.al, 2012).

6.1 Limits of Hydrate Stability for Mixtures of CO2 and N2 – Eileen Area

The one of the major goal of this study is to assess the gas hydrate resources in Northern Alaska. As mentioned previously the direct evidence for the presence of gas hydrates on the North Slope of Alaska comes from a GH containing core and indirect evidence has been obtained from well logging data which indicate the presence of a number of gas hydrate containing layers. The analysis shows that the presence of three hydrate bearing sedimentary units; Unit C, Unit D, Unit E at the depth interval between 564 m to 680.5 m from the surface where temperature ranges from 0.35 °C to ≈ 5 °C (Details can be seen in schematic representation, figure 16).

The evaluation of hydrate stability limits in Alaska region is carried out by considering temperature from 268 K to 288 K. In this case the heat released can assist in dissociating the in-situ hydrate. The estimated results makes it possible for newly formed CO2 dominated hydrate to re-dissociate due to low CO2 concentration in surrounding gas and local temperature increase from the released heat of hydrate formation. This is of course a positive aspect in terms of reducing pore blocking due to new hydrate but also an efficiency limitation (Kvamme, 2015b).

From figure 6.1.1 it is seen that hydrate formation at 90 bar is not possible for mole-fractions of CO2 less than 5% at 274 K and hydrate is not stable for mole fractions of CO2 less than 80 mole % at 288 K. For 150 bar (figure 6.1.3) hydrate is not stable at 288 K for mole fractions of CO2 less than 35 mole % CO2.

Figure 6.1.1: Estimated water chemical potential in hydrate (solid line) and liquid water chemical potential (dashed line) as a function of temperature for **90 bar** and CO2 mole percentage 100, 70, 50, 30, 20, 5, 2, 1 with 100 mole percentage CO2 at bottom & 1 mole percentage curve on the top. Estimated water chemical potential in pure CH4 hydrate (dash-dot line).

Figure 6.1.2: Estimated water chemical potential in hydrate (solid line) and liquid water chemical potential (dashed line) as a function of temperature for **100 bar** and CO2 mole percentage 100, 70, 50, 30, 20, 5, 2, 1 with 100 mole percentage CO2 at bottom & 1 mole percentage curve on the top. Estimated water chemical potential in pure CH4 hydrate (dash-dot line).

Figure 6.1.3: Estimated water chemical potential in hydrate (solid line) and liquid water chemical potential (dashed line) as a function of temperature for **150 bar** and CO2 mole percentage 100, 70, 50, 30, 20, 5, 2, 1 with 100 mole percentage CO2 at bottom & 1 mole percentage curve on the top. Estimated water chemical potential in pure CH4 hydrate (dash-dot line).

Figure 6.1.4: Estimated water chemical potential in hydrate (solid line) and liquid water chemical potential (dashed line) as a function of temperature for **200 bar** and CO2 mole percentage 100, 70, 50, 30, 20, 5, 2, 1 with 100 mole percentage CO2 at bottom & 1 mole percentage curve on the top. Estimated water chemical potential in pure CH4 hydrate (dash-dot line).

Figure 6.1.5: Estimated water chemical potential in hydrate (solid line) and liquid water chemical potential (dashed line) as a function of temperature for **250 bar** and CO2 mole percentage 100, 70, 50, 30, 20, 5, 2, 1 with 100 mole percentage CO2 at bottom & 1 mole percentage curve on the top. Estimated water chemical potential in pure CH4 hydrate (dash-dot line).

6.1.1 Limits of Hydrate Stability for mixtures of CO2 and N2 — Unit C

In this section, the limits of hydrate stability as a function of temperature for different mixtures of CO2 & N2 in terms hydrate water chemical potential and liquid water chemical potential for the hydrate bearing unit C in the Northwest Eileen State-2 well has been carried out. The temperature range has chosen a bit wider for the sake of uncertainty i.e. temperature ranges considered are from 266.3 K to 283.31 K. According to (Collett, 2002) the hydrate layer is 29 m thick and the average gas hydrate saturation in the Unit C is around 60.9 % (As shown in Table 3).

The estimated water chemical potential in hydrate and liquid or ice water chemical potential for pressures of 90 bar, 100 bar, 150 bar, 200 bar & 250 bar are plotted in figure 6.1.6 to 6.1.10.

Figure 6.1.6: Estimated water chemical potential in hydrate (solid line) and liquid water chemical potential (dashed line) as a function of temperature for **90 bar** and CO2 mole percentage 100, 70, 50, 30, 20, 5, 2, 1 with 100 mole percentage CO2 at bottom & 1 mole percentage curve on the top. Estimated water chemical potential in pure CH4 hydrate (dash-dot line).

From above figure 6.1.6 it is observed that, for 90 bar hydrate is not stable for gas mole fraction of CO2 less than 20 mole % at 276 K & less than 50 mole % at 282 K.

Figure 6.1.7: Estimated water chemical potential in hydrate (solid line) and liquid water chemical potential (dashed line) as a function of temperature for **100 bar** and CO2 mole percentage 100, 70, 50, 30, 20, 5, 2, 1 with 100 mole percentage CO2 at bottom & 1 mole percentage curve on the top. Estimated water chemical potential in pure CH4 hydrate (dash-dot line).
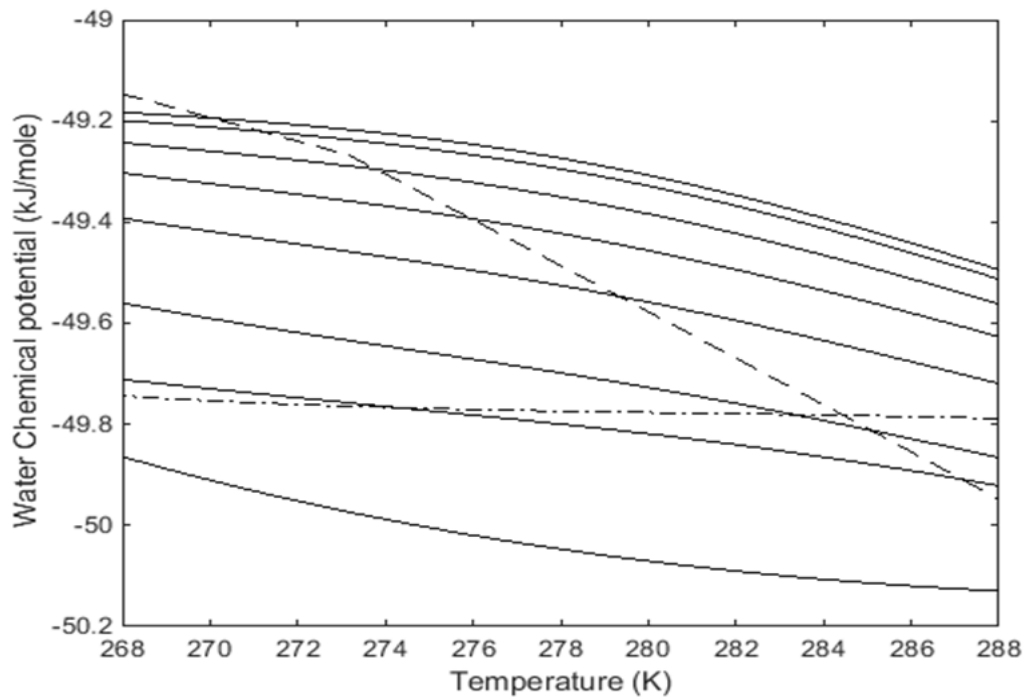

Figure 6.1.8: Estimated water chemical potential in hydrate (solid line) and liquid water chemical potential (dashed line) as a function of temperature for **150 bar** and CO2 mole percentage 100, 70, 50, 30, 20, 5, 2, 1 with 100 mole percentage CO2 at bottom & 1 mole percentage curve on the top. Estimated water chemical potential in pure CH4 hydrate (dash-dot line).
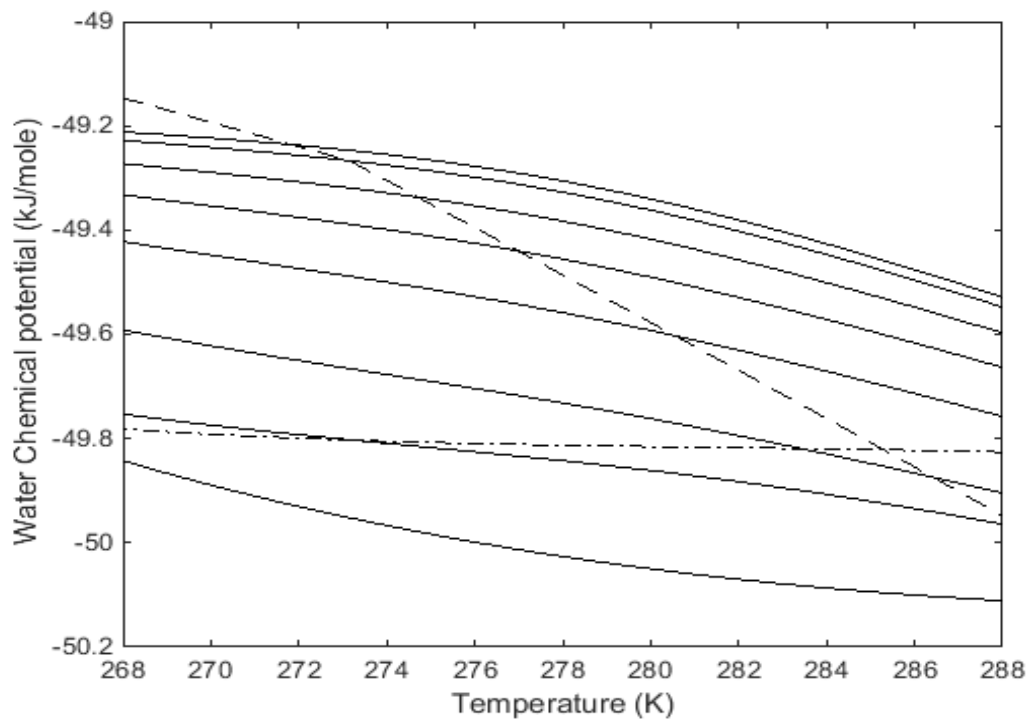
Figure 6.1.9: Estimated water chemical potential in hydrate (solid line) and liquid water chemical potential (dashed line) as a function of temperature for **200 bar** and CO2 mole percentage 100, 70, 50, 30, 20, 5, 2, 1 with 100 mole percentage CO2 at bottom & 1 mole percentage curve on the top. Estimated water chemical potential in pure CH4 hydrate (dash-dot line).
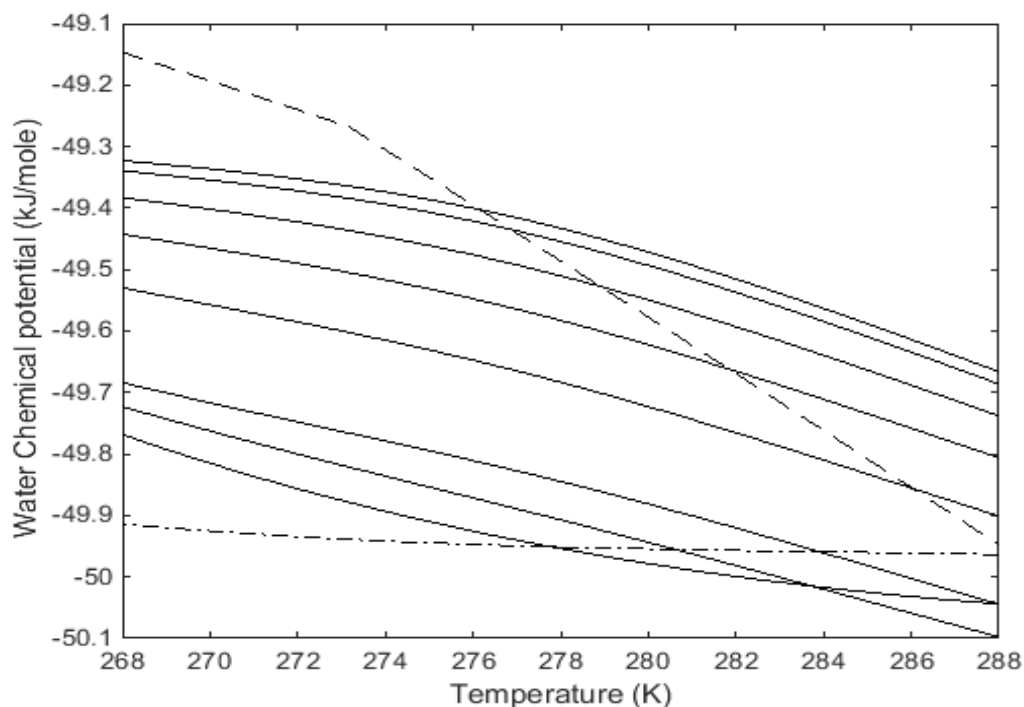

Figure 6.1.10: Estimated water chemical potential in hydrate (solid line) and liquid water chemical potential (dashed line) as a function of temperature for **250 bar** and CO2 mole percentage 100, 70, 50, 30, 20, 5, 2, 1 with 100 mole percentage CO2 at bottom & 1 mole percentage curve on the top. Estimated water chemical potential in pure CH4 hydrate (dash-dot line).

6.1.2 Limits of Hydrate Stability for mixtures of CO2 and N2 — Unit D

In this section, limits of hydrate stability for different mixtures of CO2 & N2 as a function of temperature in terms of hydrate water chemical potential & liquid water chemical potential, for Unit D in the Northwest Eileen State-2 well has been carried out. Temperature range considered for Unit D from 264.74 K to 284.95 K. Thickness of the hydrate bearing zone Unit D is around 6.7 m & gas hydrate saturation of corresponding zone is around 33.9% (Collett, 2002).

Estimated water chemical potential in hydrate & liquid or ice water chemical potential for pressures of 90 bar, 100 bar, 150 bar, 200 bar & 250 bar are plotted in figures from 6.1.11 to 6.1.15.
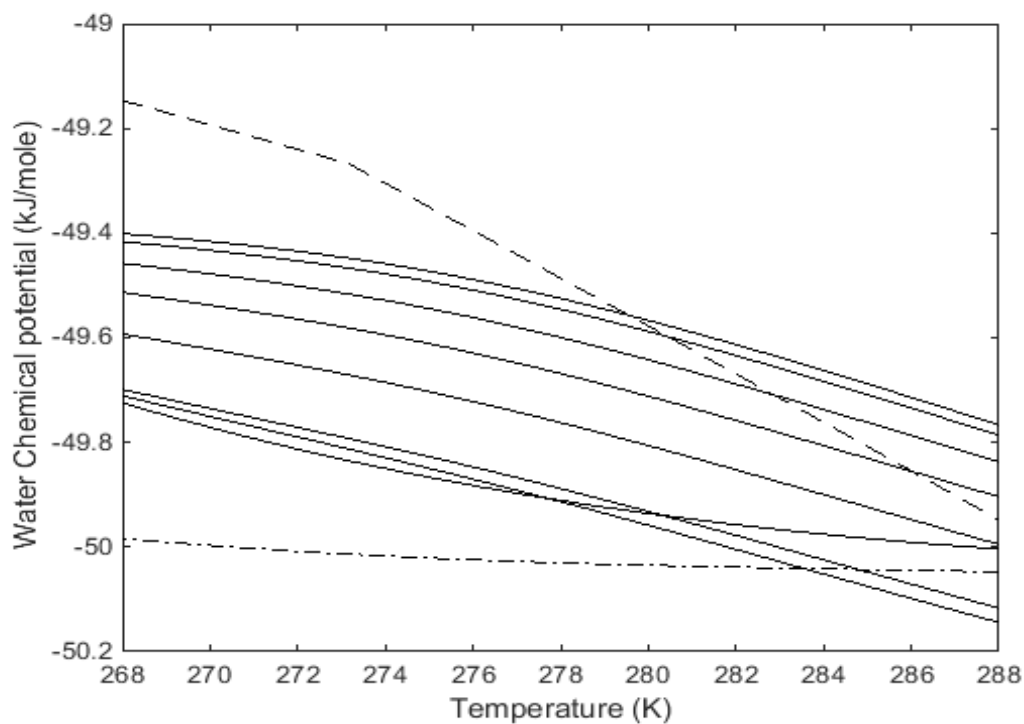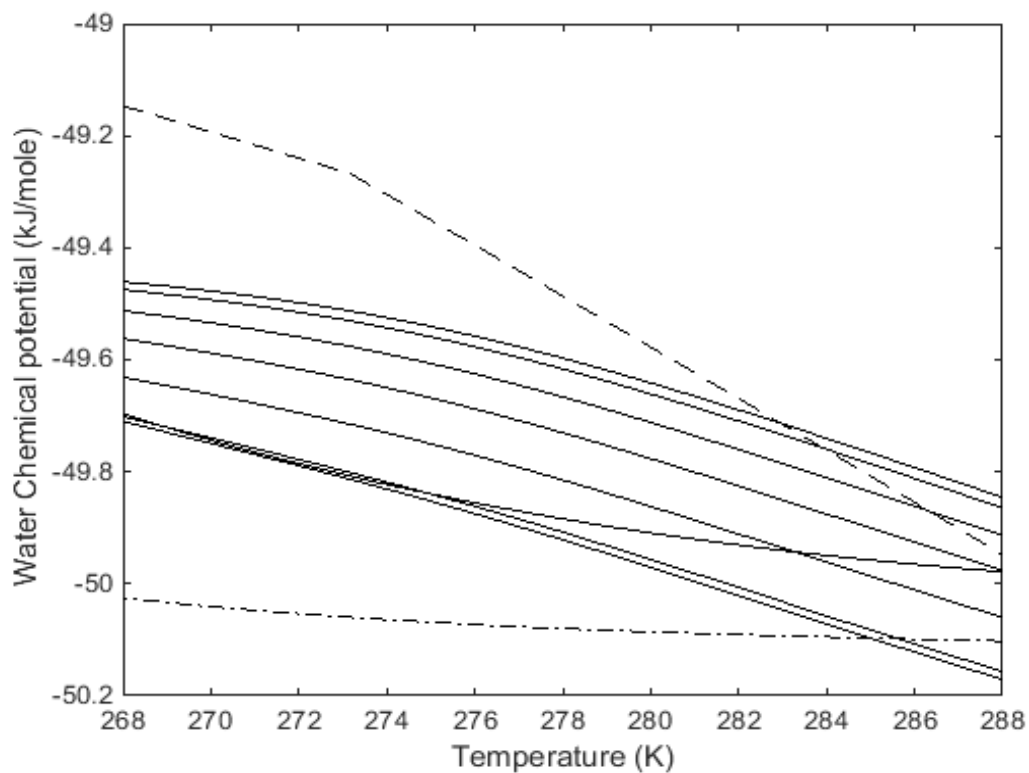

Figure 6.1.11: Estimated water chemical potential in hydrate (solid line) and liquid water chemical potential (dashed line) as a function of temperature for **90 bar** and CO2 mole percentage 100, 70, 50, 30, 20, 5, 2, 1 with 100 mole percentage CO2 at bottom & 1 mole percentage curve on the top. Estimated water chemical potential in pure CH4 hydrate (dash-dot line).

In above figure 6.1.11, it is seen that for 90 bar hydrate is not stable for mole-fraction of CO2 less than 30% at 280 K & less than 50% at 285 K.

Figure 6.1.2: Estimated water chemical potential in hydrate (solid line) and liquid water chemical potential (dashed line) as a function of temperature for **100 bar** and CO2 mole percentage 100, 70, 50, 30, 20, 5, 2, 1 with 100 mole percentage CO2 at bottom & 1 mole percentage curve on the top. Estimated water chemical potential in pure CH4 hydrate (dash-dot line).

Figure 6.1.13: Estimated water chemical potential in hydrate (solid line) and liquid water chemical potential (dashed line) as a function of temperature for **150 bar** and CO2 mole percentage 100, 70, 50, 30, 20, 5, 2, 1 with 100 mole percentage CO2 at bottom & 1 mole percentage curve on the top. Estimated water chemical potential in pure CH4 hydrate (dash-dot line).
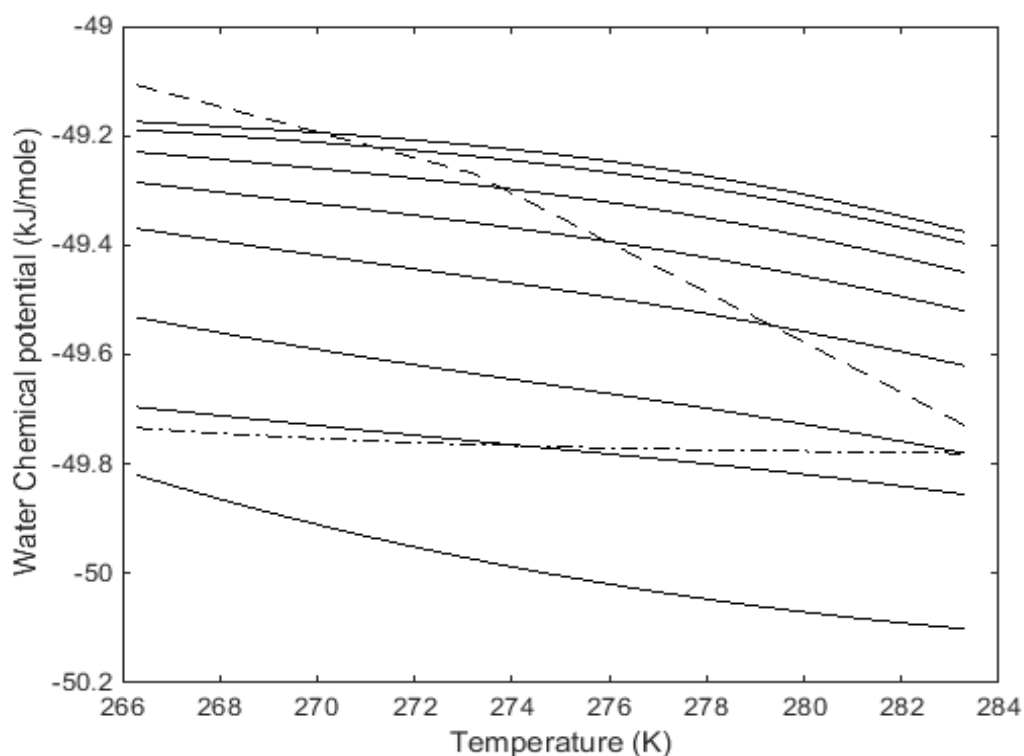
Figure 6.1.14: Estimated water chemical potential in hydrate (solid line) and liquid water chemical potential (dashed line) as a function of temperature for **200 bar** and CO2 mole percentage 100, 70, 50, 30, 20, 5, 2, 1 with 100 mole percentage CO2 at bottom & 1 mole percentage curve on the top. Estimated water chemical potential in pure CH4 hydrate (dash-dot line).
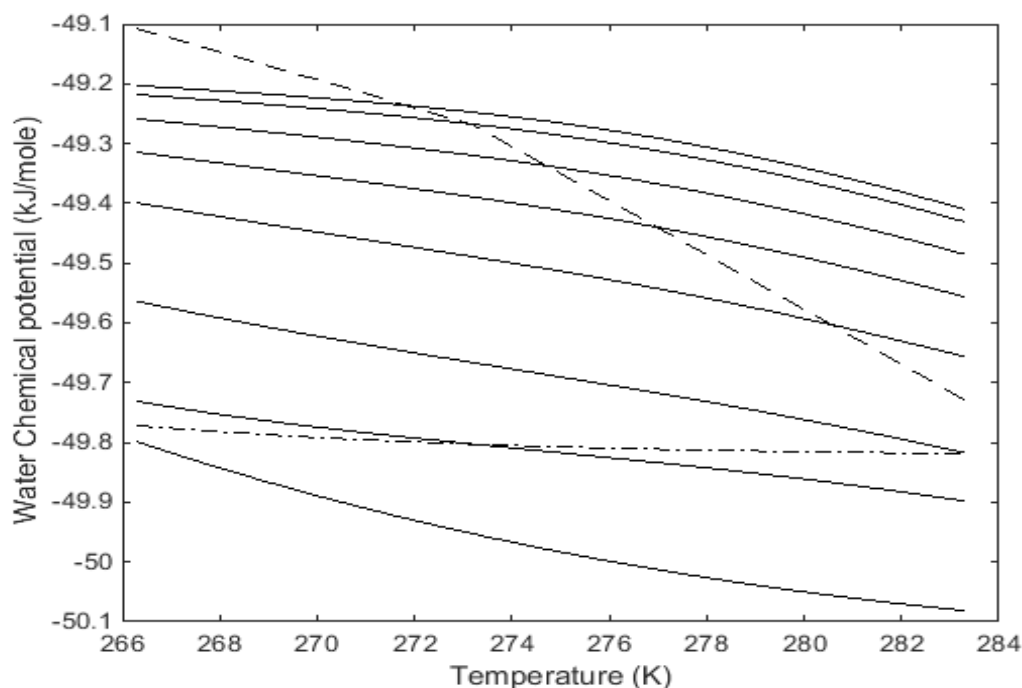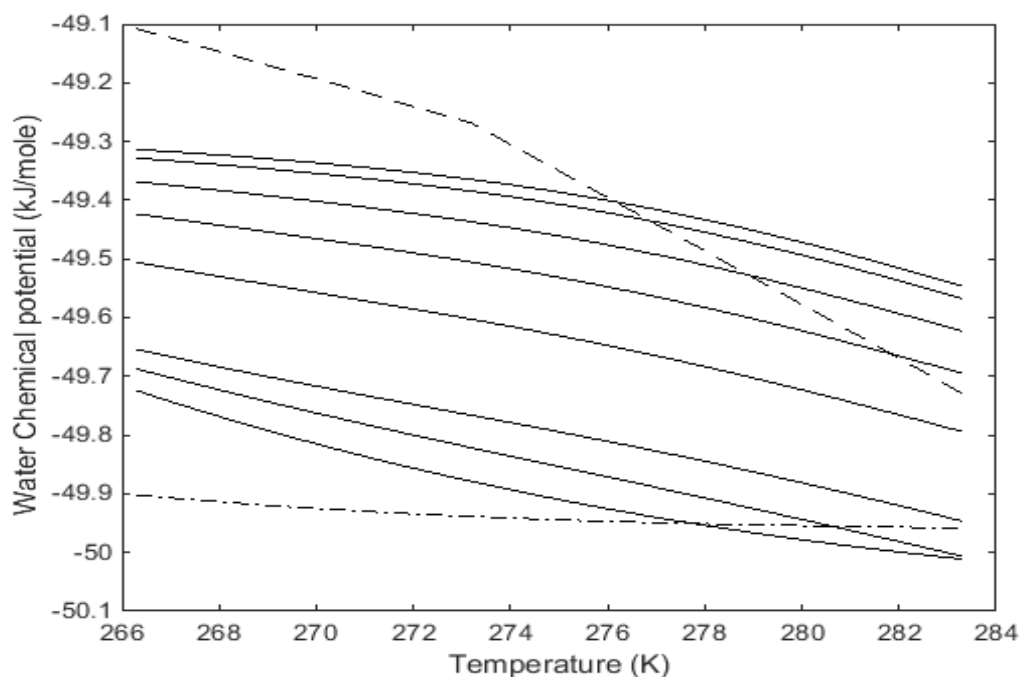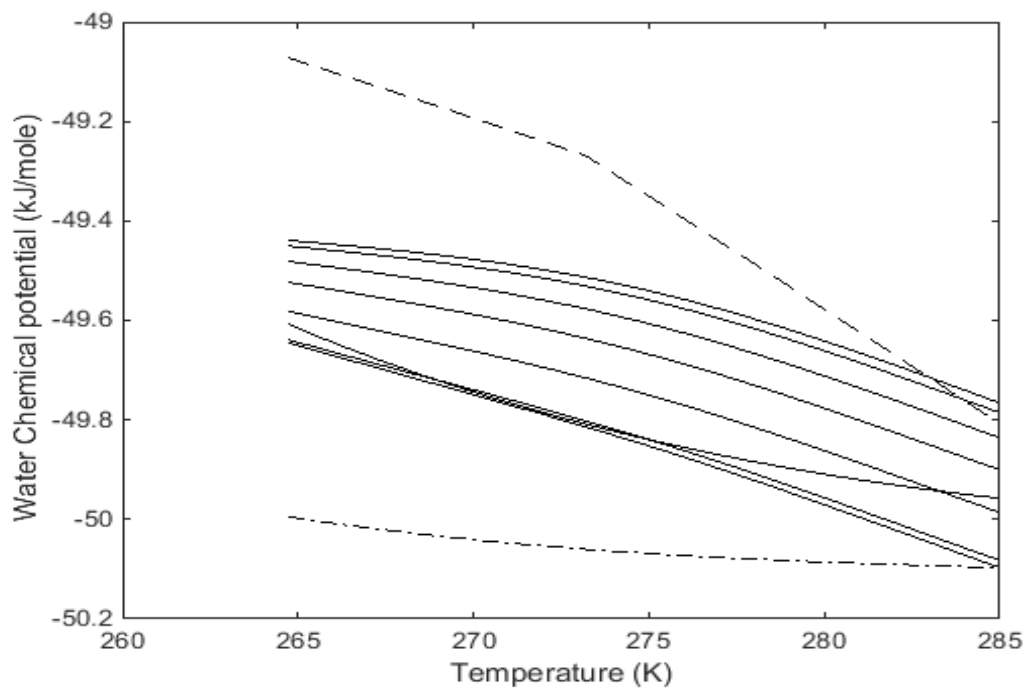

Figure 6.1.15: Estimated water chemical potential in hydrate (solid line) and liquid water chemical potential (dashed line) as a function of temperature for **250 bar** and CO2 mole percentage 100, 70, 50, 30, 20, 5, 2, 1 with 100 mole percentage CO2 at bottom & 1 mole percentage curve on the top. Estimated water chemical potential in pure CH4 hydrate (dash-dot line).

6.1.3 Limits of Hydrate Stability for Mixtures of CO2 and N2 — Unit E

In this section, we investigate the stability of hydrates from different CO2:N2 ratios with reference to chemical potential of water as ice or liquid water for Unit E in the Northwest Eileen State-2 well. Thickness of the hydrate bearing Unit E ≈ 16.8 m and average gas hydrate saturation in this Unit E is around 32.6% (Collett, 2002).

The estimated water chemical potential in hydrate and liquid or ice water for pressures of 90 bar, 100 bar, 150 bar, 200 bar, & 250 bar are plotted in figure 6.1.16 to 6.1.21. In the graphs constructed below at 90 bar, hydrate is not stable for gas mole fraction of CO2 less than 2 mole % at 272 K and less than 30 mole % at 278 K.
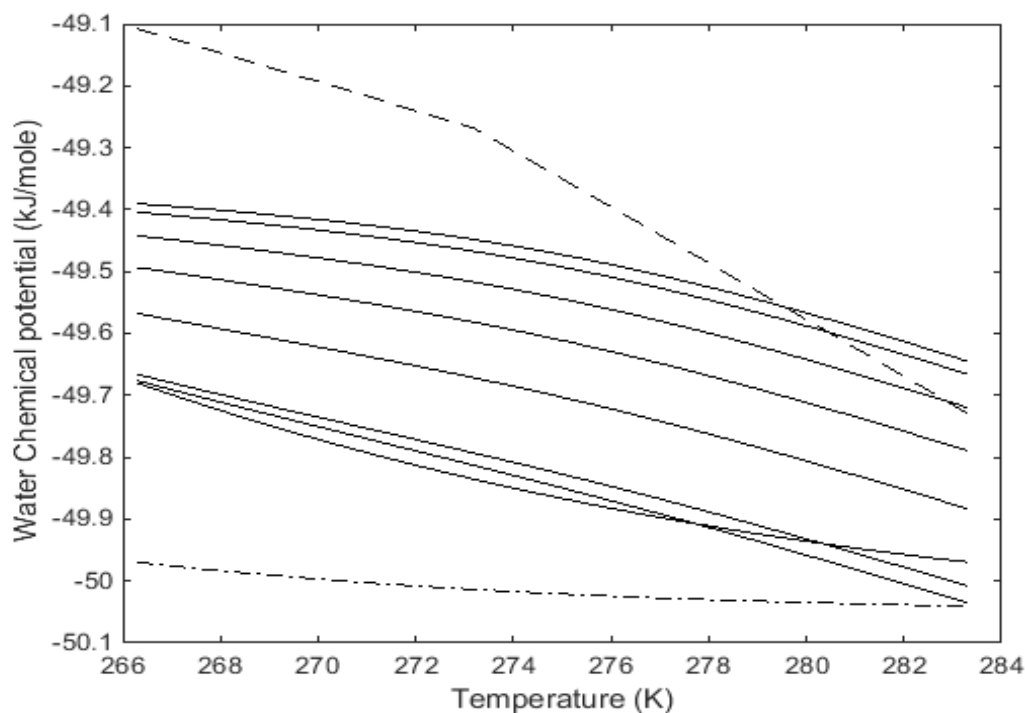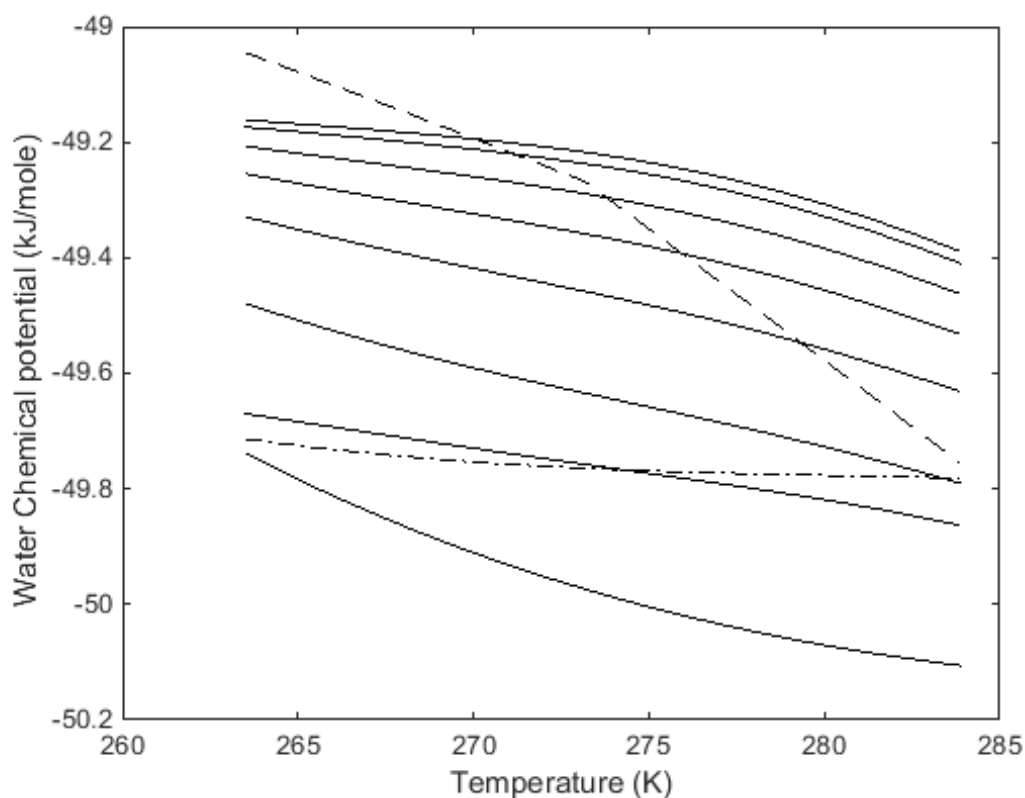

Figure 6.1.16: Estimated water chemical potential in hydrate (solid line) and liquid water chemical potential (dashed line) as a function of temperature for **90 bar** and CO2 mole percentage 100, 70, 50, 30, 20, 5, 2, 1 with 100 mole percentage CO2 at bottom & 1 mole percentage curve on the top. Estimated water chemical potential in pure CH4 hydrate (dash-dot line).
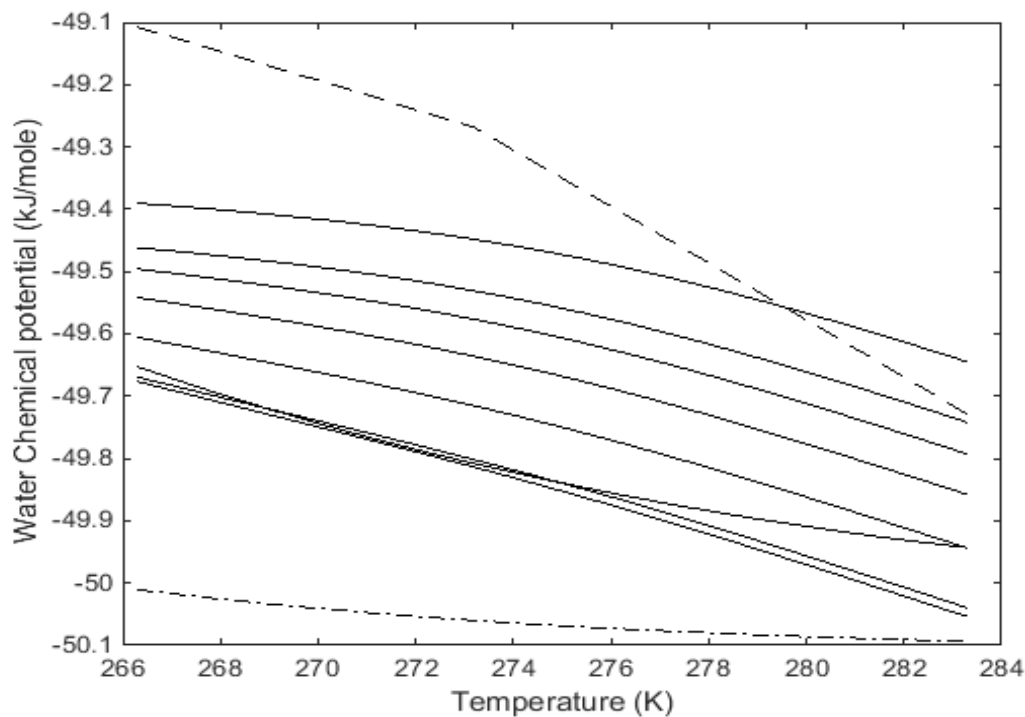
Figure 6.1.17: Estimated water chemical potential in hydrate (solid line) and liquid water chemical potential (dashed line) as a function of temperature for **100 bar** and CO2 mole percentage 100, 70, 50, 30, 20, 5, 2, 1 with 100 mole percentage CO2 at bottom & 1 mole percentage curve on the top. Estimated water chemical potential in pure CH4 hydrate (dash-dot line).

Figure 6.1.18: Estimated water chemical potential in hydrate (solid line) and liquid water chemical potential (dashed line) as a function of temperature for **150 bar** and CO2 mole percentage 100, 70, 50, 30, 20, 5, 2, 1 with 100 mole percentage CO2 at bottom & 1 mole percentage curve on the top. Estimated water chemical potential in pure CH4 hydrate (dash-dot line).

Figure 6.1.19: Estimated water chemical potential in hydrate (solid line) and liquid water chemical potential (dashed line) as a function of temperature for **200 bar** and CO2 mole percentage 100, 70, 50, 30, 20, 5, 2, 1 with 100 mole percentage CO2 at bottom & 1 mole percentage curve on the top. Estimated water chemical potential in pure CH4 hydrate (dash-dot line).
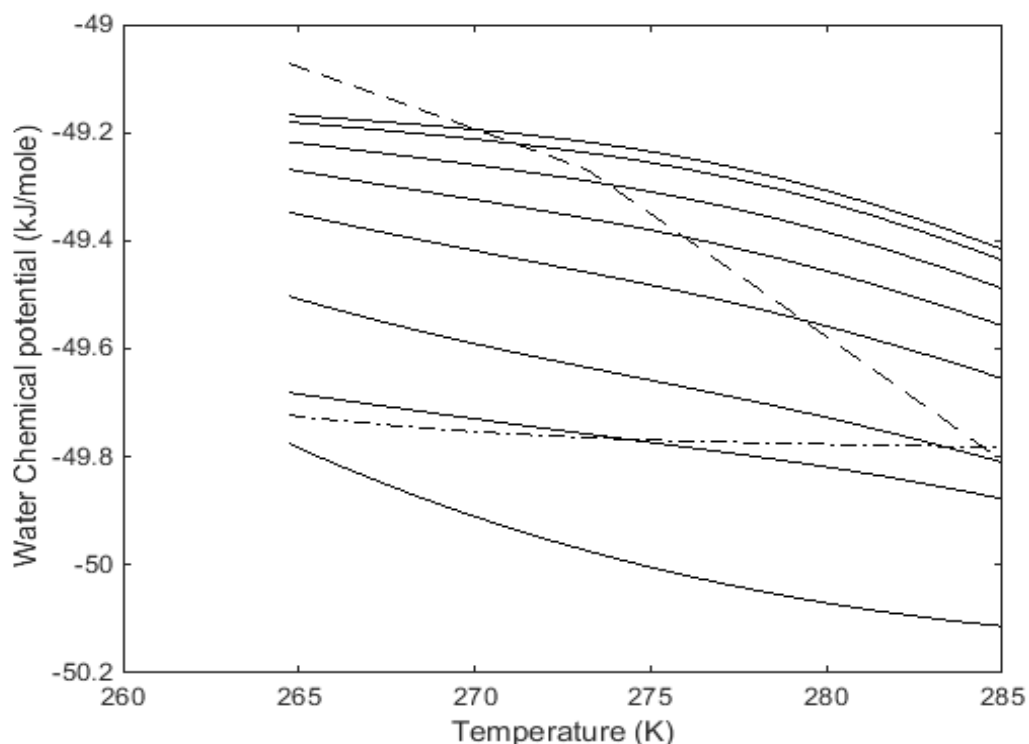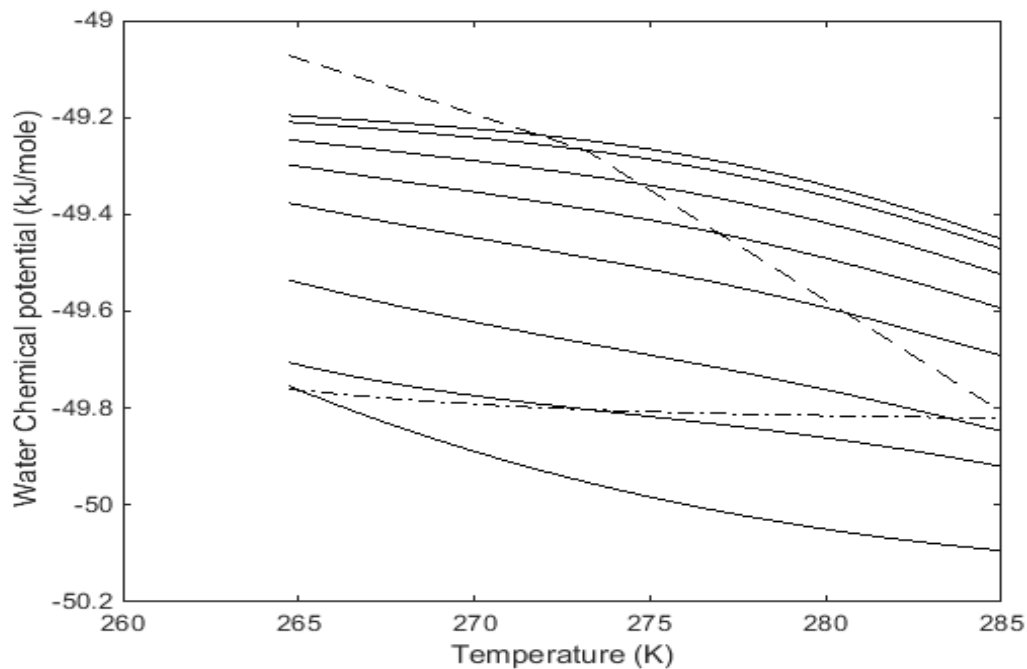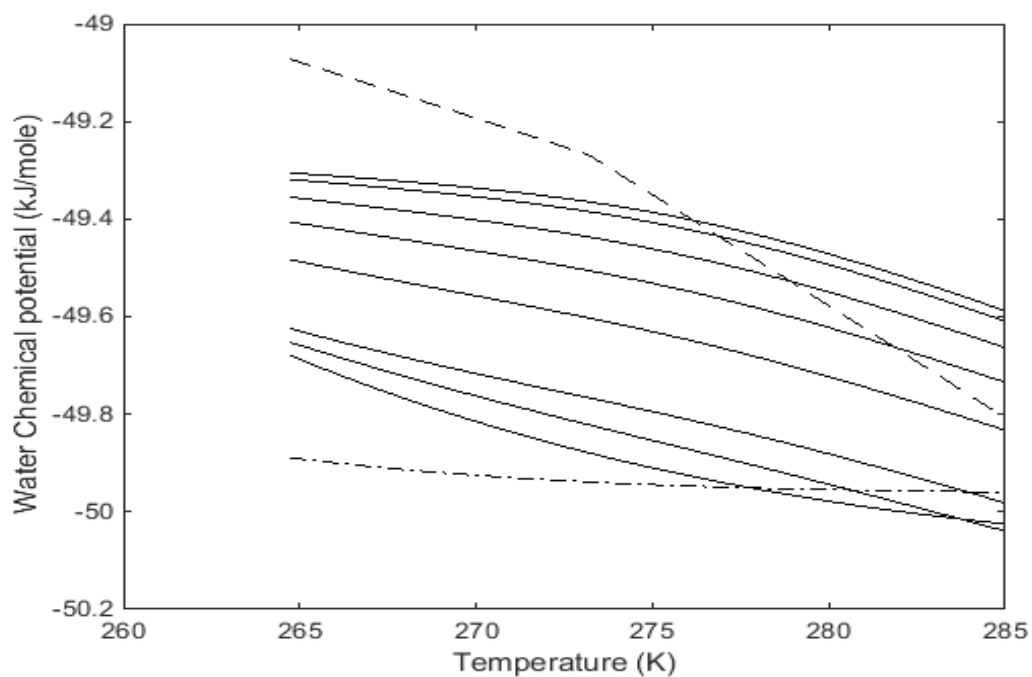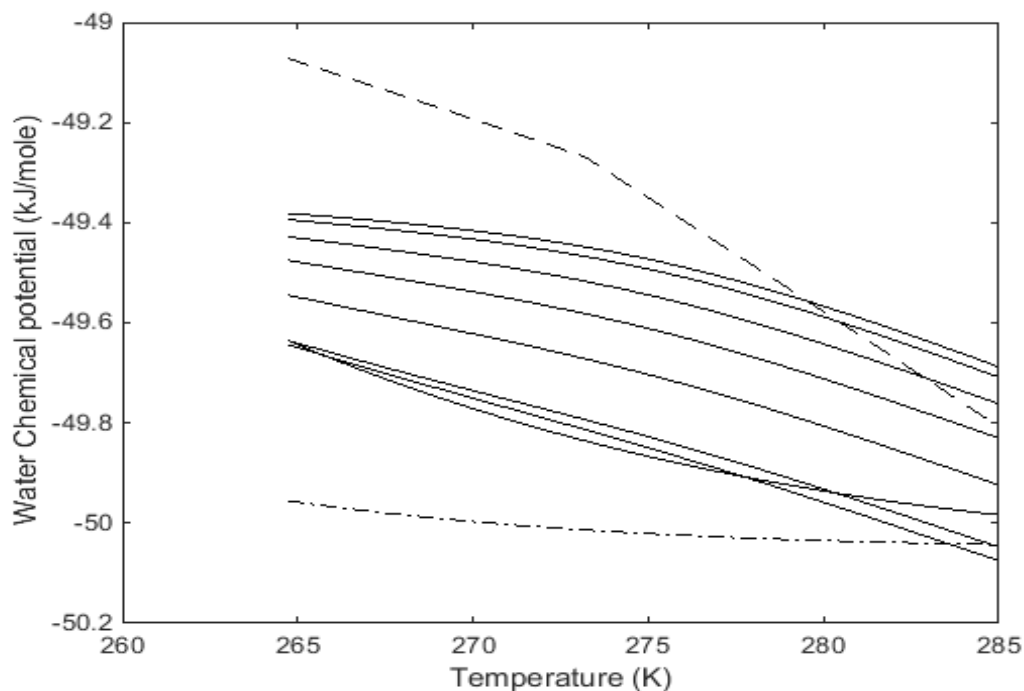

Figure 6.1.20: Estimated water chemical potential in hydrate (solid line) and liquid water chemical potential (dashed line) as a function of temperature for **250 bar** and CO2 mole percentage 100, 70, 50, 30, 20, 5, 2, 1 with 100 mole percentage CO2 at bottom & 1 mole percentage curve on the top. Estimated water chemical potential in pure CH4 hydrate (dash-dot line).

6.1.4 Chemical Potential Gradients for CH4 between Gas and Hydrate

In this section it has been examined that the differences in chemical potential of methane between methane hydrate & methane diluted in CO2\N2 mixtures to shed light on the thermodynamic driving force for dissociation of hydrate towards gas due to guest (methane) chemical potential.

Chemical potential of methane as pure component at 90 bar and given temperatures is plotted in figure 6.1.21 below to illustrate that an equilibrium pure methane hydrate (in which methane chemical potential in hydrate is the same as chemical potential of methane in gas phase) will dissociate due to guest chemical potential gradient. Dashed lines are 0.1 per cent methane in different mixtures of CO2 and N2. The calculated temperature for hydrate bearing units in the Eileen area on the Alaska North Slope ranges from 268 K to 288 K.
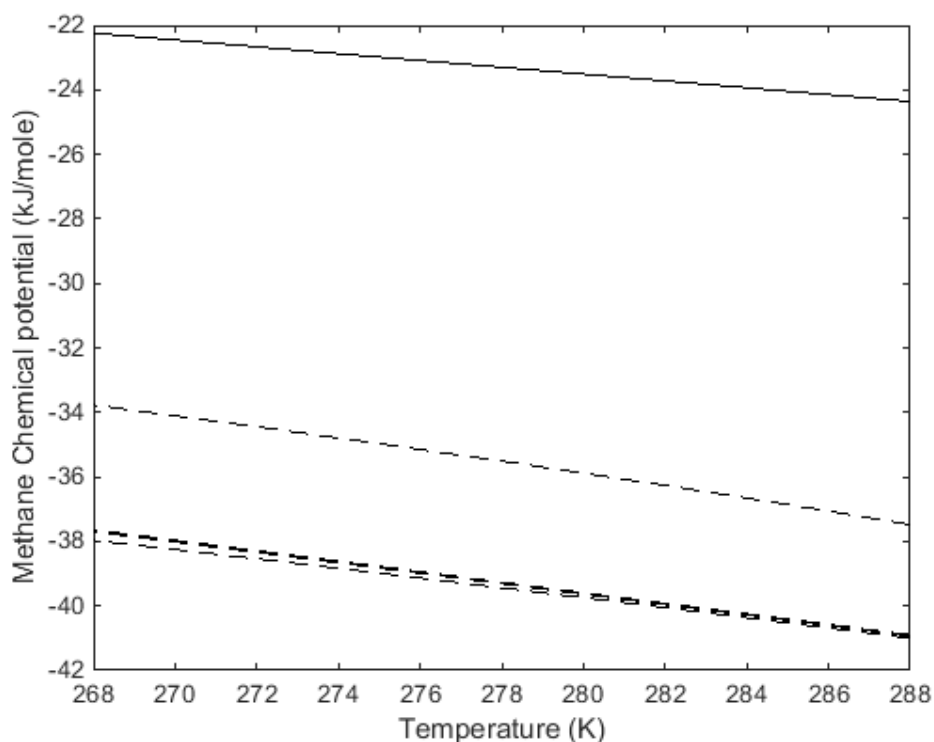
Figure 6.1.21: Chemical potential of CH4 in pure methane hydrate (as created from CH4 gas and water so equal to pure methane gas chemical potential) (solid line) and 0.1 mole % CH4 in surrounding gas of varying mole-fraction of CO2 (dashed). Top to bottom in mole percentage CO2: 100, 70, 50, 20, 10, 5, 2, 1. Liquid water chemical potential (dashed). Pressure is **90 bar**.

From figure 6.1.21, it is observed that CH4 hydrate will dissociate towards gas due to chemical potential gradient of CH4.

6.1.5 CO2 Solubility in Liquid Water Needed to Keep Hydrate Stable

Hydrates dominated by CO2 as guest will also dissociate towards water if the mole-fraction of CO2 dissolved in liquid water is lower than the CO2 concentration in liquid water needed to keep hydrate stable. When the gas gets diluted for CO2, it won't be able to support enough CO2 into the water phase to keep CO2 hydrate stable so even formed CO2 hydrate may dissolve towards lean gas if the gas concentration of CO2 becomes less than required for stability.

In this section the estimated CO2 mole-fractions are plotted as a function of temperature for varying concentration of CO2 in the mixture. The values are estimated by using "Thermocode" generated by Prof. Bjørn Kvamme. The code is in "FORTRAN" language and Microsoft Developer Studio (MSDEV) has been used as compiler.
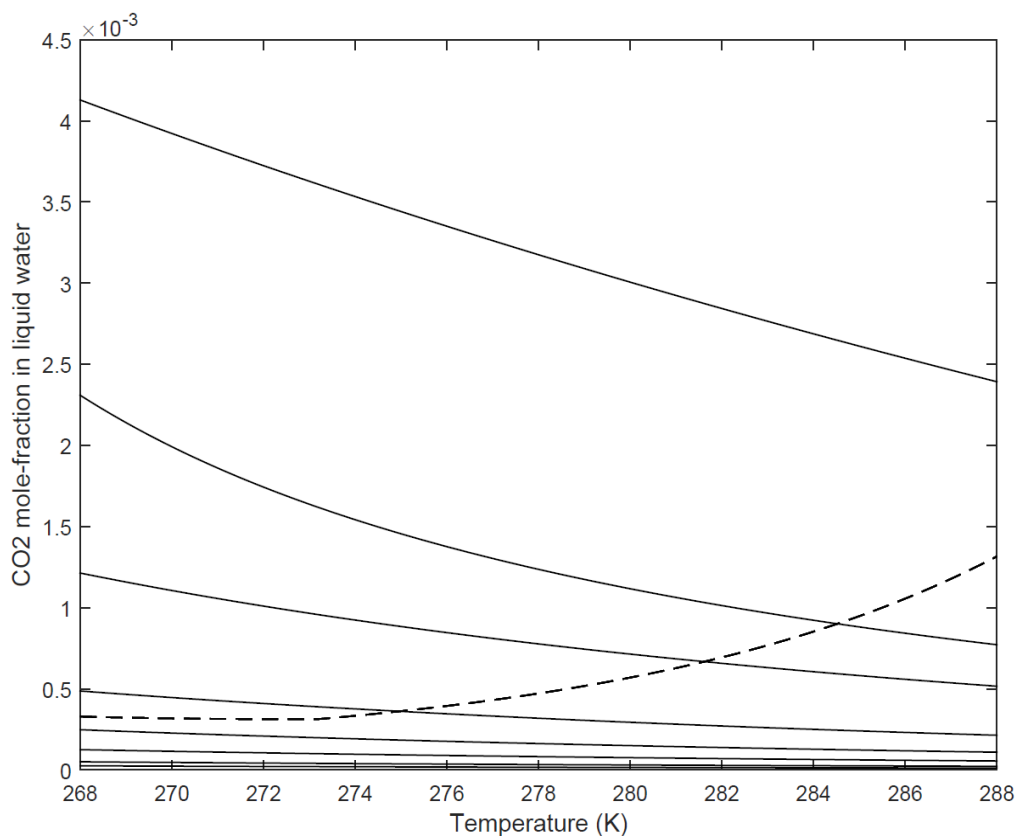
Figure 6.1.22: Mole-fraction of CO2 dissolved in liquid water (solid line) for varying concentrations of CO2 in gas. Top to bottom in mole percentage CO2 of gas: 100, 70, 50, 20, 10, 5, 2, 1. CO2 concentration in liquid water needed to keep hydrate stable (dashed line). Pressure is **90 bar**.

The figure illustrates that the CO2 dominated hydrate will dissociate towards water if the chemical potential of CO2 dissolved in water is lower than the chemical potential of CO2 in the aqueous solution. From above figure 6.1.22, it is observed that if the CO2 concentration in liquid water becomes lower than the ≈ 45% at 280 K, then hydrate may dissolve towards lean gas.

6.2 Limits of Hydrate Stability for Mixtures of CO2 and N2 – Mallik Field

In this section, the stability of hydrates inferred to occur in the Mallik L-38 well in the Mackenzie River Delta - Beufort Sea Region, Canada for different mixtures of CO2 has been estimated. The stability of the hydrates has been evaluated on the basis of estimated values of chemical potential of hydrate water & liquid water chemical potential as a function of temperature. The temperature and pressure range for the hydrate zone in the Mallik area considered here are from 276.75 K – 284.63 K & 79.38 bar – 108.03 bar respectively.

In the following graphs, the limits of hydrate stability for different mixtures of CO2 (100% CO2, 70% CO2, 50% CO2, 30% CO2, 20% CO2, 5% CO2, 2% CO2, 1% CO2) in terms of the estimated hydrate water chemical potential & liquid or ice water chemical potential as a function of temperature at pressures 90 bar, 100 bar, 150 bar, 200 bar, 250 bar has been calculated.

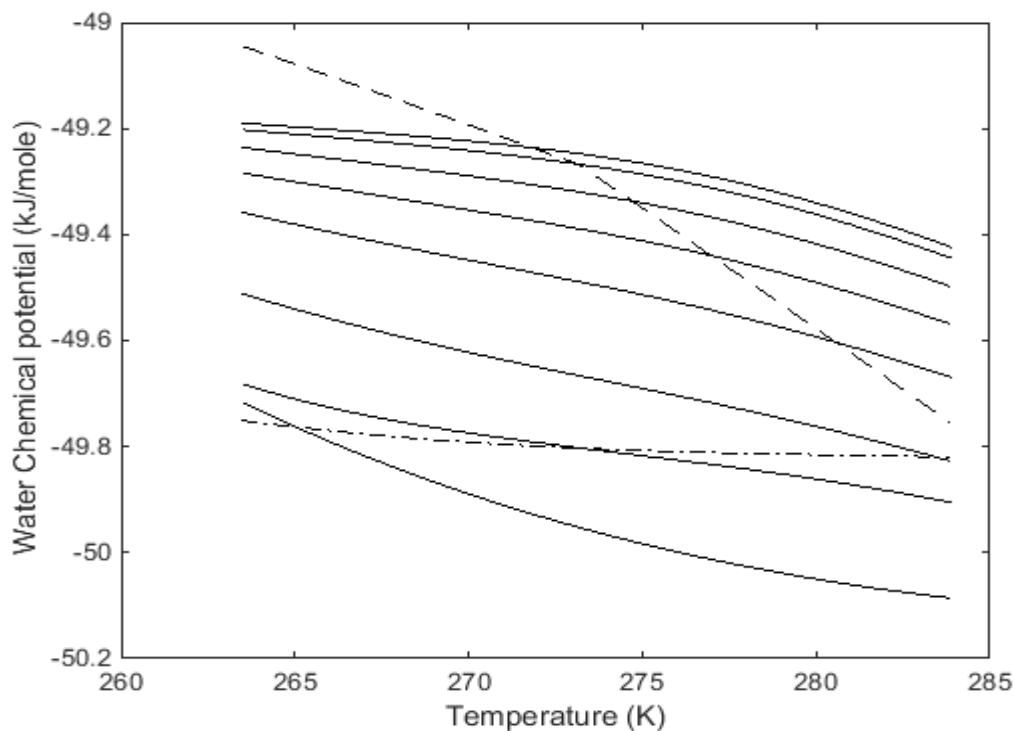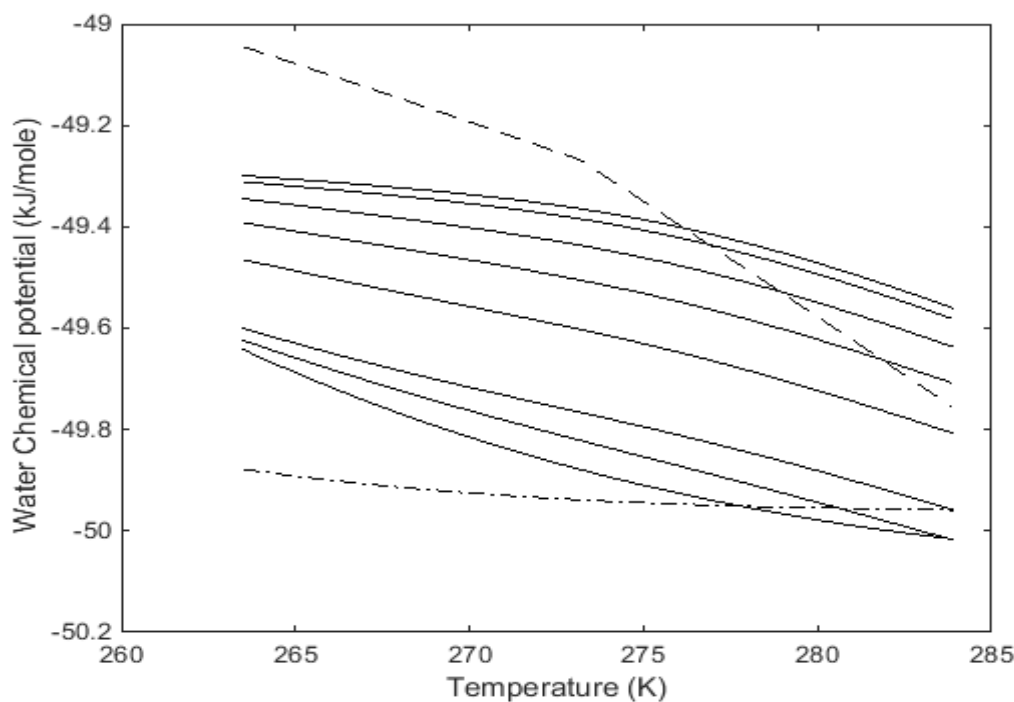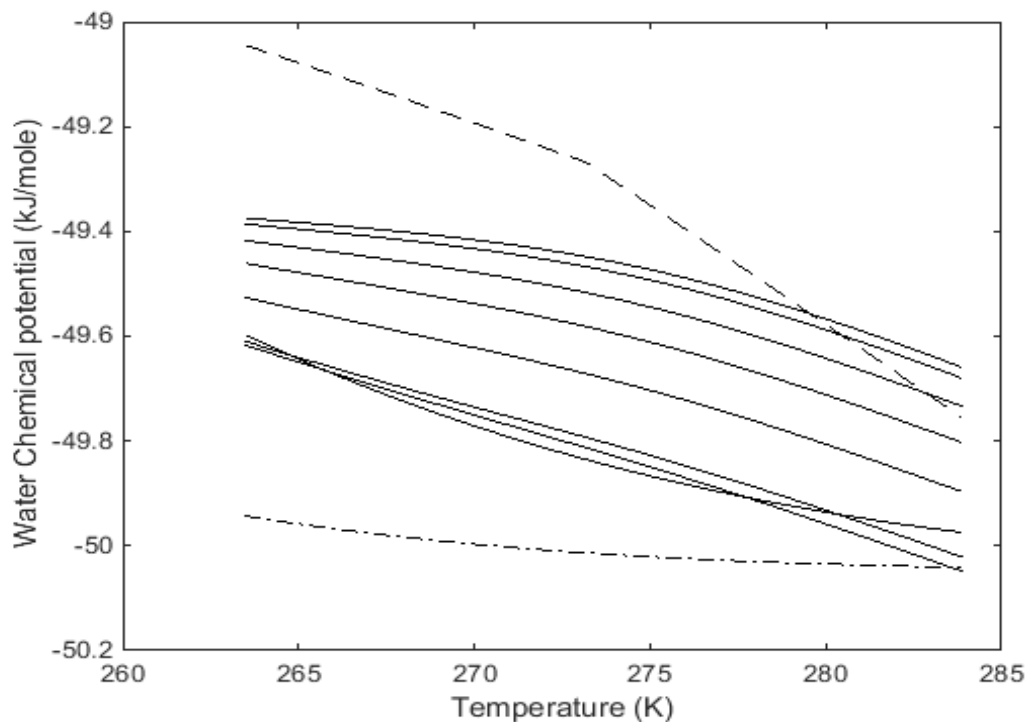

Figure 6.2.1: Estimated water chemical potential in hydrate (solid line) and liquid water chemical potential (dashed line) as a function of temperature for **90 bar** and CO2 mole percentage 100, 70, 50, 30, 20, 5, 2, 1 with 100 mole percentage CO2 at bottom & 1 mole percentage curve on the top. Estimated water chemical potential in pure CH4 hydrate (dash-dot line).

In above figure, the hydrate is not stable for mole fraction of CO2 less than 30% at 279 K & less than 50% at 284 K.

In figure 6.2.1 hydrate is not stable for mole fractions of CO2 less than 40% at temperature 282 K. From figure 6.2.1 to 6.2.5, it is observed that the region of instability has been reduced by increasing pressure from 90 bar to 250 bar.
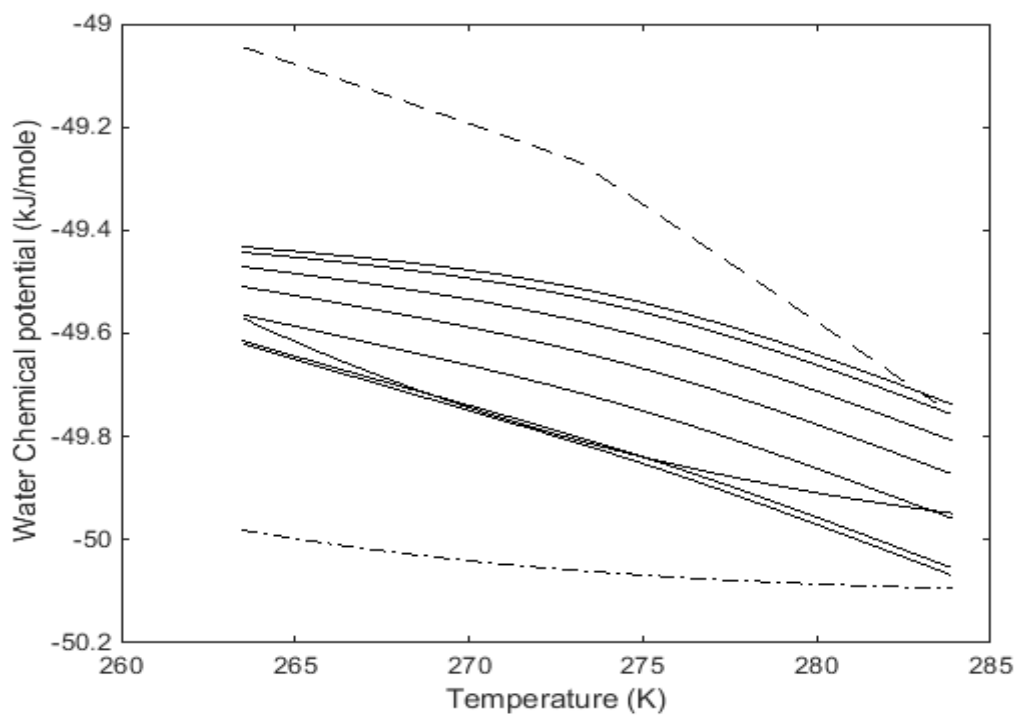
Figure 6.2.2: Estimated water chemical potential in hydrate (solid line) and liquid water chemical potential (dashed line) as a function of temperature for **100 bar** and CO2 mole percentage 100, 70, 50, 30, 20, 5, 2, 1 with 100 mole percentage CO2 at bottom & 1 mole percentage curve on the top. Estimated water chemical potential in pure CH4 hydrate (dash-dot line).

Figure 6.2.3: Estimated water chemical potential in hydrate (solid line) and liquid water chemical potential (dashed line) as a function of temperature for **150 bar** and CO2 mole percentage 100, 70, 50, 30, 20, 5, 2, 1 with 100 mole percentage CO2 at bottom & 1 mole percentage curve on the top. Estimated water chemical potential in pure CH4 hydrate (dash-dot line).

Figure 6.2.4: Estimated water chemical potential in hydrate (solid line) and liquid water chemical potential (dashed line) as a function of temperature for **200 bar** and CO2 mole percentage 100, 70, 50, 30, 20, 5, 2, 1 with 100 mole percentage CO2 at bottom & 1 mole percentage curve on the top. Estimated water chemical potential in pure CH4 hydrate (dash-dot line).

Figure 6.2.5: Estimated water chemical potential in hydrate (solid line) and liquid water chemical potential (dashed line) as a function of temperature for **250 bar** and CO2 mole percentage 100, 70, 50, 30, 20, 5, 2, 1 with 100 mole percentage CO2 at bottom & 1 mole percentage curve on the top. Estimated water chemical potential in pure CH4 hydrate (dash-dot line).

6.2.1 Chemical Potential Gradients for CH4 between Gas and Hydrate

In this section, chemical potential of methane as pure component at 90 bar and temperatures (calculated temperature for the region of log-inferred hydrate bearing zones in the Mallik field i.e. from 276 K to 285 K) is plotted. Figure 6.2.6 illustrates that the equilibrium pure methane hydrate (in which methane chemical potential in hydrate is same as the chemical potential of methane in gas phase) will dissociate due to guest chemical potential gradient.

Figure 6.2.6: Chemical potential of CH4 in pure methane hydrate (as created from CH4 gas and water so equal to pure methane gas chemical potential) (solid line) and 0.1 mole % CH4 in surrounding gas of varying mole-fraction of CO2 (dashed). Top to bottom in mole percentage CO2: 100, 70, 50, 20, 10, 5, 2, 1. Liquid water chemical potential (dashed). Pressure is **90 bar**.

6.2.2 CO2 Solubility in Liquid Water Needed to Keep Hydrate Stable

As mentioned previously in section 6.1.5, when gas gets diluted for CO2 it will not be able to support enough CO2 into the water phase to keep CO2 hydrate stable, so even formed CO2 hydrate may dissolve towards lean gas if the gas concentration of CO2 becomes less than needed.

In figure below the mole-fractions of CO2 in liquid water for varying concentration of CO2 in gas Vs CO2 concentration in liquid water needed to keep hydrate stable as a function of temperature has been plotted. In figure below 60% CO2 concentration in liquid water at 283 K is needed to keep hydrate stable.

Figure 6.2.7: Mole-fraction of CO2 dissolved in liquid water (solid line) for varying concentrations of CO2 in gas. Top to bottom in mole percentage CO2 of gas: 100, 70, 50, 20, 10, 5, 2, 1. CO2 concentration in liquid water needed to keep hydrate stable (dashed line). Pressure is **90 bar**.

6.3 Limits of Hydrate Stability for Mixtures of CO2 and N2- Nankai Trough

In this section the hydrate stability limits for different mixtures of CO2 & N2 in hydrate bearing units at depth between 190 m to 300 m below sea floor has been estimated in terms of chemical potentials. The hydrate bearing layer in Nankai Trough is found to be 16 m thick. The geophysical properties needed for the calculation of temperature and pressure for this region has been studied in detail in section 4.3. The calculated temperature range for hydrate bearing sediments in Nankai Trough corresponds to 285 K to 290 K.
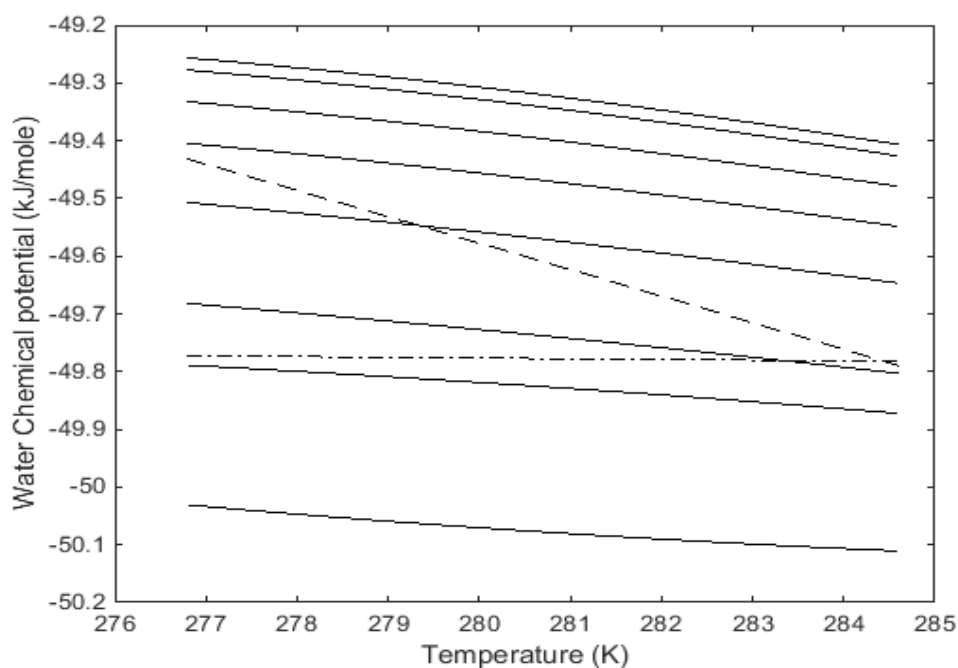

Figure 6.3.1: Estimated water chemical potential in hydrate (solid line) and liquid water chemical potential (dashed line) as a function of temperature for **90 bar** and CO2 mole percentage 100, 70, 50, 30, 20, 5, 2, 1 with 100 mole percentage CO2 at bottom & 1 mole percentage curve on the top. Estimated water chemical potential in pure CH4 hydrate (dash-dot line).

In above figure 6.3.1, hydrates are not stable for mole-fractions of CO2 less than 45% in gas mixture of CO2 & N2 at 282 K. At temperature 286 K, 70% CO2 in gas mixture is needed for hydrate stability.
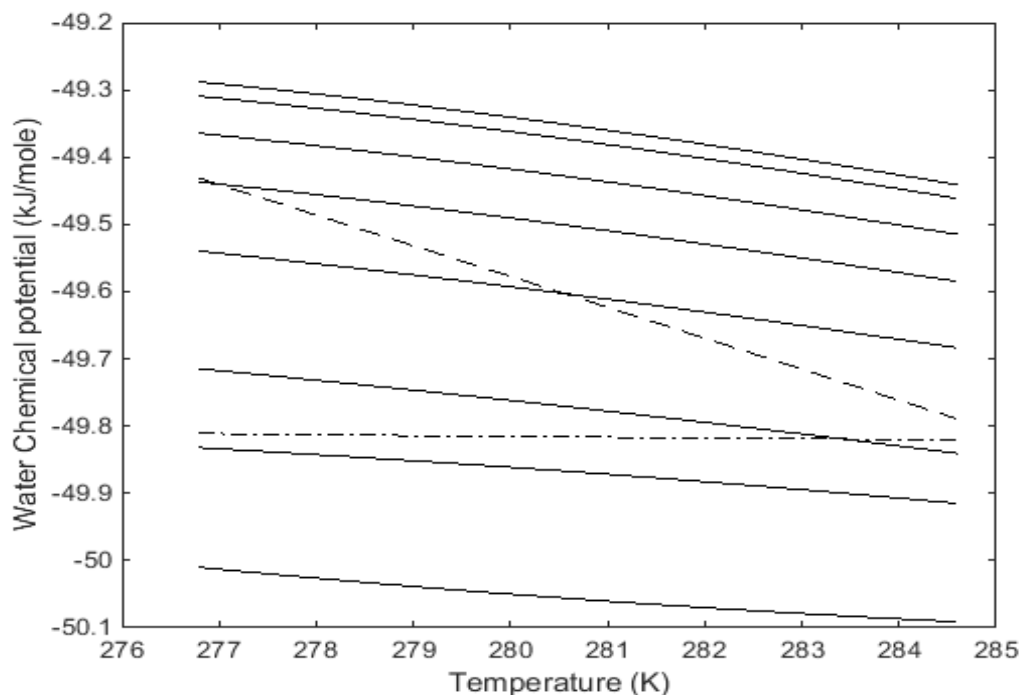
Figure 6.3.2: Estimated water chemical potential in hydrate (solid line) and liquid water chemical potential (dashed line) as a function of temperature for **100 bar** and CO2 mole percentage 100, 70, 50, 30, 20, 5, 2, 1 with 100 mole percentage CO2 at bottom & 1 mole percentage curve on the top. Estimated water chemical potential in pure CH4 hydrate (dash-dot line).
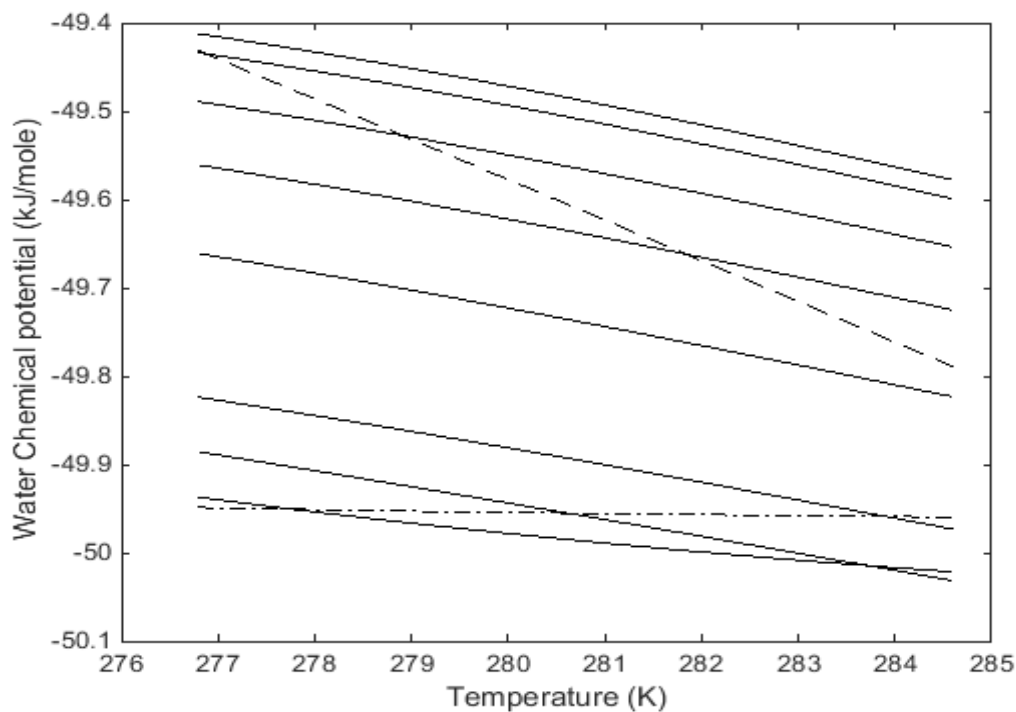

Figure 6.3.3: Estimated water chemical potential in hydrate (solid line) and liquid water chemical potential (dashed line) as a function of temperature for **150 bar** and CO2 mole percentage 100, 70, 50, 30, 20, 5, 2, 1 with 100 mole percentage CO2 at bottom & 1 mole percentage curve on the top. Estimated water chemical potential in pure CH4 hydrate (dash-dot line).
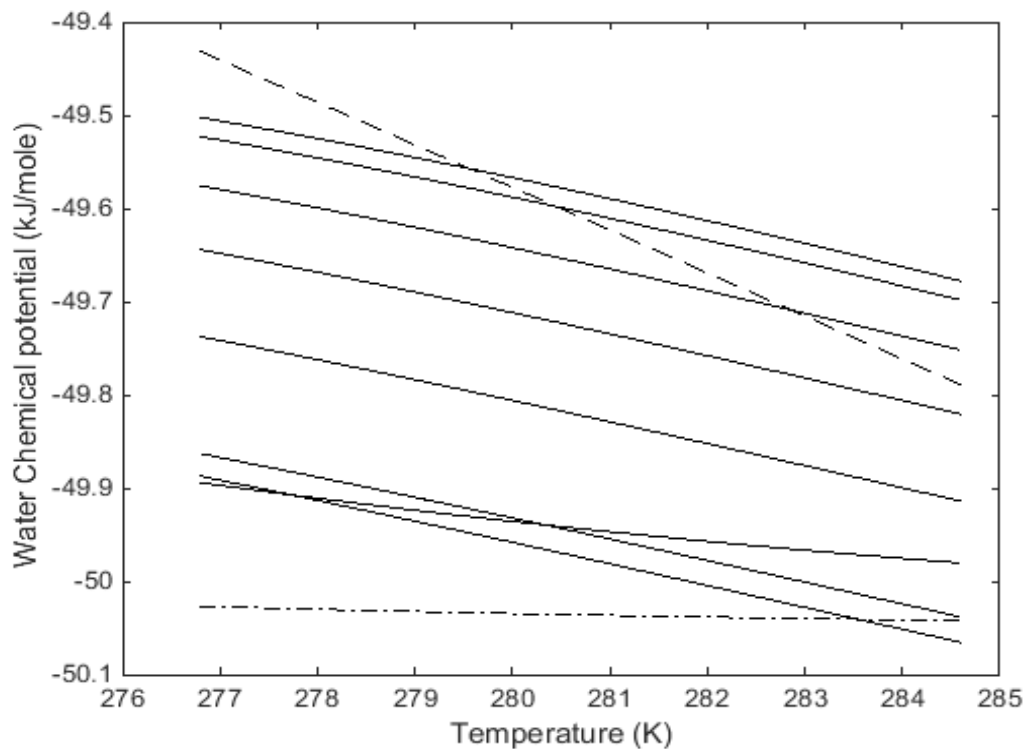
Figure 6.3.4: Estimated water chemical potential in hydrate (solid line) and liquid water chemical potential (dashed line) as a function of temperature for **200 bar** and CO2 mole percentage 100, 70, 50, 30, 20, 5, 2, 1 with 100 mole percentage CO2 at bottom & 1 mole percentage curve on the top. Estimated water chemical potential in pure CH4 hydrate (dash-dot line).
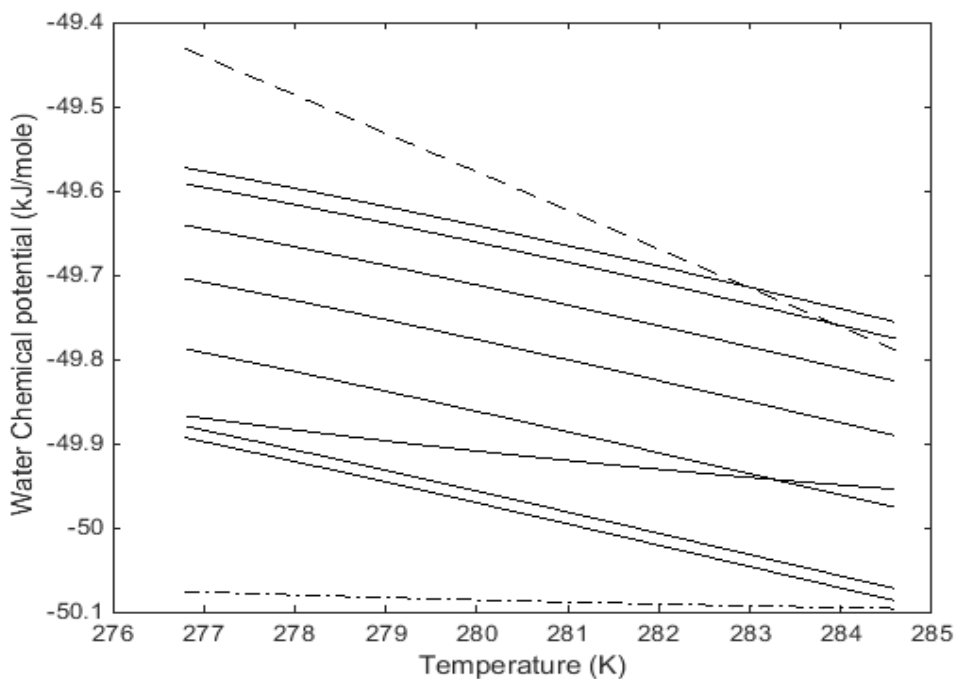

Figure 6.3.5: Estimated water chemical potential in hydrate (solid line) and liquid water chemical potential (dashed line) as a function of temperature for **250 bar** and CO2 mole percentage 100, 70, 50, 30, 20, 5, 2, 1 with 100 mole percentage CO2 at bottom & 1 mole percentage curve on the top. Estimated water chemical potential in pure CH4 hydrate (dash-dot line).

6.3.1 Chemical Potential Gradient for CH4 between Gas and Hydrate

In figure below 6.3.6, chemical potential of methane as pure component at pressure 90 bar vs temperature is plotted. The calculated temperature range for log-inferred hydrate bearing sediments in Nankai Trough vary from 284.35 K to 290 K. Gas hydrate occurrences are strongly related to temperatures.
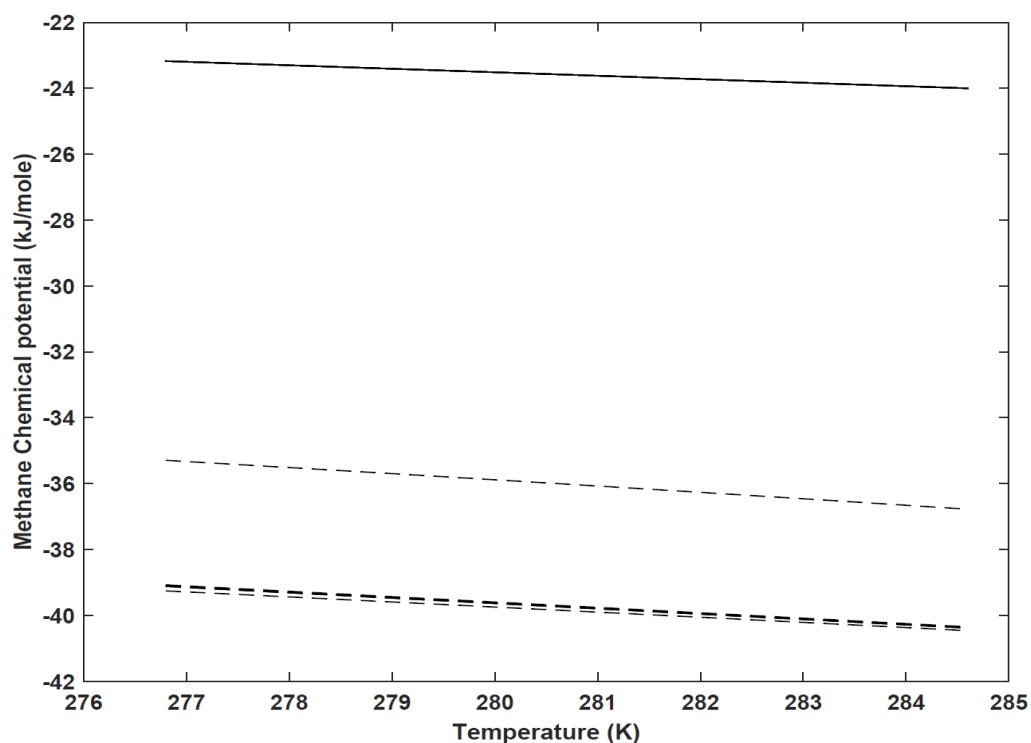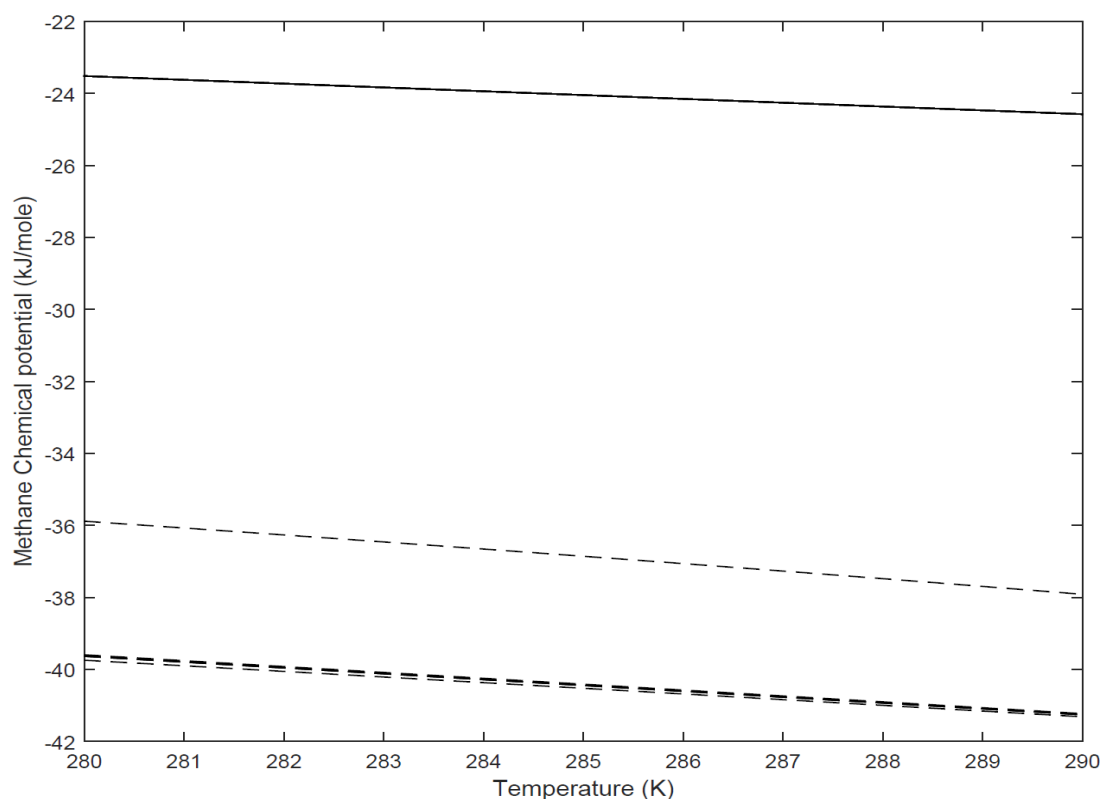

Figure 6.3.6: Chemical potential of CH4 in pure methane hydrate (as created from CH4 gas and water so equal to pure methane gas chemical potential) (solid line) and 0.1 mole % CH4 in surrounding gas of varying mole-fraction of CO2 (dashed). Top to bottom in mole percentage CO2: 100, 70, 50, 20, 10, 5, 2, 1. Liquid water chemical potential (dashed). Pressure is **90 bar.**

6.3.2 CO2 Solubility in Liquid Water Needed to Keep Hydrate Stable

In the graph constructed below, CO2 mole-fraction in liquid water for varying concentration of CO2 in gas mixtures and CO2 concentration in liquid water needed to keep hydrate stable as a function of temperature has been plotted. The figure 6.3.7 shows that 70% CO2 must be dissolved in liquid water to keep hydrate stable at temperature 284 K. At slightly lower temperature of 280 K, 40% CO2 concentration in liquid water needed to keep hydrate stable.
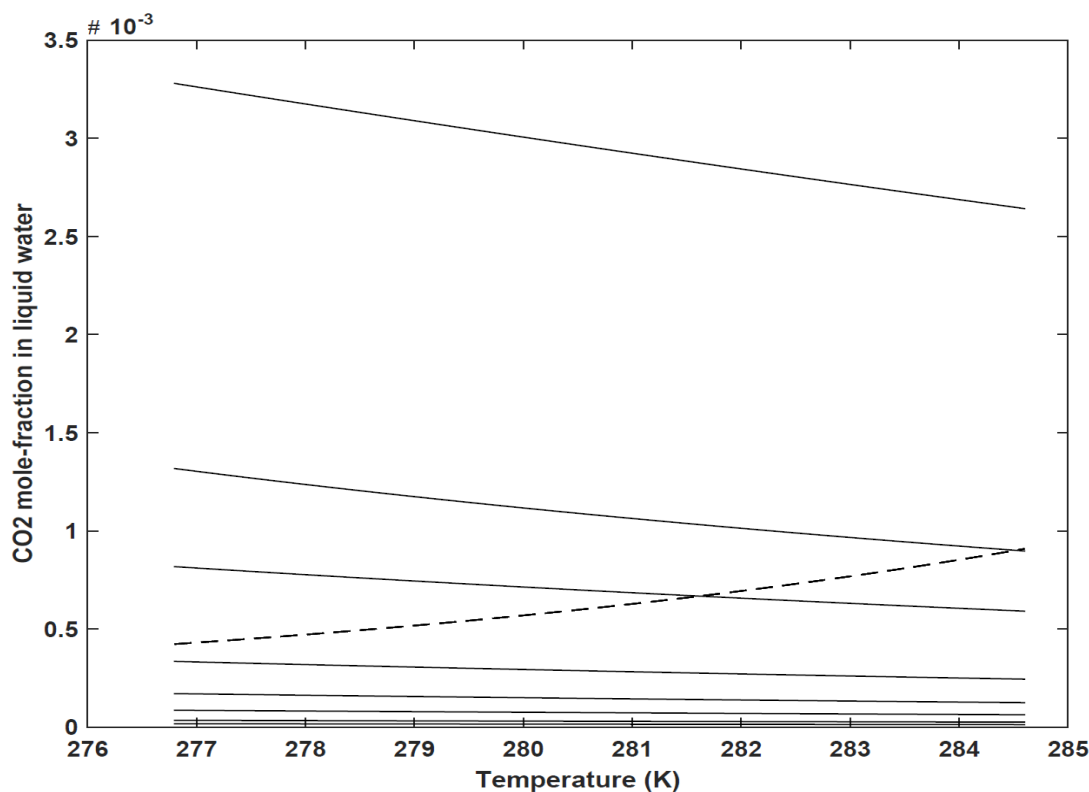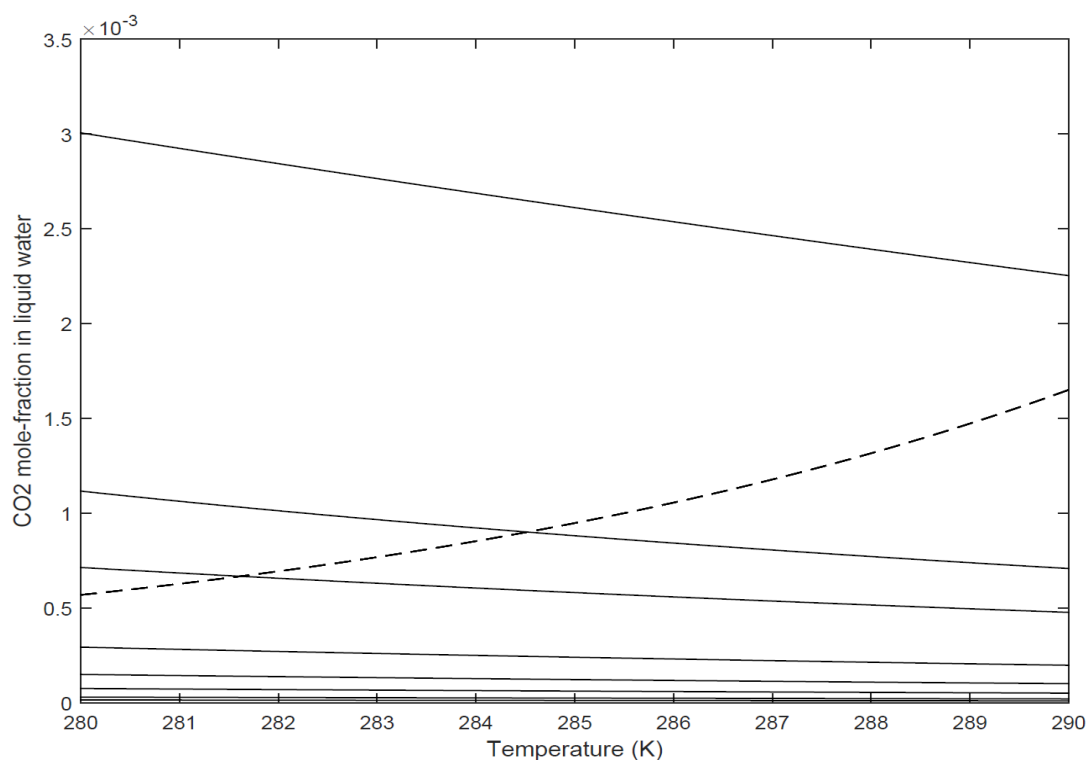

Figure 6.3.7: Mole-fraction of CO2 dissolved in liquid water (solid line) for varying concentrations of CO2 in gas. Top to bottom in mole percentage CO2 of gas: 100, 70, 50, 20, 10, 5, 2, 1. CO2 concentration in liquid water needed to keep hydrate stable (dashed line). Pressure is **90 bar.**

6.4 Limits of Hydrate Stability for Mixtures of CO2 & N2 – Bjørnøya Basin

The graph constructed below evaluates the limits of hydrate stability as a function of temperature for different mixtures of CO2 & N2 for hydrate bearing units in Bjørnøya Basin in Barents Sea at pressure 90 bar, 100 bar, 150 bar, 200 bar & 250 bar. Thickness of the suspected GH bearing zone in Barents Sea corresponds to 100 m. Temperature calculated at the bottom of suspected hydrate zone is approximately 9.7 °C i.e. 282.85 K.
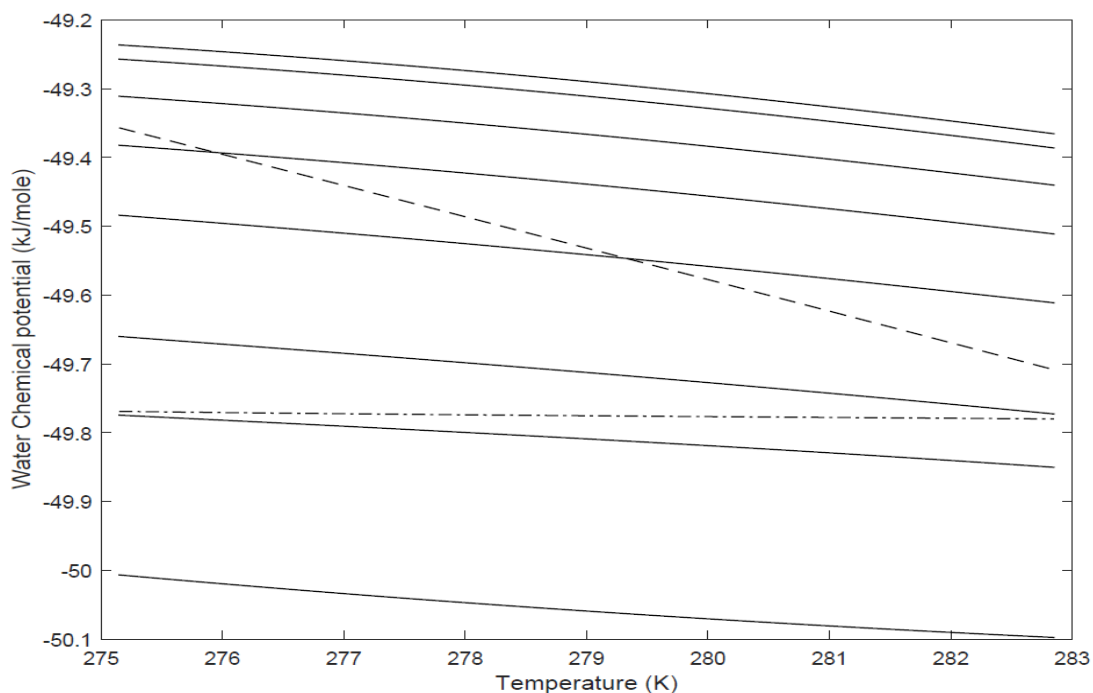
Figure 6.4.1: Estimated water chemical potential in hydrate (solid line) and liquid water chemical potential (dashed line) as a function of temperature for **90 bar** and CO2 mole percentage 100, 70, 50, 30, 20, 5, 2, 1 with 100 mole percentage CO2 at bottom & 1 mole percentage curve on the top. Estimated water chemical potential in pure CH4 hydrate (dash-dot line).

In above figure 6.4.1, hydrate is not stable for mole-fraction of CO2 less than 20% at 276 K. At temperature 279 K, 30% CO2 is needed for hydrate stability & 50% CO2 is needed at 283 K.
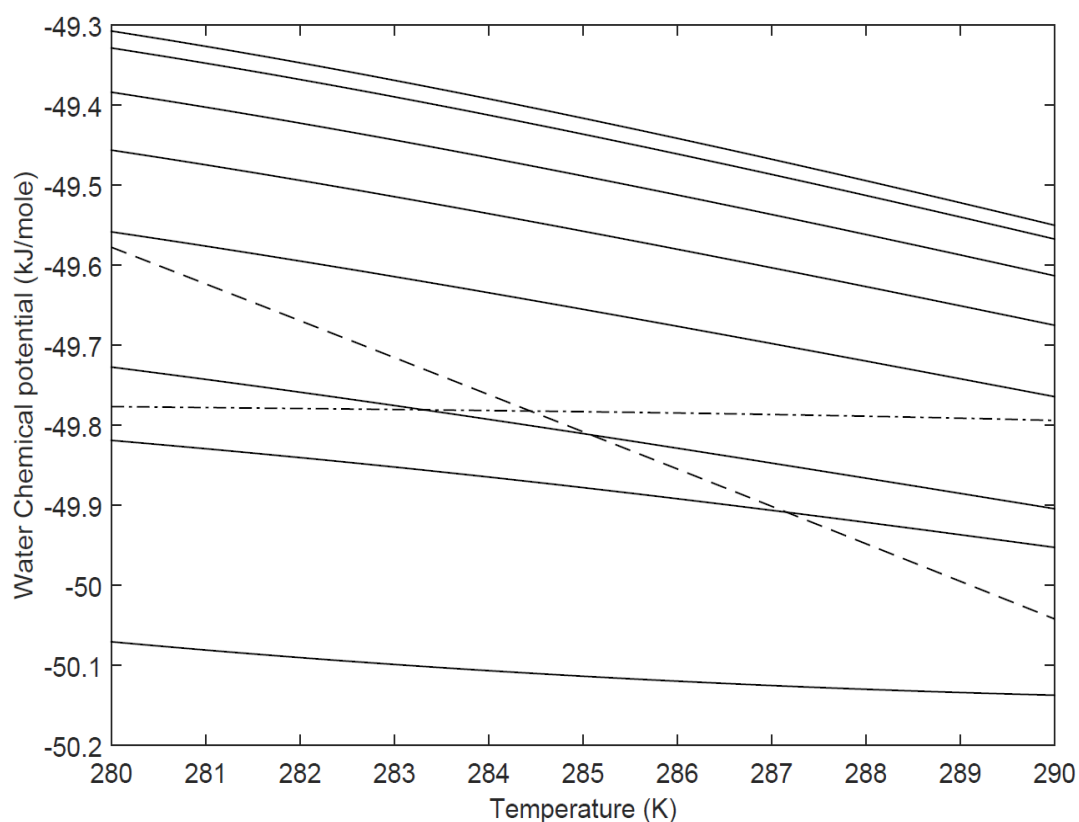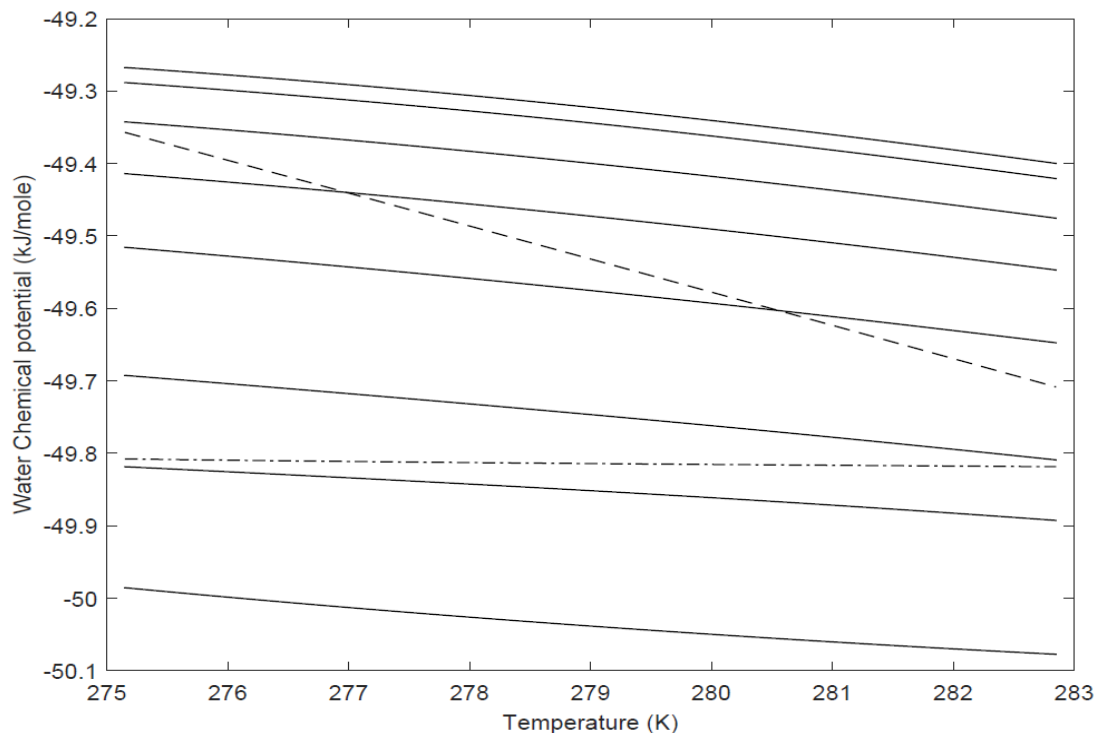
Figure 6.4.2: Estimated water chemical potential in hydrate (solid line) and liquid water chemical potential (dashed line) as a function of temperature for **100 bar** and CO2 mole percentage 100, 70, 50, 30, 20, 5, 2, 1 with 100 mole percentage CO2 at bottom & 1 mole percentage curve on the top. Estimated water chemical potential in pure CH4 hydrate (dash-dot line).
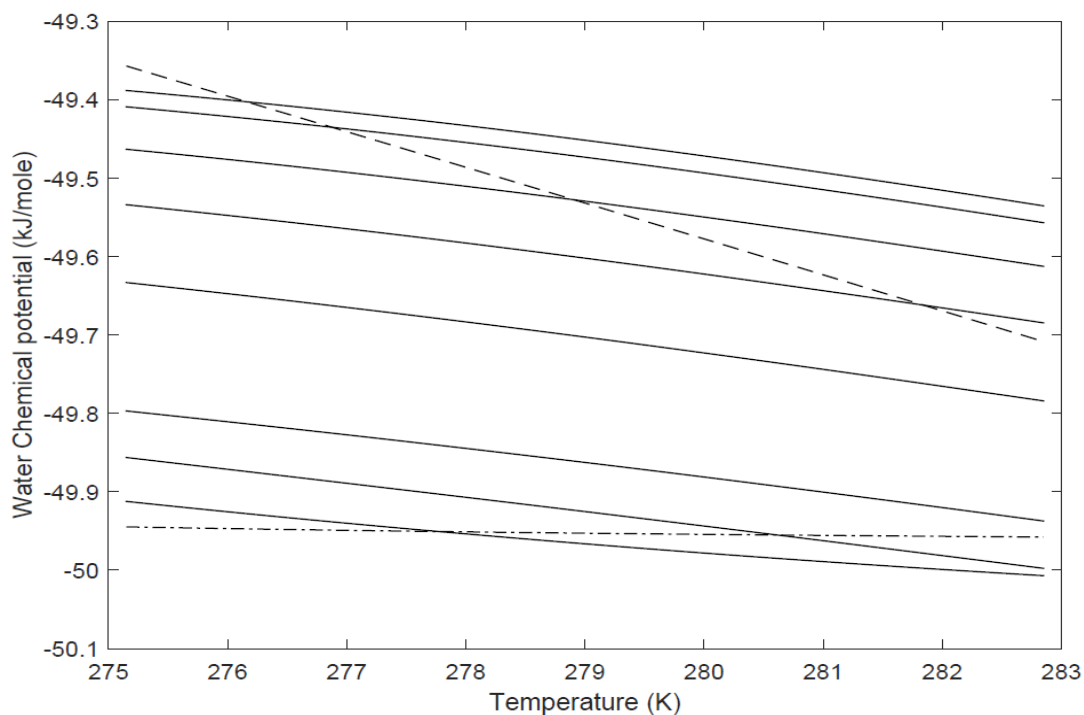
Figure 6.4.3: Estimated water chemical potential in hydrate (solid line) and liquid water chemical potential (dashed line) as a function of temperature for **150 bar** and CO2 mole percentage 100, 70, 50, 30, 20, 5, 2, 1 with 100 mole percentage CO2 at bottom & 1 mole percentage curve on the top. Estimated water chemical potential in pure CH4 hydrate (dash-dot line).
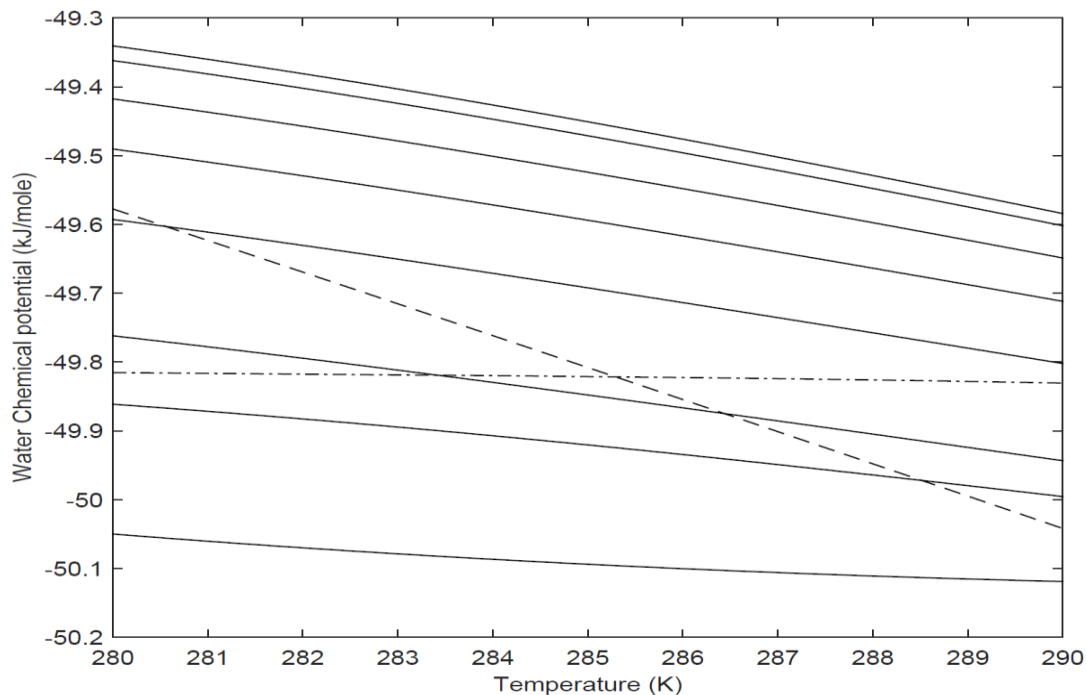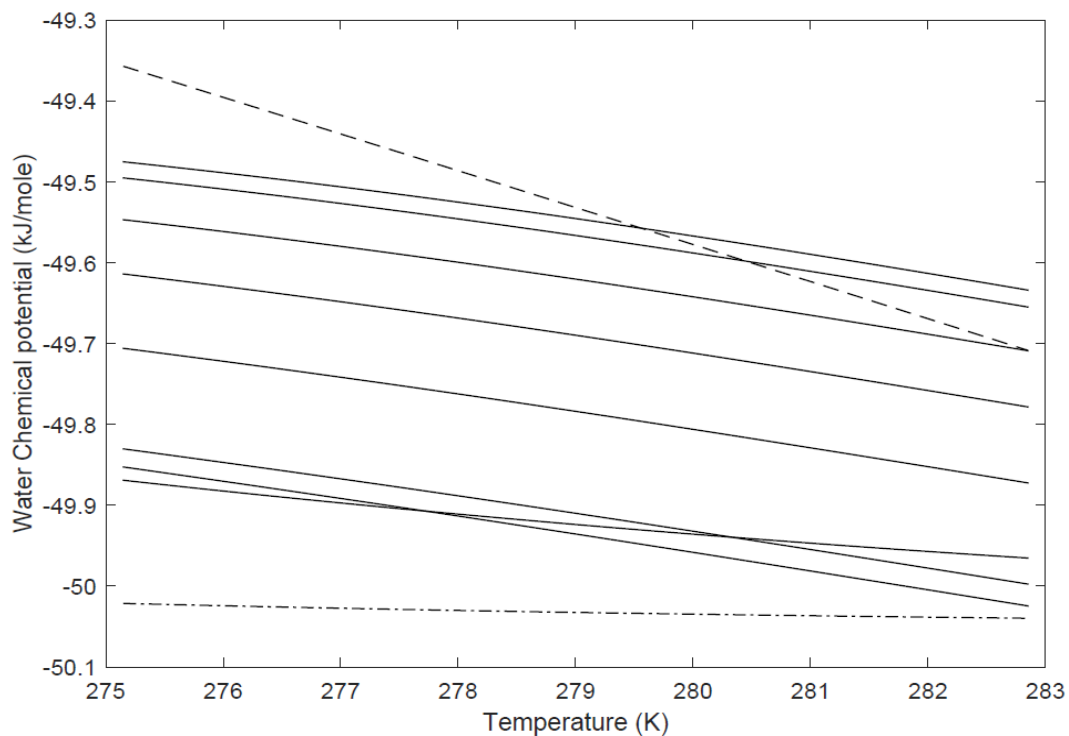
Figure 6.4.4: Estimated water chemical potential in hydrate (solid line) and liquid water chemical potential (dashed line) as a function of temperature for **200 bar** and CO2 mole percentage 100, 70, 50, 30, 20, 5, 2, 1 with 100 mole percentage CO2 at bottom & 1 mole percentage curve on the top. Estimated water chemical potential in pure CH4 hydrate (dash-dot line).
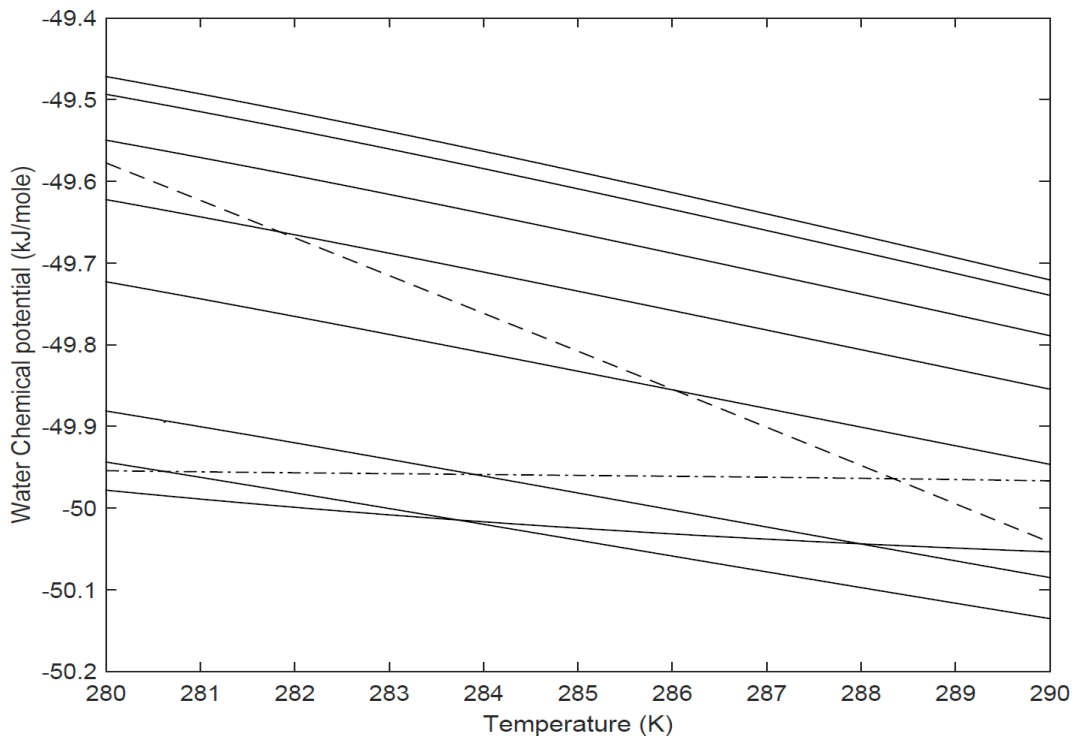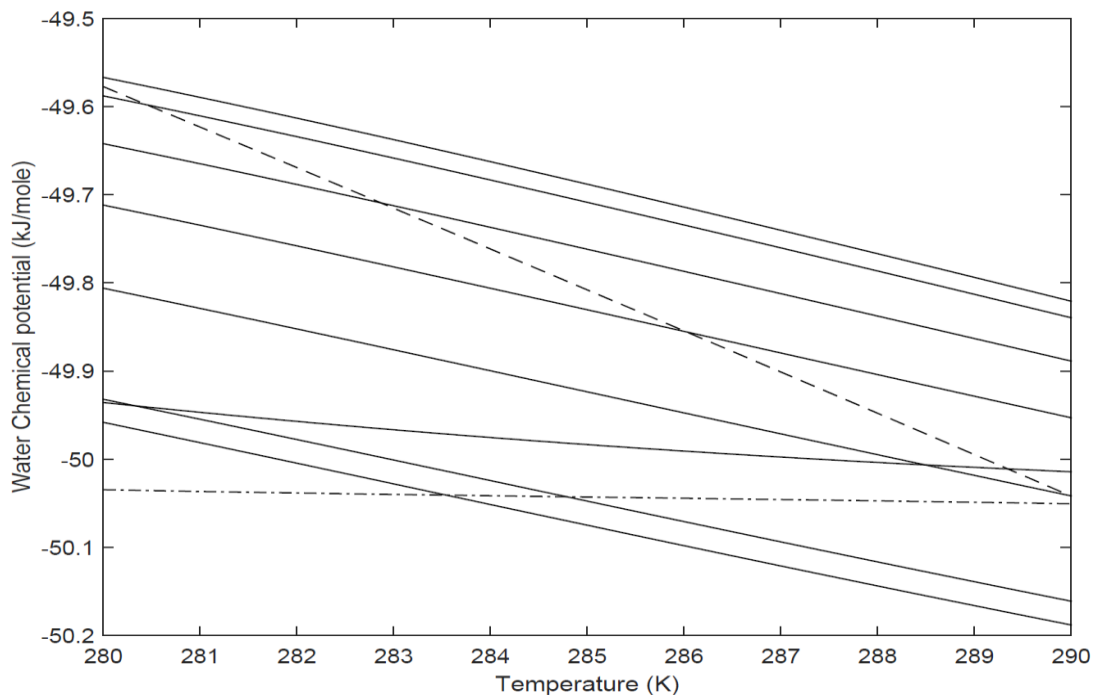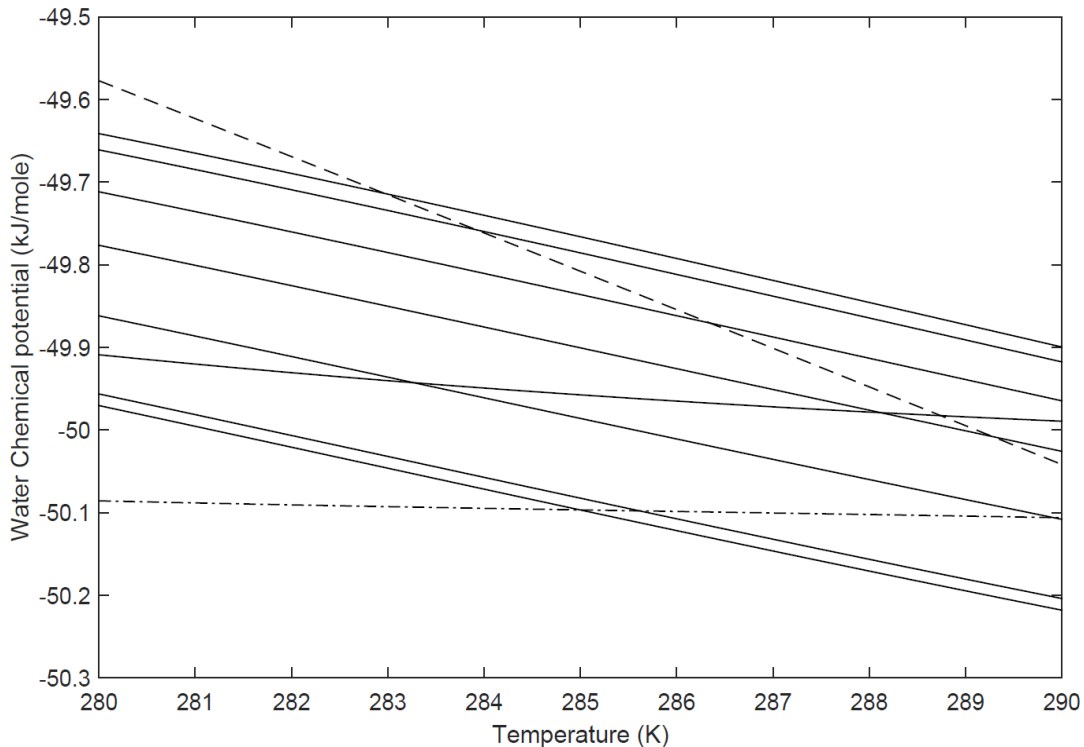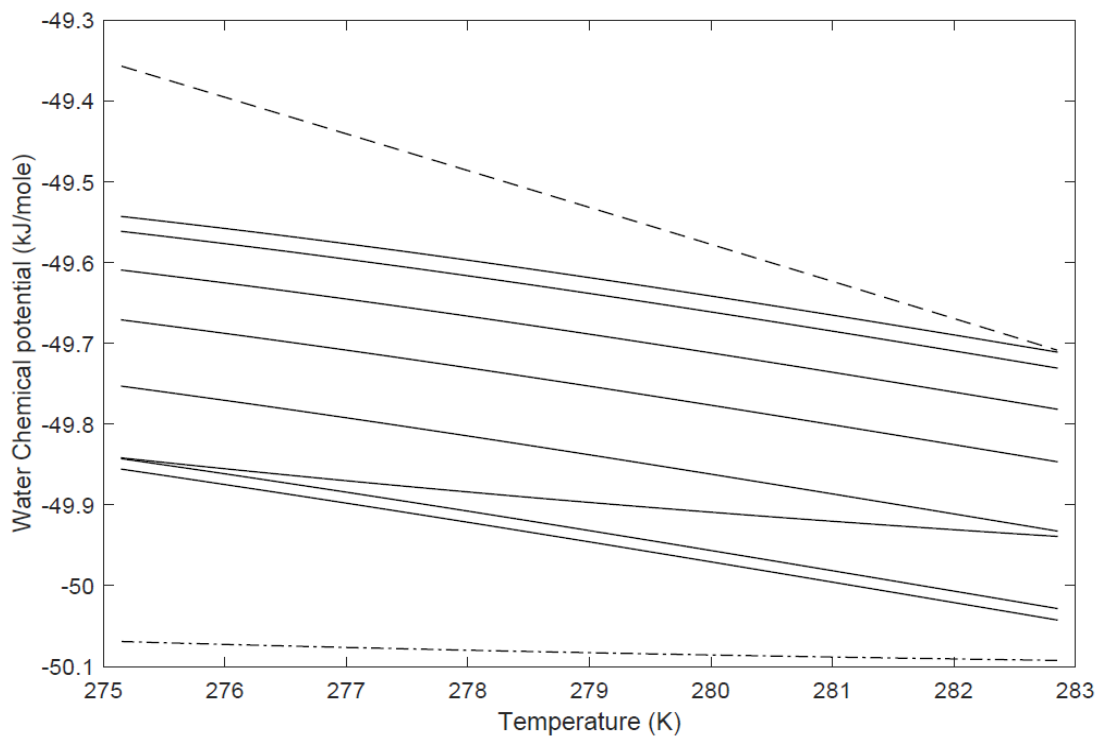

Figure 6.4.5: Estimated water chemical potential in hydrate (solid line) and liquid water chemical potential (dashed line) as a function of temperature for **250 bar** and CO2 mole percentage 100, 70, 50, 30, 20, 5, 2, 1 with 100 mole percentage CO2 at bottom & 1 mole percentage curve on the top. Estimated water chemical potential in pure CH4 hydrate (dash-dot line).

6.4.1 Chemical Potential Gradient for CH4 between Gas and Hydrate

In the graph constructed below the chemical potential of methane as a pure component has been plotted against the temperature at pressure 90 bar. Dashed lines in figure 6.4.6 are for 0.1% methane in different mixtures of CO_2 and N_2.
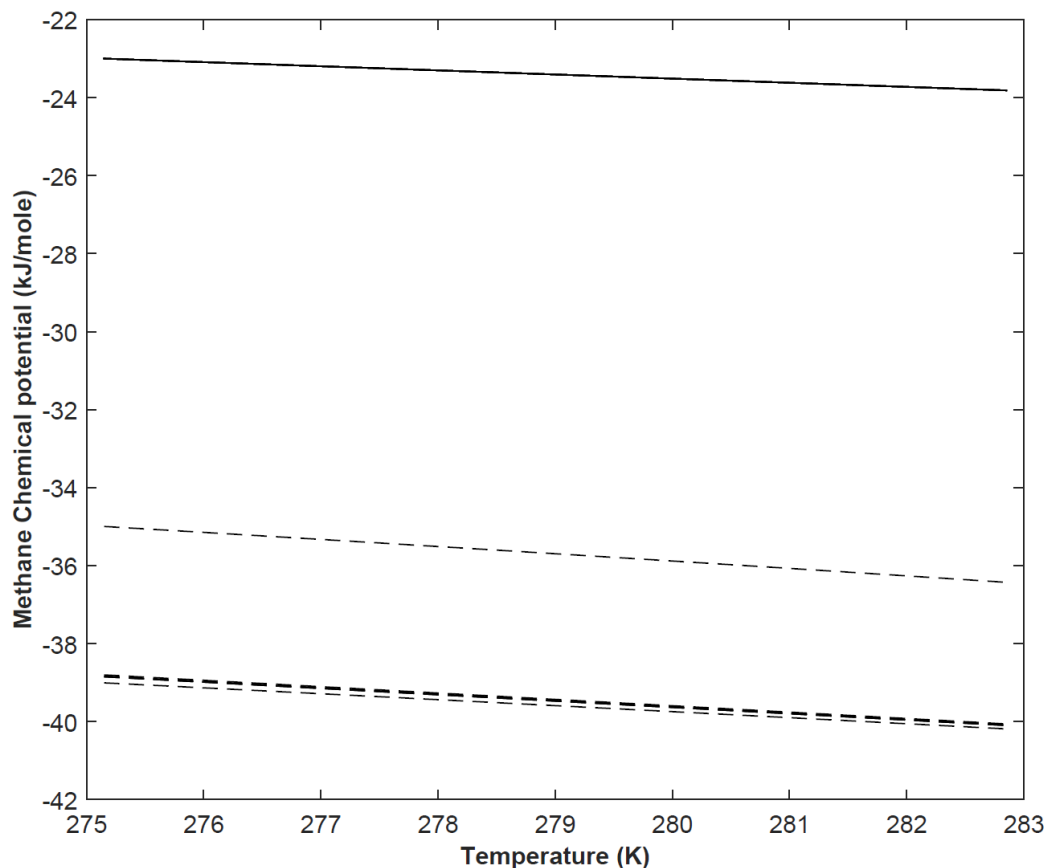
Figure 6.4.6: Chemical potential of CH4 in pure methane hydrate (as created from CH4 gas and water so equal to pure methane gas chemical potential) (solid line) and 0.1 mole % CH4 in surrounding gas of varying mole-fraction of CO_2 (dashed). Top to bottom in mole percentage CO2: 100, 70, 50, 20, 10, 5, 2, 1. Liquid water chemical potential (dashed). Pressure is **90 bar.**

Figure 6.4.6 illustrates that hydrate dissociates towards gas due to guest (methane) chemical potential i.e. due to the difference in chemical potential of methane in methane hydrate and methane diluted in CO2/N2 mixture.

6.4.2 CO2 Solubility in Liquid Water Needed to Keep Hydrate Stable

In the graph constructed below, the mole-fraction of CO2 dissolved in liquid water for varying concentration of CO2 in gas Vs temperature at pressure 90 bar has been plotted. The dashed line in figure indicates the amount of CO2 required to be dissolved in CO2 to be hydrate stable.
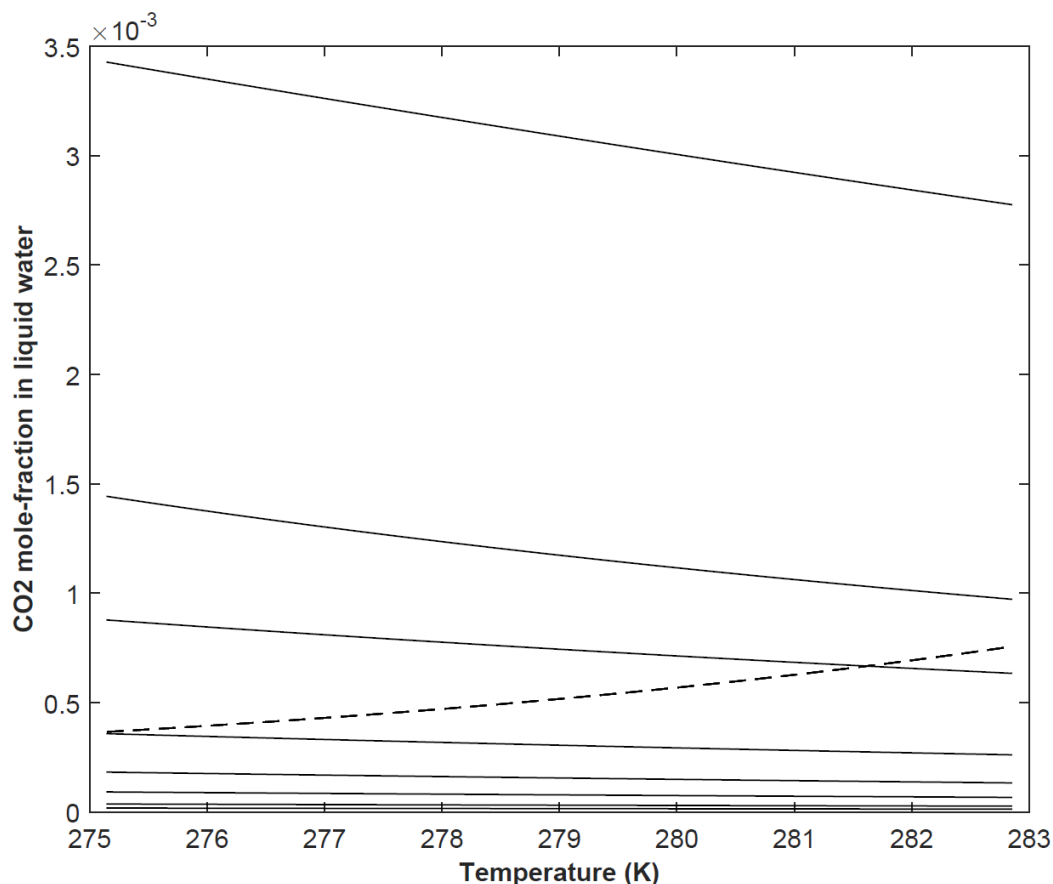
Figure 6.4.7: Mole-fraction of CO2 dissolved in liquid water (solid line) for varying concentrations of CO2 in gas. Top to bottom in mole percentage CO2 of gas: 100, 70, 50, 20, 10, 5, 2, 1. CO2 concentration in liquid water needed to keep hydrate stable (dashed line). Pressure is **90 bar**.

In above figure 6.4.7, 20% CO2 is needed to be dissolved in liquid water at temperature 275 K for hydrate stability. If the gas concentration of CO2 becomes less than 50% at temperature 281 K then CO2 hydrate may dissociate towards lean gas.

6.5 Maximum water content in gas

The hydrocarbons containing water in transport pipelines may cause hydrate formation and deposition which results in severe problems like pipeline plugging. The transport of CO2 in offshore pipelines involves high pressure and low temperature and these conditions are suitable for hydrate formation from residual water dissolved in CO2 and CO2 gas. Hydrate formation in pipeline generally leads to increase of the pressure drop. In worst situation, it is associated with the growth of plugs which can leads to complete blockage in pipeline. Many companies are investing both time and money to avoid such problems. So in this section it has been evaluated the amount of water that can be permitted in gas stream in order to avoid the risk of formation of hydrate deposits in pipeline which results in pipeline plugging while transporting hydrocarbons on the sea floor or in cold regions. In this case two approximations for water are considered, first water at certain temperature and pressure will drop out as liquid droplets and forms hydrate, or another possibility is that water adsorbs on pipeline surfaces and subsequently forms hydrates heterogeneously (Kivelæ et.al, 2012a).

In this section estimated the maximum limits of water content in the gas before dropping out as liquid water, hydrate and as adsorbed onto hematite (rust) surface, based on the thermodynamic model by (Kvamme & Tanaka, 1995). The SRK (Soave-Redlich-Kwong) equation of state has been applied for the gas phase in these calculations and also for water dissolved in the gas as an approximation.

The classical method of hydrate problem evaluation is based on assumption of equilibrium. In thermodynamics the basic fundamental principle of Gibbs Phase Rule has been used to determine whether the system can reach equilibrium or not. Gibbs Phase Rule can be represented as,

$$F = n - \prod + 2 \tag{18}$$

Where F = Number of degrees of freedom

n = Number of components

$\prod$ = Number of phases

Gibbs Phase Rule tells us that if the number of degrees of freedom is equal to the number of variables defined, then the system can reach equilibrium. If number of degrees of freedom is greater than what is thermodynamically defined then the system is said to be underdetermined and if F is less than what is defined then the system said to be thermodynamically overdetermined (Kvamme, 2013b). In summary Gibbs phase rule is a balance of mass conservation under the constraints of equilibrium. But according to Gibbs Phase Rule systems undergoing hydrate formation during transport and processing of hydrocarbons & carbon dioxide will not reach equilibrium, specifically when the adsorption on solid surfaces and hydrate formation close to these surfaces are considered (Kivelæ et.al, 2012a). Hence the transport of gases through pipelines becomes challenging issue due to hydrate risk associated with it.

In view of the above, the maximum water content permitted in gas stream while transport of gas at the North Slope of Alaska has been evaluated. Because of the Alaska region being very cold, temperature range considered here during transport vary between -50 °C to 10 °C. So the relevant temperature – pressure transport conditions considered here ranges from 220 K to 280 K and 50 bar to 250 bar respectively.

So once theoretical amount of allowable water content while transport of gas through pipelines is calculated, the appropriate action can be taken for hydrate risk management.

The results are plotted for following three cases

1. Mole-fraction of water before drop out as liquid
2. Mole-fraction of water before hydrate drop out
3. Mole-fraction of water before adsorption on hematite.

6.5.1 Estimation of Mole- fraction of water in pure CO2

In this section, the maximum amount of water before drop out as liquid, maximum amount of water before hydrate drop out and the maximum amount of water before adsorption on hematite for pure CO2 gas stream.
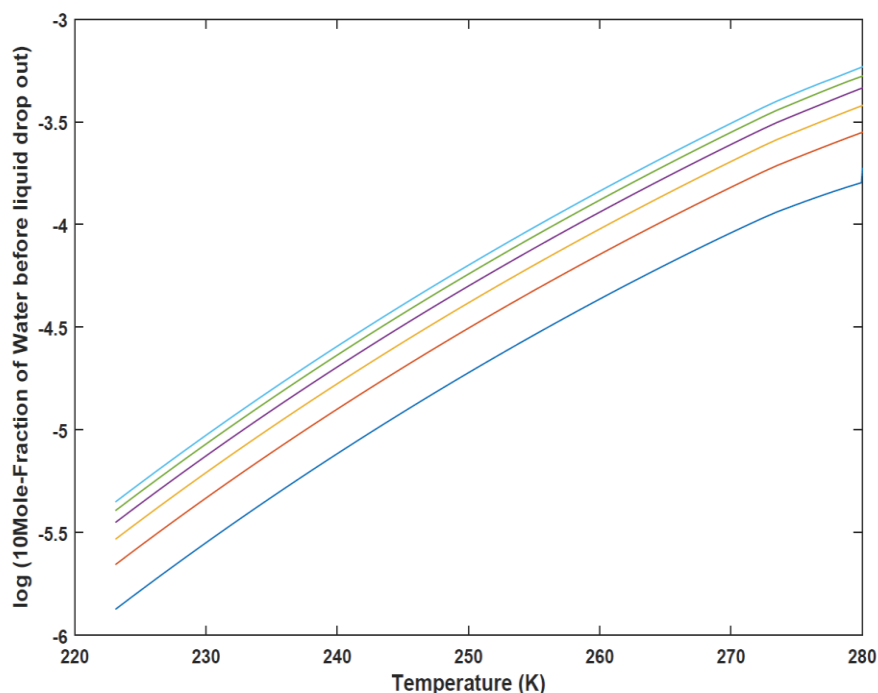
Figure 6.5.1: Maximum Water content before water drop out for mole fraction of 99.9% CO2, 0.01% H2S, 0.01% N2. Curves from bottom to top correspond to pressure 50 bar, 90 bar, 130 bar, 170 bar, 210 bar, 250 bar.
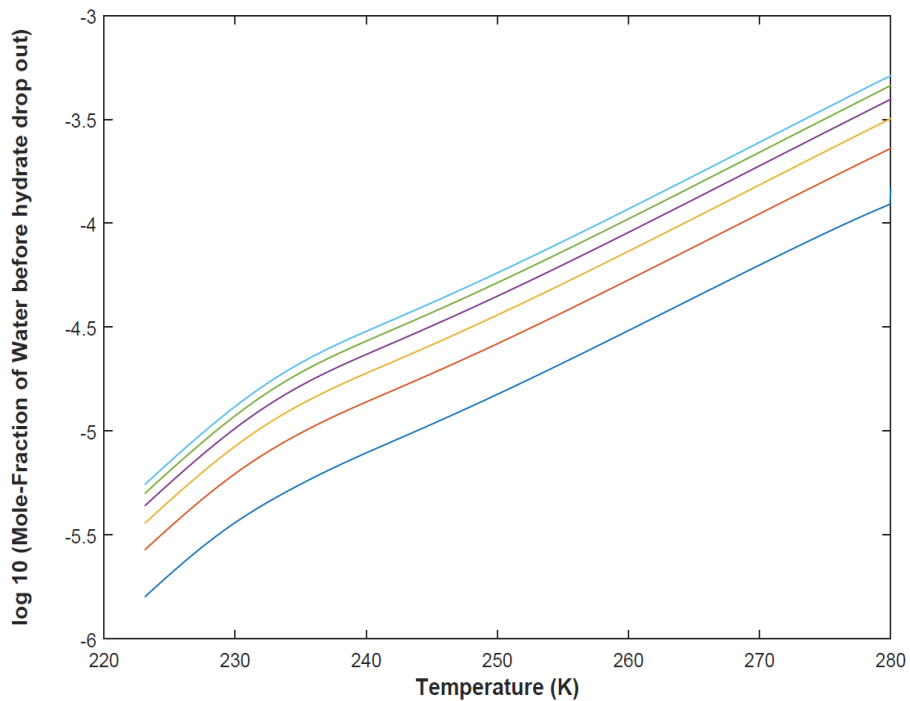
Figure 6.5.2: Maximum Water content before hydrate drop out for mole fraction of 99.9 % CO2, 0.01% H2S, 0.01% N2. Curves from bottom to top correspond to pressure 50 bar, 90 bar, 130 bar, 170 bar, 210bar, 250 bar.
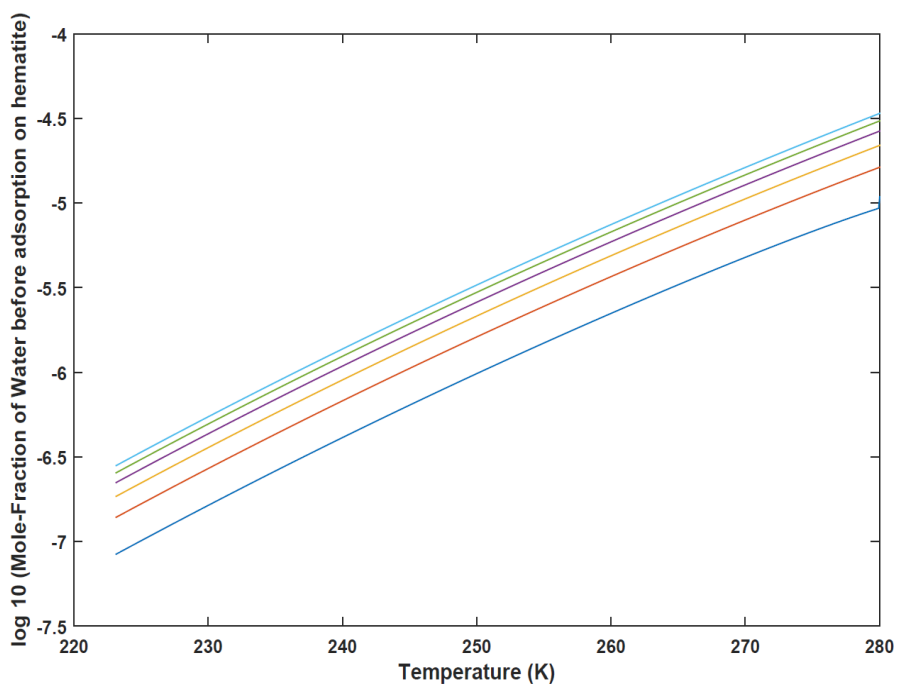
Figure 6.5.3: Maximum Water content before adsorption on hematite for mole fraction of 99.9 % CO2, 0.01% H2S, 0.01% N2. Curves from bottom to top correspond to pressure 50 bar, 90 bar, 130 bar, 170 bar, 210bar, 250 bar.

6.5.2 Estimation of Mole-fraction of water in 1/3 CO2 and 2/3 N2 mixture

In this section, the maximum amount of water before drop out as liquid, maximum amount of water before hydrate drop out and the maximum amount of water before adsorption on hematite in system containing 33.33% CO2 + 66.66% N2 + 0.01% H2S mixture has been plotted.
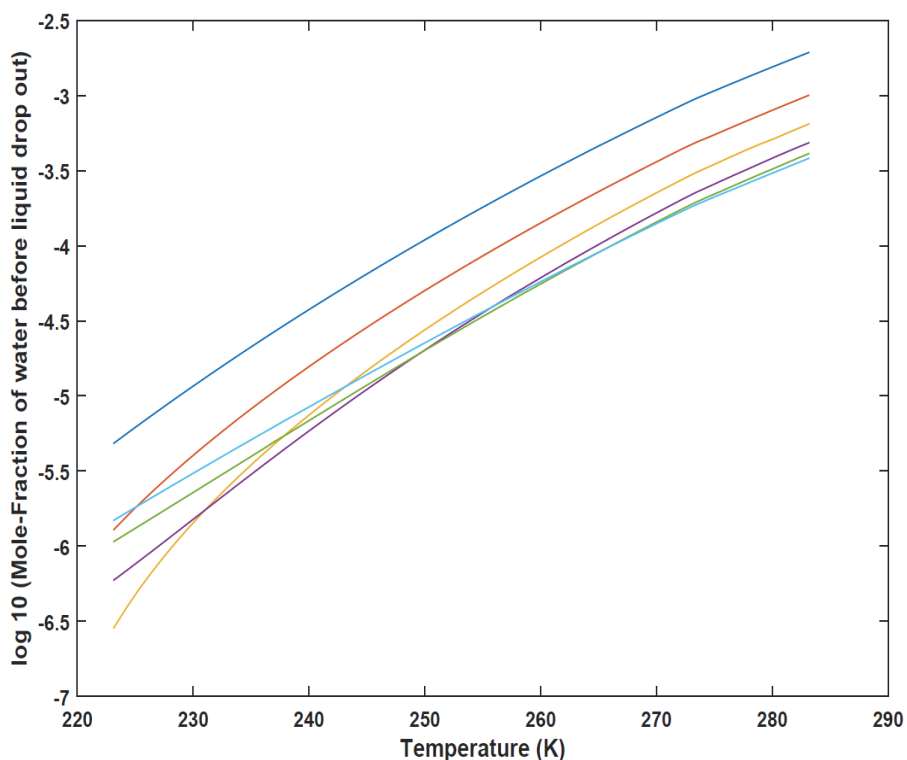
Figure 6.5.4: Maximum Water content before water drop out for mole fraction of 33.33% CO2, 0.01% H2S, 66.66% N2. Curves from top to bottom correspond to pressure 50 bar, 90 bar, 130 bar, 170 bar, 210 bar, 250 bar.

In above figure 6.5.4 it is observed that there is not much difference in maximum water content before water drop out at high pressures like 210 bar & 250 bar. In contrast considerable difference is observed at low pressures.

In figure 6.5.5 & 6.5.6 illustrated the maximum water content before hydrate drop out & before adsorption on hematite respectively for system containing 33.33% CO2 + 66.66% N2 + 0.01%.
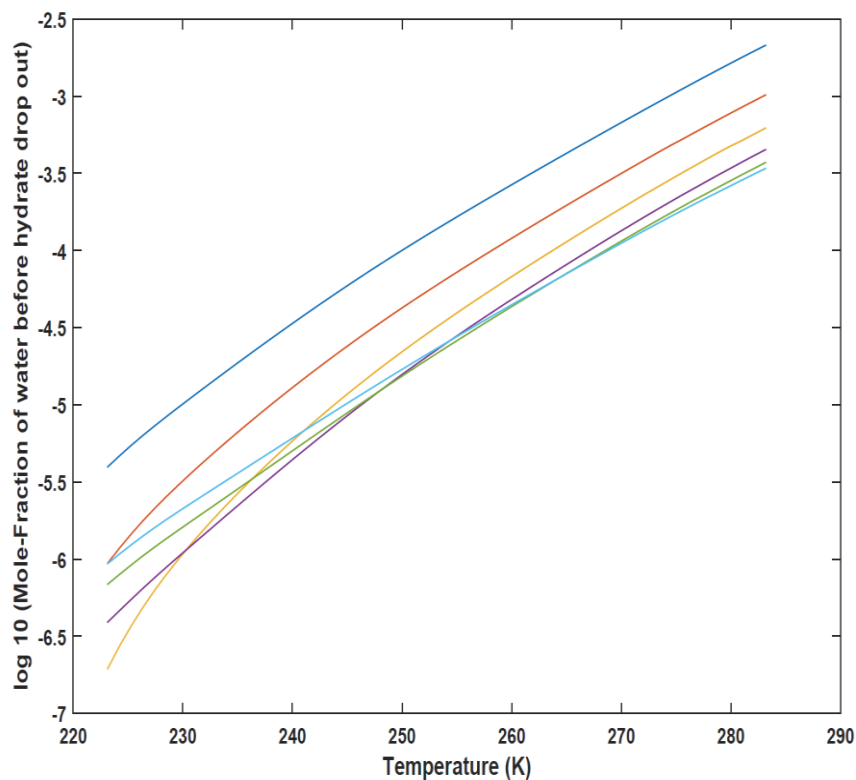
Figure 6.5.5: Maximum Water content before hydrate drop out for mole fraction of 33.33% CO2, 0.01% H2S, 66.66% N2. Curves from top to bottom correspond to pressure 50 bar, 90 bar, 130 bar, 170 bar, 210 bar, 250 bar.
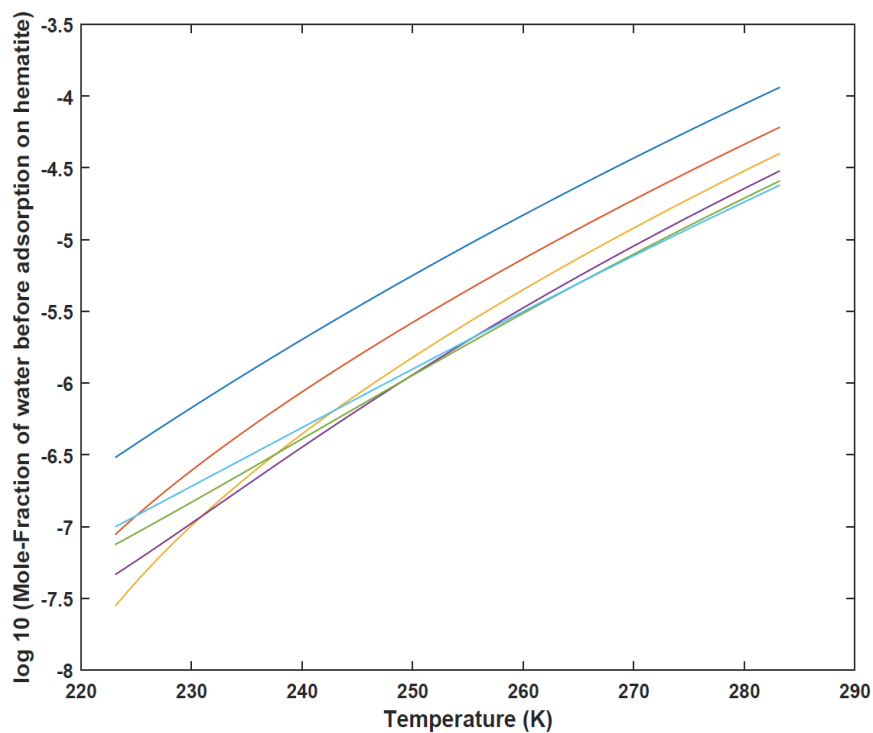
Figure 6.5.6: Maximum water content before adsorption on hematite for mole fraction of 33.33% CO2, 0.01% H2S, 66.66% N2. Curves from top to bottom correspond to pressure 50 bar, 90 bar, 130 bar, 170 bar, 210 bar, 250 bar.

6.5.3 Estimation of Mole-fraction of water in 20% CO2 and 80% N2 mixture

In this section, the maximum amount of water before drop out as liquid, maximum amount of water before hydrate drop out as hydrate and the maximum amount of water before adsorption on hematite in system containing 19.99% CO2 + 79.99% N2 + 0.01% H2S mixture has been evaluated.
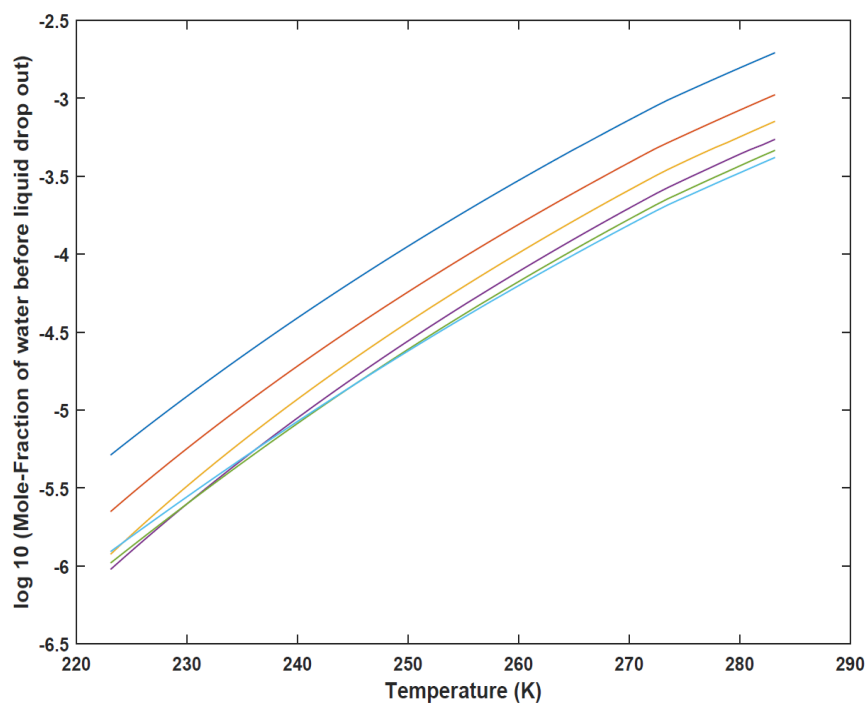
Figure 6.5.7: Maximum Water content before water drop out for mole fraction of 19.99% CO2, 0.01% H2S, 79.99% N2. Curves from top to bottom correspond to pressure 50 bar, 90 bar, 130 bar, 170 bar, 210 bar, 250 bar.
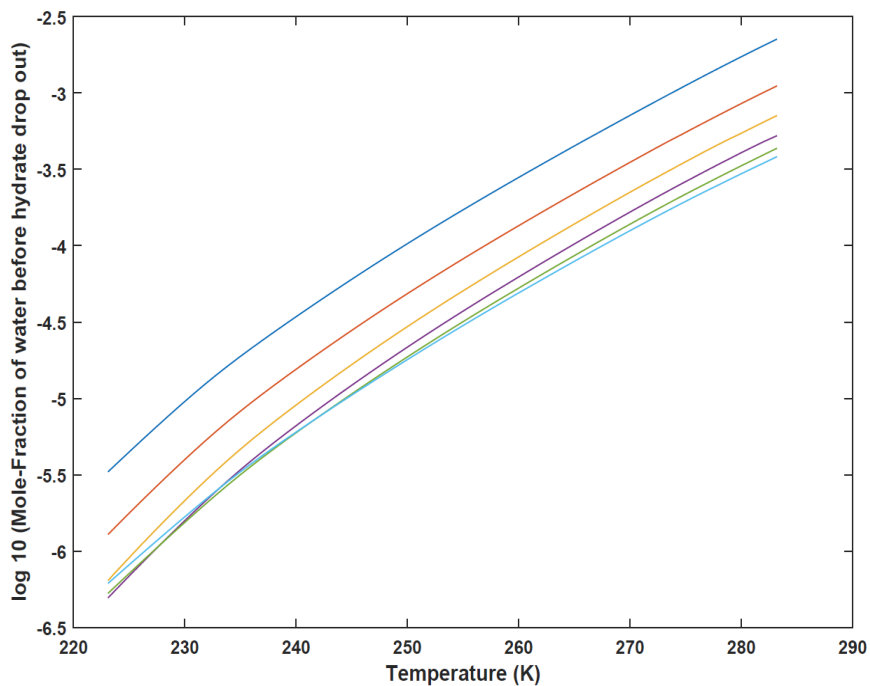
Figure 6.5.8: Maximum Water content before hydrate drop out for mole fraction of 19.99% CO2, 0.01% H2S, 79.99% N2. Curves from top to bottom correspond to pressure 50 bar, 90 bar, 130 bar, 170 bar, 210 bar, 250 bar.
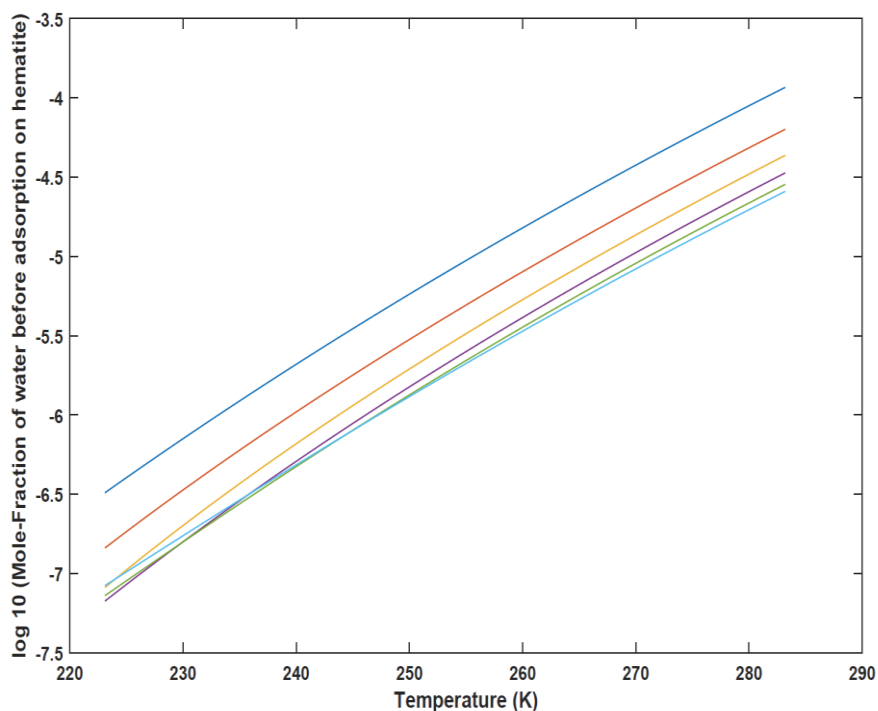
Figure 6.5.9: Maximum water content before adsorption on hematite for mole fraction of 19.99 % CO2, 0.01% H2S, 79.99% N2. Curves from top to bottom correspond to pressure 50 bar, 90 bar, 130 bar, 170 bar, 210 bar, 250 bar.

7. Discussion

Injection of CO2 into in-situ methane hydrate is a promising technology for both serving methane recovery and underground storage of greenhouse gas, CO2. However, this method is practically challenging due to injectivity and flow permeability issues associated with it. When injected CO2 comes in contact with residual water it forms new CO2 hydrate or mixed CO2-CH4 hydrate resulting in reduction in available pore spaces for flow, further reducing flow permeability of CO2. The situation becomes even more complicated when hydrate saturation is high. This can be solved by addition of N2 to CO2. N2 increases the flow permeability. In CO2/N2 injection method, the risk of blocking the flow path due to formed new CO2-hydrate will be less compared to using pure CO2. The exchange process of CO2-CO2/N2 is based on two primary mechanisms; these mechanisms are discussed in detail in section 2.

The replacement process of CH4-CO2/N2 mixture has been proven beneficial for overall improved CH4 recovery instead of using pure CO2. Addition of N2 to CO2 enhance the methane recovery up to 84% which was 64% using pure CO2. Hence the ideal efficiency of this method is 85%, but the experimental results suggest that the exchange efficiency can be as low as 50% (Dong-Yeun Koh et.al, 2014).

Methane hydrate production by CH4-CO2/N2 replacement has been successfully implied at Ignik Sikumi #1 test on the North Slope of Alaska in 2012. In this field trial test program, in total 210,000 standard cubic feet (scf) of gas mixture containing 77.5% N2 and 22.5% CO2 was injected and produced 855 Mscf of methane within a short period of 12 days (details can be seen in section 1.6.2). In 2013 gas hydrate field production was carried out on the Eastern Nankai Trough of Japan by using depressurization method. Thermal stimulation method has been implied at hydrate bearing layers in Mackenzie Delta River of Canada, producing 470 m^3 of gas within five days. The nitrogen concentration applied for simulations reported in this work vary from 30% to 90%.

The primary focus of this thesis is to investigate the lowest amount of carbon dioxide in nitrogen that can produce hydrate with liquid water, and the stability of hydrates after extraction of CO2 for the formation on new CO2-hydrate in the environment of nitrogen dominated gas mixture of CO2/N2. In the pursuit of this goal the hydrate stability limits for individual hydrate bearing fields (studied in section 4), as a function of gradually decreasing CO2 content in the gas mixture of CO2 & N2 have been evaluated. Hydrate stability limits are evaluated by calculating chemical potential of components in different phases for various concentration of CO2 in the CO2/N2 mixtures, by assuming that the guest chemical potentials are same in the hydrate and in the gas but no equilibrium constraints for water. This makes it possible to compare the difference in chemical potential for water in hydrate and the liquid water chemical potential.

The simulation results indicate that hydrate is not stable for mole-fraction of CO2 less than 30% at 280 K and at pressure 90 bar for the hydrate bearing units in Eileen area on the North Slope of Alaska (figure 6.1.1). If pressure increases from 90 bar to 150 bar at same temperature then 10% CO2 requires for hydrate stability (figure 6.1.3).

The inferred GH zone is observed in the depth interval between 810.1 m to 1102.3 m in Mallik area of Mackenzie Delta River of Canada. The calculated temperature range for hydrate bearing zone in the Mallik area vary from 277 K to 285 K. The simulation results indicate that at temperature 277 K and pressure 100 bar, 20% CO2 is required for hydrate stability in the mixture of CO2 & N2 (figure 6.2.2). But if temperature increases from 277 K to 284 K at same pressure, hydrate will not be stable for mole-fraction of CO2 less than 50%. These results indicate that if temperature increases in the reservoir, then the limitations of addition of N2 to CO2 decreases.

In the Nankai Trough, the theoretical base of GH stability is observed at shallower depth than the depth of GH inferred layer, but this discrepancy is not fully understood yet. The estimated results for hydrate stability limits for different mixture of CO2 & N2 indicate that at temperature 283 K and pressure 90 bar, hydrate is not stable for mole-fraction of CO2 less than 40% (figure 6.3.1). If pressure increases form 90 bar to 200 bar at same temperature then only 5% CO2 is required in CO2/N2 gas mixture for hydrate stability. This indicates that increase in pressure consequently reduces the region of hydrate instability as well as increases the limitations of addition of N2 to CO2.

Even though the GH accumulation in Barents Sea is not fully understood geographically yet, some evidences suspect the presence of GHs at comparatively shallower depth interval between 400 m to 620 m in Bjørnøya Basin. The simulation results for limits of hydrate stabilities suggests that at temperature 275 K and pressure 100 bar, 5% CO2 is needed for hydrate stability (figure 6.4.2). If pressure increases up to 200 bar only 2% CO2 is required for hydrate to be stable at 280 K (figure 6.4.4). In this region hydrate is not stable for mole-fraction of CO2 less than 20% at temperature 277 K and at pressure 100 bar (figure 6.4.2).

The second part of this study deals with the transport of hydrocarbons or other hydrate forming fluids containing water through the pipelines. The transport of gases occurs at high pressure and low temperature which are the suitable conditions for hydrate formation. According to Gibbs phase rule system containing water, gas, adsorbed phase & hydrate phase are not in thermodynamic equilibrium since T and P are defined locally through coupling to fluid dynamics and heat transport dynamics. Impact of presence of solid surfaces induces phase transitions. According to 1st and 2nd law of thermodynamics, minimum free energy principle determines in which direction a system will prefer to develop.

In non-equilibrium situation simulations for phase transition kinetics is basically free energy minimization under mass and heat transport constraints (Kvamme et.al, 2014d). The different phase transitions will have different kinetic rates and hydrate formed from different phases will have different free energies since chemical potential of all guest molecules will be different. Hence in case of hydrate formation and dissociation, each phase transition is modelled as pseudo reactions with corresponding changes in free energies as driving force for

phase transition itself and dynamically coupled to mass transport & heat transport (Vafai et.al, 2014). Impact of competing phase transitions needs to couplings to kinetics of mass and heat transport.

By using equation (19) free energy changes of all phase transitions are evaluated using absolute values of water chemical potentials (ice, liquid water, empty structure sI & sII) based on (Kvamme & Tanaka, 1995) and SRK equation of state for fluids.

$$\Delta G_i = d[x_w^{H,i}(\mu_w^{H,i} - \mu_w^p) + x_{gas}^{H,i}(\mu_{gas}^{H,i} - \mu_{gas}^p)] \qquad (19)$$

In equation (19), i is phase transition scenario, p is liquid, gas & adsorbed phases, H is hydrate phase, μ is chemical potential and x is composition.

There are several different routes to hydrate formation depending on number of phases, these routes are discussed in detail in (Kvamme et.al, 2014e), but in this study only three possible routes of hydrate formation has been evaluated. Among the three routes evaluated for hydrate formation, the route of hydrate formation through water dissolved in gas is thermodynamically feasible but mass transport is limitation. In this case mass transport limitation that remain a major uncertainty and provides a challenge for hydrate formation (Kvamme, 2014d). In this case heat transport is limited due to low heat conductivity and low heat convection.

Uncertainties in hydrate formation would induce new sources of errors. In this study the assumption that all of the free methane present in the form of solid hydrate is produced by injecting CO2/N2 mixture may induce error & significantly affects the calculation of methane recovery.

In this thesis the maximum permissible water content in gas stream containing pure CO2, 33.3% CO2 + 66.6% N2 + 0.01% H2S and 19.9% CO2 + 79.9% N2 + 0.01% H2S have been evaluated in section 6.5. In order to evaluate the maximum mole-fraction of water that can be permitted in gas without risk of hydrate plugging in pipelines, the temperature range has been chosen from 220 K to 280 K. The range of transport pressure might be up to 50 bar to 250 bar. The water available for hydrate formation exists in three different states. First is water dissolved in CO2 gas forms hydrate and either water dropped out as liquid or adsorbed on rusty surfaces (hematite in this work since it is more stable than the other oxides). The simulation results obtained for maximum water content for mole-fraction of water before drop out as liquid, mole-fraction of water before hydrate drop out & mole-fraction of water before adsorption on hematite in different gas mixture is discussed below.

Comparing system containing 99.9% CO2 + 0.01% N2 + 0.01% H2S with system containing 33.3% CO2 + 66.6% N2 + 0.01% H2S at temperature 222 K and at pressure 50 bar, it is observed that the mole-fraction of water before liquid drop out (figure 6.5.1) is 0.89 times higher than the mole-fraction of water before adsorption on hematite (figure 6.5.6). If pressure

increases from 50 bar to 250 bar, then the ratio between mole-fraction of water before liquid drop out to before adsorption on hematite will be 0.82.

In a system containing 33.3% CO2 + 66.6% N2 + 0.01% H2S at comparatively higher pressure 210 bar and temperature 222 K, the mole-fraction of water before hydrate drop out (figure 6.5.5) is 0.86 times higher than mole-fraction of water before adsorption on hematite (figure 6.5.6).

Comparing system containing 99.8% CO2 + 0.01% N2 + 0.01% H2S with system containing 19.9% CO2 + 79.9% N2 + 0.01% H2S at temperature 222 K and pressure 130 bar, mole-fraction of water before liquid drop out (figure 6.5.1) is 0.78 times higher than the mole-fraction of water before adsorption on hematite (figure 6.5.9).

In system containing 19.9% CO2 + 79.9% N2 + 0.01% H2S at temperature 250 K and pressure 90 bar, it is observe that the mole-fraction of water before adsorption on hematite (figure 6.5.9) is -0.13 times lower than the mole-fraction of water before hydrate drop out (figure 6.5.8).

From the graph constructed in section 6.5 it is observed that, as the nitrogen concentration in gas mixture of CO2/N2 increases, the mole-fraction of water before liquid drop out, mole-fraction of water before hydrate drop out & mole-fraction of water before adsorption on hematite increases at lower pressures. At comparatively lower pressures 50 bar to 130 bar the considerable difference between mole-fractions of water is observed but at higher pressures 170 bar to 250 bar this difference almost disappears (refer section 6.5).

From the estimated simulation results it is observed that at higher pressures water will prefer to drop out as adsorbed on hematite more quickly than water drop out as liquid or drop out as hydrate, suggesting that the most favorable route for hydrate formation is through the adsorbed water on hematite.

8. Conclusions

Substantial amount of methane is trapped worldwide in the form of solid hydrate. In order to produce gas from in-situ methane hydrate beyond the conventional methods, a new sustainable technology of injection of CO2/N2 mixtures has been investigated experimentally over the last two decades and also tested in pilot plant study recently.

The exchange reaction between in-situ methane hydrate & injected CO2/N2 mixture is governed by two mechanisms, if free water is available then through the formation of new hydrate dominated by the injected CO2 and corresponding release of heat which will assist in dissociating the in-situ CH4 hydrate. In lack of sufficient free water in the pores then solid state exchange mechanism will convert the in-situ CH4 hydrate over to a mixed CO2-CH4 hydrate in which CO2 will dominate filling of large cavities. The direct solid state exchange process is comparatively slow due to mass transport limitations.

In this CH4-CO2 replacement process, addition of N2 to the CO2 will lead to depletion of CO2 from the gas mixture during formation of new hydrate. In a dynamic situation most stable hydrate will be formed first, in which CO2 dominates the filling of 75% large cavities (CO2 consumed three times faster than N2) and heterogeneous CO2 hydrate nucleation on liquid water/CO2 interface as well as on mineral surfaces will further enhance this process of depletion of CO2 from the injected gas. Eventually this may lead to a situation of depleted gas which is not able to create a new hydrate. It does not mean that the in-situ hydrate will not dissociate towards this gas lean on CO2. CH4 in the hydrate will have lower chemical potential than in the gas phase when it is initially free of CH4. So the in-situ CH4 hydrate will dissociate to a certain level of CH4 concentration in the surrounding gas. But the CO2 storage aspect is more uncertain since even the formed CO2 hydrate may dissociate towards surrounding gas of mainly N2 and some CH4. For this reason the limit of CO2 content needed for formation of new hydrate from the injected gas has been estimated for some real hydrate occurrences which have been characterized to sufficient extent. A summary of the obtained results are given in table 8.

Site/well identification	Depth of log inferred GHs (m)	Calculated T range (K)	Calculated P range (bar)	CO2 required for stability (%), (when T= 275 K, P= 100 bar)	CO2 required for stability (%), (when T=280 K, P=100 bar)
Northwest Eileen State-2 Well					
Unit C	651.5– 680.5	276 – 277	63 – 66	≈ 7	≈ 30
Unit D	602.7– 609.4	274 – 275	59 – 60	≈ 5	≈ 35
Unit E	564.0– 580.8	273– 274	55 – 57	≈ 3	≈ 32
Mallik L-38 well	810.1-1102.3	277 – 285	79 – 108	≈ 10	≈ 30
MITI Nankai Trough Well	190 – 268	284 – 288	113 – 121	-	≈ 31
Bjørnøya Basin	400 – 620	275 – 283	40 – 62	≈ 6	≈ 32

Table 8: Depth – Temperature - Pressure profile of hydrate bearing units in different fields in the world and amount of CO2 required for hydrate stability in those range of thermodynamic conditions.

The estimated simulation results for limits of hydrate stabilities as a function of gradual decrease in CO2 content in CO2/N2 gas mixture, for different hydrate bearing fields indicate that the hydrate stability region is increased by increasing pressure. The estimated results also indicate that for higher pressures new hydrate formation is possible from a substantially lower amount of CO2 in the gas phase.

In the open literature the main focus on hydrate stability of hydrates in sediments has been estimated on the temperature and pressure dependency despite the fact that any phase stability depends also on concentration (and corresponding chemical potentials) of all co-existing phases. The work presented in this thesis confirms that the thermodynamic stability of hydrate depends on concentration i.e. corresponding chemical potential of all components entering the hydrate in all co-existing phases rather than only temperature and pressure. The study is based on change in free energy associated with all thermodynamic independent variables. On the basis of the results obtained from this study, it seems feasible to produce in-situ methane hydrate by injection of CO2 and N2 mixtures.

The maximum water that can be permitted in gas stream passing through the pipelines without facing the problem of hydrate formation has also been evaluated. Three of the possible routes for hydrate formation in pipelines and process equipment have been evaluated. From the simulation results it has become clear that the most favorable route for hydrate formation in pipelines is through the adsorption of water on rusty pipeline surfaces from water dissolved in gas, and subsequent hydrate formation from dropped out water and hydrate formers form the gas phase. From the results obtained it is observed that increase in pressure and increase in N2 content in the CO2/N2 gas mixtures both reduce the amounts of water that can be permitted during pipeline transportation.

Once the theoretical amount of water that can be permitted in gas stream is evaluated, then it becomes possible to take appropriate action to reduce risk of hydrate formation in pipelines and in process equipment. In that case hydrate formation can be prevented by reducing the water content to a level below the concentration leading to water drop out or adsorb on solid surfaces.

9. Suggestions for Future Works

Hydrate Stability Limits

In this thesis work, theoretical case studies of different hydrate bearing fields (Eileen area on the North Slope of Alaska, Nankai Trough at Japan, Mallik field on Canada & Bjørnøya Basin in Barents Sea) have been carried out. The amount of H2S used in these mixtures 0.01% is quite low as compared to CO2 & N2. This work can be extended by increasing quantity of H2S which is stronger hydrate former. The effect of addition of H2S in varying quantity in CO2 and N2 mixture is not adequately evaluated yet and we propose further feasibility evaluation of H2S usage in methane production from gas hydrate.

Routes to Hydrate Formation

There are several routes to hydrate formation, but this study does not cover all the possible routes. In this thesis only three possible routes of hydrate formation in pipelines have been evaluated. The simulation performed during this thesis indicates that the route of hydrate formation via adsorption of water on solid surfaces is dominating. In this case further analysis of routes can be done by including addition impurities. In this work, maximum permissible water content in gas stream is calculated for transport of gas through pipelines on the North Slope of Alaska. Further extension of this work could be to estimate the maximum amount of water permitted in gas stream during transport through pipelines at Mallik field, Nankai Trough & Bjørnøya Basin.

Solid Surfaces

The dominating route of hydrate formation is via adsorption of water on solid surfaces. Since in the thermodynamic point of view hematite might be among the most stable on longer term aging of rust, the solid surface considered in this work is hematite (Fe2O3). Hence the work can be extended using other possible surfaces of iron oxides such as magnetite (Fe3O4), FeO.

- The iron oxide rust when comes in contact with solution containing CO2, forms iron carbonates (FeCO3).

  $Fe \Rightarrow Fe^{2+} + 2e^{-}$

  $Fe^{2+} + CO_3^{2-} \Rightarrow FeCO_3$
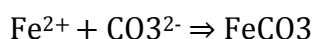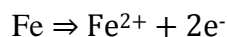
  Further study on how these iron carbonates affects the results is recommended.

- The minerals present in the reservoirs such as calcite, kaolin, quartz have direct effect on reservoir characteristics. Further work need to be done by considering these mineral surfaces.

- The data available until now for the late Cenozoic paleoenvironment in Svalbard & Barents Sea is limited, and gas hydrate accumulation in Barents Sea is not fully understood geographically yet. Further research efforts are needed for the successful production of natural gas from hydrate deposits.

10. References

Allen, D.M., Michel, F A & Judge, A S., The permafrost regime in the Mackenzie Delta, Beaufort sea region N.W.T and its significance to the reconstruction of the paleoclimatic history, Journal of quaternary science, (1988), Vol 3, p. 3-13.

Bily, C., and Dick, J.W.L., Natural occurring gas hydrates in the Mackenzie delta, N.W.T. Bulletin of Canadian Petroleum Geology, (1974), Vol. 22, p. 340–352.

Chand ,S., Thorsnes, T., Rise , L., Brunstad, H., Stoddart, D., Bøe, R., Lågstad, P., Svolsbru, T., Multiple episodes of fluid flow in the SW Barents Sea (Loppa High) evidenced by gas flares, pockmarks and gas hydrate accumulation., Earth and Planetary Science Letters, (2012), Vol 33, p. 305–314.

Chejara Ashok Kumar., Gas Hydrates in Porous Media: CO2 Storage and CH4 Production., Dissertation for the degree of philosophiae doctor at the University of Bergen, Norway, (2012).

Chersky, N. & Makogon, Yu., Solid gasworld reserves are enormous., Oil and Gas International, (1970), Vol 10, p. 82-84.

Christian Hågenvik., CO2 Injection IN Hydrate Bearing Sandstone with Excess Water, Master thesis in reservoir physics, Department of Physics and Technology, University of Bergen, Norway, (2013).

Collett, T. S., Detection and evaluation of natural gas hydrates from well logs, Prudhoe Bay, Alaska., In Proc. of the Fourth International Conference on Permafrost, Fairbanks, Alaska, Washington D.C., National Academy of Sceiences, (1983), p. 169-1 74.

Collett, T.S., & Kvenvolden, K.A., Evidence On Naturally Occurring Gas Hydrates On The North Slope of Alaska, United States Department of The Interior Geological Survey, Open-File Report 87-255, (1987).

Collette, T. S., Natural gas hydrates of the Prudhoe Bay and Kuparuk River area, North Slope, Alaska: AAPG Bulletin, (1993a), Vol 77, p. 793–812.

Collett, T. S., Natural gas production from Arctic gas hydrates in D. G. Howell, ed., The Future of Energy Gases - U.S. Geological Survey Professional Paper 1570: Washington, United States Government Printing Office,(1993b), p. 299-311.

Collett, T.S, & Dallimore, S.R., Quantitative Assessments of Gas Hydrates In The Mallik L -38 Well, Mackenzie Delta, N.W.T., Canada, 7th International Conference (Proceedings), Yellowknife (Canada), Collection Nordicana No 55, (1998).

Collett T S., Energy resource potential of natural gas hydrates, AAPG Bulletin, (2002), Vol 86, p. 1971–1992.

Collett, T.S., Arctic Gas Hydrate Energy Assessment Studies, the Arctic Energy Summit, Anchorage, Alaska. Presentation held in October 15-18, (2007).

Collett, T.S., Geology of Marine Gas Hydrates and Their Global Distribution, Presentation at the 2008 Offshore Technology Conference held in Houston, Texas, U.S.A, (2008).

Collett, T.S., Myung W. Lee., Warren F. Agena., John J. Miller., Kristen A. Lewis., Margarita V. Zyrianova., Ray Boswell., Tanya L. Inks., Permafrost-associated natural gas hydrate occurrences on the Alaska North Slope, Marine and Petroleum Geology, (2009), Vol 28, p. 279–294.

Dallimore, S.R., & Collett, T.S., Intra-permafrost gas hydrates from a deep core hole in the Mackenzie Delta, Northwest Territories, Canada, (1995), Vol 23, p. 527-530.

Dallimore, S. R., & Collett, T, S., Gas hydrates associated with deep permafrost in the Mackenzie Delta, N.W.T., Canada: Regional overview: In Proceedings Of the 7th International Conference on Permafrost, Yellowknife, Canada., (1998).

Dallimore, S. R., T. Uchida., and Collett, T.S., Scientific results from JAPEX/JNOC/GSC Mallik 2L-38 gas hydrate research well, Mackenzie delta, Northwest Territories, Canada: Geological Survey of Canada Bulletin 544,(1999), p. 403.

Dallimore, S.R., Wright, J.F., Nixon, F.M., Kurihiara, M., Yamamoto, K., Fujii, T., Fujii, K., Numasawa, M., Yasuda, M., Imasato, Y., Geologic and porous media factors affecting the 2007 production response characteristics of the JOGMEC/ NRCAN/AURORA Mallik gas hydrate production research well, In Proceedings of the 6th International Conference on Gas Hydrates, Vancouver, British Columbia, Canada, (2008a), p. 10.

Dallimore, S.R., Wright, J.F., Yamamoto, K., Appendix D: update on Mallik., In: Energy from Gas Hydrates: Assessing the Opportunities and Challenges for Canada, Report of the Expert Panel on Gas Hydrates, (2008b), p. 196–200.

Demirbas Ayhan, Methane hydrates as potential energy resource: Part 2 – Methane production processes from gas hydrates, Energy Conversion and Management, (2010), Vol 61, p.1662-1671.

Dixon, J., Dietrich, J.R., & McNeil, D.H., Upper Cretaceous to Pleistocene Sequence Stratigraphy of the Beufort-Mackenzie and Blanks Island Areas, Northwest Canada, Geological Survey of Canada Bulletin 407, (1992), p. 1-90.

Dong-Yeun Koh, Yun-Ho Ahn, Hyery Kang, Seongmin Park, Joo Yong Lee , Se-Joon Kim, Jaehyoung Lee and Huen Lee., 1-Dimensional Productivity Assessment for On-Field Methane Hydrate Production Using CO2/N2 Mixture Gas., Thermodynamic and Molecular-scale phenomena., AIChE Journal, DOI 10.1002/aic.14687., 2014.

Ginley David S., Cahen David, Fundamentals of Materials for energy and Environmental sustainability, (2012), p. 752.

Guo, D B., Song, D. S., Chacko J., Ghalambor D. A., Offshore Pipelines, Gulf Professional Publishing, (2005), ISBN:0-07506-7847-X.

Herri, J.M., Bouchemoua, A., Kwaterski, M., Fezoua, A., Ouabbas, Y., Cameirao, A., Gas hydrate equilibria for CO2-N2 and CO2-CH4 gas mixtures – Experimental studies and thermodynamic modelling., Fluid Phase Equilibria, (2010), Vol 301, P. 171-190.

Husebø Jarle., Monitoring depressurization and CO2-CH4 exchange production scenarios for natural gas hydrates, Dissertation for the degree of philosophiae doctor at the University of Bergen, Norway, (2012), p. 146.

Jeffrey, G.A., Hydrate inclusion compounds, Journal of inclusion phenomena 1, (1984), p. 211-222. doi: 10.1007/bf00656757.

Katz, D.L., Depths to which frozen gas fields (gas hydrates) may be expected, Journal of Petroleum Technology, (1971), Vol 23, p. 419-423.

Khaled Jemai., Bjørn Kvamme., Mohammad Taghi Vafaei., Theoretical studies of CO2 hydrates formation and dissociation in cold aquifers using RetrasoCodeBright simulator., WSEAS Transactions on Heat & Mass Transfer, (2014), Vol. 9, p.150.

Khameneh Niloofar Aslankhani., Bahmani Samira., Mushtaq Waqas., Methane hydrates as potential energy resource, Project report-Natural gas TPG 4140, NTNU, Trondheime, Norway, (2012).

Khuram, B., Kvamme, B., Kuznetsova, T., The impact of water thickness on the rate of mixed hydrate formation, Proceedings of the 8th International Conference on Gas Hydrates (ICGH8-2014), At Beijing, China, (2014a).

Kivelæ, P. H., Kvamme, B., Muhammad Quasim., Khuram Baig., Jordan Baumann., Phase field theory modeling of methane fluxes from exposed natural gas hydrate resrvoirs., International Journal of Greenhouse Gas Control, 2014, 29,263-278., 2012.

Kvamme, B., Tanaka H, Thermodynamic Stability of Hydrates for Ethane, Ethylene, and   carbon Dioxide, Journal of Physical Chemistry, (1995), p. 7114-7119.

Kvamme, B., Graue, A., Kuznetsova, T., Ersland, G., Storage of CO2 in natural gas hydrate reservoirs and the effect of hydrate as an extra sealing in cold aquifers, International Journal of Greenhouse Gas Control, (2007), p. 236-246, DOI: 10.1016/S1750-5836(06)00002-8.

Kvamme, B., Kuznetsova, T., and Kivelæ, P.H., Adsorption of water and carbon dioxide on hematite and consequences for possible Hydrate Formation., Physical Chemistry Chemical Physics, (2012), Vol 14, p. 4410-4424, DOI :10.1039/c2cp23810A.

Kvamme, B., Kuznetsova, T., Kivelæ, P.H., and Bauman, J., Can hydrate form in carbon dioxide from dissolved water?, Phys.Chem.Chem.Phys, (2013a), Vol 15(6), p. 2063-2074.

Kvamme, B., Oil and Gas Processing, PTEK 231, Course Material, Bergen, autumn (2013b).

Kvamme, B., Fundamentals of Natural Gas Hydrates and Practical Implications, PTEK 232, Course Material, Bergen, Spring Session, (2014b).

Kvamme, B., Kuznetsova, T., Jensen, B., Stensholt, S., Sjøblom, S. and Lervik, K.N., Investigating chemical potential of water and H2S dissolved into CO2 using molecular dynamics simulation and Gibbs-Duhem relation, Submitted to fluid phase equilibria, 2014c.

Kvamme, B., Kuznetsova, T., Jensen, B., Stensholt, S., Bauman, J., Sjøblom, S. and Lervik, K.N., Consequences of solubility for hydrate formation from carbon dioxide containing water and other impurities., Phys.Chem.Chem.Phys, (2014d), 16(18), 8623-8638.

Kvamme, B., Kuznetsova, T., Jensen, B., Sjoblom, S., Routes to hydrate formation during transport of carbon dioxide containing water and other impurities., Proceedings of the 8th International Conference on Gas Hydrate, (ICGH8-2104), Beijing, China., 2014e.

Kvamme, B., Qasim M., Baig K., Pilvi-Helinä Kivelä, Bauman Jordan., Hydrate phase transition kinetics from Phase Field Theory with implicit hydrodynamics and heat transport., International Journal of Greenhouse Gas, (2014f), p. 263–278.

Kvamme, B., Feasibility of simultaneous CO_2 storage and CH_4 production from natural gas hydrate using mixture of CO_2 & N_2, Canadian Journal of Chemistry, (2015a).

Kvamme, B., Injection of CO_2/N_2 mixtures into CH_4 hydrate-will it provide safe long terms storage of CO_2?, AAPG Interpretation, Submitted, (2015b).

Kvenvolden, K.A., & McMenamin, M.A., Hydrates of Natural Gas: A Review of Their Geologic Occurrence, U.S. Geological Survey Circular 825, (1980), p. 11.

Kvenvolden, K.A., Methane hydrate-A major reservoir of carbon in the shallow geosphere?, Chemical Geology, (1988), Vol 71, p. 41-51.

Kvenvolden, K. A., A primer on the geological occurrence of gas hydrates, in J.-P. Henriet, and J. Mienert, eds., Gas Hydrates - Relevance to World Margin Stability and Climate Change: London, The Geological Society Special Publication, (1998), p. 9-30.

Laberg, J.S., Andreassen, K., Gas hydrate and free gas indications within the Cenozoic succession of the Bjørnøya Basin, western Barents Sea, , Marine and Petroleum Geology, (1996), Vol 13, p. 921-940.

Laberg, J.S., Andreassen, K., Knutsen, S.M., Inferred gas hydrate on the Barents Sea shelf — a model for its formation and a volume estimate, Geo-Marine Letters, (1998), Vol 18, p. 26-33.

Lachenbruch, A.H., Sass, J.H., Marshall, B.V., & Moses, T.H., Thermal Regime of Permafrost at Prudhoe Bay, Alaska, United States Department of the Interior Geological Survey, Preliminary Open-File Report 82-535, (1982).

Lachenbruch, A.H., Sass, J.H., & Galanis, S.P., Heat flow in southern California and the origin of the Salton Trough, Journal of Geophysical Research, (1985), Vol 90, p. 6709-6736.

Majorowickz, J.A., Jones, F.W., Judge, A.S., Deep subpermafrost thermal regime in the Mackenzie Delta basin, Northern Canada - Analysis from petroleum bottom hole temperature data, Geophysics,(1990), Vol 55, p. 362-371.

Majorowicz, J. A., & Hanigan, P. K., Stability Zone of Natural Gas Hydrates in a Permafrost- Bearing Region of the Beaufort–Mackenzie Basin: Study of a Feasible Energy Source1., Natural Resources Research, (2000), Vol. 9.

Makogon, Y.F., Hydrates Of Natural Gas, Petroleum Engineering-UPSTREAM.

Makogon, Y.F., Specialties of exploitation of the natural gas hydrate fields in permafrost conditions, VNIIGAZPROM, (1966), Vol 11(4), p. 1-12.

Makogon, Y.F., V.I.Tsarev., & N.V.Cherskiy., Formation of large Natural gas fields in zones of permanently low temperatures., Doklady Academii Nauk SSSR, (1972), 205:700-703.

Makogon, Y.F., Production from Natural Gas hydrates deposits., Gazovaya Promishlennost, (1984), Vol 10, p. 24-26.

Makogon, Y.F., & Sayakhov, F.L., Physical principals and models of decomposition of the hydrates of natural gases, VNIIEGazprom, Moscow, (1988).

Mathews, M. A. and von Huene, R., Site 570 methane hydrate zone, Initial report in Deep Sea Drilling Projects and Publications, (1985), Vol 84, p. 773-790.

Mingjian Luo., Peisheng M.A., Shuqian XIA., A Modification of α in SRK equation of state and Vapor-Liquid Equilibria Prediction, Chin. J. Chem. Eng, (2007), Vol 15(1), p. 102-109.

Moridis, G., Collett T., Dallimore, S., Satoh, T., Hancock, S, Weatherhill, B., Numerical studies of gas production from several methane hydrate zones at the Mallik site, Mackenzie Delta, Canada, Journal of Petroleum Science Engineering, (2004), Vol 43, p. 219–238.

Pecher, I. A., T. A. Minshull, S. C. Singh, and R. von Huene., Velocity structure of a bottom simulating reflector offshore Peru: Results from full waveform inversion, Earth Planet. Sci. Lett, (1996), Vol 139, p. 459– 469.

Ruppel Carolyn., Methane Hydrates and the Future of Natural Gas, Gas Hydrates Project, U.S. Geological Survey, Woods Hole, MA, (2011).

Ryo MATSUMOTO, Hitoshi TOMARU and Hailong LU*, Detection and Evaluation of Gas Hydrates in the Eastern Nankai Trough by Geochemical and Geophysical Methods, RESOURCE GEOLOGY, (2004), Vol 54, p. 53–67.

Satoh, M.T., Maekawa, & Y. Okuda., Estimation of amount of methane and resources of natural gas hydrates in the world and around Japan, Journal of the geological society of Japan, (1996), Vol 102, p. 959-971.

Schoderbek & Boswell., Iġnik Sikumi #1, Gas Hydrate Test Well, Successfully Installed on the Alaska North Slope, Fire in the Ice, (2011), Vol 11.

Schoderbek, D., Farrell, H., Hester, K., Howard, J., Raterman, K., Silpngarmlert, S., Kenneth Lloyd Martin, Bruce Smith, and Perry Klein., Oil and Natural Gas Technology., ConocoPhillips Gas Hydrate Production Test Final Technical Report, United States Department of Energy, National Energy Technology Laboratory, (2013).

Seo, Y.T., Lee, H., Yoon, J.H., Hydrate phase equilibria of the carbon dioxide, methane, and water system, J. Chem. Eng. Data, (2001), Vol 46, p. 381–384.

Singh, S.C., Minshull, T.A., & Spence, G.D., Velocity structure of gas hydrate reflector, Science 260, (1993), 204-207.

Sinquin, A., Palermo T., & Peysson Y., Rheological and Flow Properties of Gas Hydrate Suspensions., Oil & Gas Science and Technology – Rev. IFP, (2004), Vol 59, p. 41-57.

Sloan, E.D, & Koh C., Clathrate Hydrates of Natural Gases, Boca Raton, Florida: CRC press, 3rd edition, (2007).

Takahashi, H., Yonezawa, T. and Takedomi, Y., Exploration for natural hydrate in Nankai Trough wells offshore Japan, OTC13040, Offshore Technology Conference Abstract, Houston, (2001).

Uchida, T., Lu, H. L., Tomaru, H. and the MITI Nankai Trough Shipboard Scientists., Subsurface occurrence of natural gas hydrate in the Nankai Trough area: Implication for gas hydrate concentration, Resource Geol., (2004), Vol 54, p. 35–44.

Uchida, T & Tsuji, T., Petrophysical Properties of Natural Gas Hydrates-Bearing Sands and Their Sedimentology in the Nankai Trough., Resource Geology, (2004), Vol 54, p. 79–87.

Vafai, M. T., Kvamme, B., Chejara, A., Jemai, K., A new reservoir simulator for studying hydrate dynamics in reservoir, International Journal of Greenhouse Gas Control, (2014), Vol 23, p. 12-21.

Vogt, P.R., Gardner, J., Crane, K., The Norwegian-Barents-Svalbard (NBS) continental margin: Introducing a natural laboratory of mass wasting, hydrates, and ascent of sediment, pore water, and methane, Geo-Marine Letters, (1999), Vol 19, p. 2-21.

Waseda, A. and Uchida, T., The geochemical context of gas hydrates in the eastern Nankai Trough, Resource Geol., (2004), Vol 54, p. 69–78.

Yamamoto Koji., Masato Yasuda., Masaaki Numasawa., Tetsuya Fujii., Kasumi Fujii., Yutaka Imasato., Masanori Kurihiara., Scott Dallimore., The Second Onshore Methane Hydrate Production Test in the Mackenzie Delta, Journal of the Japanese Association for Petroleum Technology, 2007-2008.
Yamamoto, K., Dallimore, S., Aurora-JOGMEC-NRCan Mallik 2006–2008 Gas Hydrate Research Project progress, In: DOE-NETL Fire In the Ice Methane Hydrate Newsletter, Summer (2008), Vol 8, p. 1–5.